Review

Critical role of toxicologic pathology in a short-term screen for carcinogenicity

Samuel M. Cohen[1]*, and Lora L. Arnold[1]

[1] Department of Pathology and Microbiology, University of Nebraska Medical Center, 983135 Omaha, NE 68198-3135, USA

Abstract: Carcinogenic potential of chemicals is currently evaluated using a two year bioassay in rodents. Numerous difficulties are known for this assay, most notably, the lack of information regarding detailed dose response and human relevance of any positive findings. A screen for carcinogenic activity has been proposed based on a 90 day screening assay. Chemicals are first evaluated for proliferative activity in various tissues. If negative, lack of carcinogenic activity can be concluded. If positive, additional evaluation for DNA reactivity, immunosuppression, and estrogenic activity are evaluated. If these are negative, additional efforts are made to determine specific modes of action in the animal model, with a detailed evaluation of the potential relevance to humans. Applications of this approach are presented for liver and urinary bladder. Toxicologic pathology is critical for all of these evaluations, including a detailed histopathologic evaluation of the 90 day assay, immunohistochemical analyses for labeling index, and involvement in a detailed mode of action analysis. Additionally, the toxicologic pathologist needs to be involved with molecular evaluations and evaluations of new molecularly developed animal models. The toxicologic pathologist is uniquely qualified to provide the expertise needed for these evaluations. (DOI: 10.1293/tox.2016-0036; J Toxicol Pathol 2016; 29: 215–227)

Key words: liver carcinogenesis, bladder carcinogenesis, genotoxicity, cell proliferation, immunosuppression, estrogen

Introduction

The standard for evaluation of carcinogenic potential for a chemical is the two year bioassay in two rodent species, usually rats and mice[1]. Although there have been some minor refinements during the past four decades, this bioassay has remained essentially the same as that developed in the 1960's as part of the National Cancer Institute Bioassay Program. Over the years, several difficulties have been identified regarding this assay, including its high cost and the length of time to perform and adequately evaluate it. Several criticisms have been raised including the use of high doses, usually the maximum tolerated dose (MTD) and fractions thereof, and the use of large numbers of animals. In addition, fundamentally the only information that is gained from this assay is whether or not the chemical increases the incidence of some type of tumor or tumors in rats and/or mice. Minimal dose response information is obtained since the doses used in these studies are in the range of only one order of magnitude, not the multiple orders of magnitude that are needed for a better assessment of the dose response, particularly down to doses relevant to human exposure. However, the most significant limitation of the two year bioassay is that it does not generate information about the relevance of the findings to human risk. Initially several chemicals were tested where a strong relationship between the findings in the animal test and human cancer development existed. These generally involved the potent, DNA-reactive (genotoxic) carcinogens such as aromatic amines, polycyclic aromatic hydrocarbons, nitrosamines, and aflatoxin[1]. However, over the past decades, numerous chemicals were tested in which either extremely high doses had to be used to produce tumors since the chemical was non-toxic, or the relevance of the tumors produced by the chemical were shown to be produced by a mechanism that was not relevant to humans. Such examples of non-relevant modes of action include the production of calcium phosphate-containing urinary precipitate by sodium saccharin and other sodium salts leading to the induction of bladder tumors in rats[2, 3], d-limonene and the induction of kidney tumors in male rats by binding to α_{2u}-globulin[3], ethyl acrylate induction of forestomach tumors in rodents[4], and a variety of others. Determining the relevance of tumors in the bioassay to humans had to be determined in follow-up mechanistic research. The proposal is to utilize a short term screen to identify potential pre-neoplastic changes, and then evaluate the mechanistic processes involved to determine both a detailed dose response and relevance to humans. The two year bioassay is not necessary for evaluation of carcinogenic potential.

Carcinogenesis

Any studies performed in animal models, whether the two year bioassay or others, are based on two fundamental assumptions: 1) the effects produced at the doses used in the bioassay will also occur at doses to which humans are exposed (dose extrapolation); and 2) the effect that is produced in rodents will produce a similar effect in humans (species extrapolation)[1, 5]. As was stated by George Box more than five decades ago, "Models: all are wrong, some are useful"[6]. As scientists, it is incumbent on us to evaluate the results of the use of a given model as to how they might extrapolate to humans. Unfortunately, evaluation of the extrapolation to humans is not always investigated.

For cancer and non-cancer endpoints, the US EPA, Health Canada, and International Programme on Chemical Safety (IPCS) have evolved a framework for a transparent, structured, disciplined evaluation of mode of action data in animal studies, followed by a detailed evaluation of the human relevance of the mode of action[7–12]. It is based on determination of the key events necessary for production of the adverse effect by the chemical in the animal model, and then an evaluation of those key events in humans qualitatively and quantitatively. The criteria for evaluating the various aspects of mode of action utilize a modification of the Bradford Hill criteria used in assessing causality in epidemiology studies[7]. These include temporality, dose response, strength of the evidence, consistency of the findings, and biological plausibility. In addition, alternative modes of action are evaluated and data gaps identified regarding a given mode of action for the induction of an adverse effect by a chemical. This framework continues to evolve, and now is incorporated into the adverse outcome pathway analysis that utilizes molecular biological investigations[13–16]. It is a fundamental understanding of the key events in the process of producing the adverse effect that is essential for our understanding of the mode of action and for extrapolating between the animal model and the human. The key event is defined as a necessary step in the process, and all of the key events together are sufficient to explain the induction of the adverse effect.

Utilizing this framework can form the basis for a short term screen for carcinogenesis that provides a much more rational approach to this assessment than the current two year bioassay.

To understand the basis for the shorter term approach to this risk assessment process, the fundamental basis for carcinogenesis needs to be understood[17, 18]. It has long been known that cancer is the result of numerous errors in the genome occurring in a single pluripotential, tissue stem cell. Cancer is a clonal disease, so all of the critical genetic errors must occur in a single cell. It is clear that more than one genetic abnormality must be present for cancer to develop, although the precise number is not usually known. Furthermore, these errors are fixed into place during DNA replication. Also, it has long been known that DNA replication, although incredibly precise, does not have 100% replica-

tion precision. Rather, rare mistakes occur every time DNA replicates. Thus, a chemical, or for that matter, any agent, can increase the risk of cancer only one of two fundamental ways[17–20]: 1) it can increase the rate of DNA damage per cell division (DNA reactivity, genotoxicity); or 2) it can increase the number of cell divisions increasing the opportunity for spontaneous errors to occur (non-DNA reactive, increased proliferation) every time DNA replicates. DNA reactive carcinogens at high doses nearly always are toxic, in addition to being DNA reactive. Thus, at high doses, DNA reactive chemicals both increase proliferation and directly damage DNA.

Synergy Between DNA Reactivity and Cell Proliferation

When there is both an increase in DNA reactivity (genotoxicity) and increased cell proliferation, there is a strong synergism. In effect, the increased proliferation provides more numerous targets for the DNA reactive effect and increases the possibility of spontaneous errors. There are numerous examples of this synergy in human cancer risk, including some instances where the increased risk is in one agent, such as cigarette smoking, and in other circumstances the increase in DNA reactivity and increase in DNA replication are induced by different sources[18, 20]. An excellent example which provides a quantitative indication of this synergy is the interaction between aflatoxin (DNA reactive) and hepatitis B virus infection (cytotoxicity with consequent regenerative cell proliferation)[5, 20]. In parts of China where there is increased exposure to aflatoxin without hepatitis B virus infection, the increased risk of hepatocellular carcinoma is approximately three times. In areas where there is no increased aflatoxin exposure but increased hepatitis B virus infection, the increased risk is approximately ten to twelve times. In populations that have both an increased exposure to aflatoxin and have hepatitis B virus infection, the overall risk is approximately sixty-five times, clearly more than additive and more than multiplicative, a true synergy.

In animal experiments, there are numerous examples of interaction between increased cell proliferation and DNA reactivity. One example is the ED01 study involving more than 24,000 mice orally administered acetylaminofluorene (AAF) at relatively low doses, with a detection limit of an increased incidence of 1% instead of the usual 10% in two year bioassays[21]. A number of subgroups were also investigated, but the results clearly showed that the incidence of liver tumors was increased at all doses, even as low as 30 ppm. In contrast, an increase in urinary bladder tumors only occurred at doses of 60 ppm and above, despite a linear dose response for DNA adduct formation in both tissues. In this study, at the doses used, there was no effect of AAF on hepatocellular proliferation, whereas in the urinary bladder, urothelial cell proliferation was increased at doses of 60 ppm and above, the same doses at which there was an increase in detectable tumor incidence. It is apparent that at the lower doses, the presence of DNA adduct formation was

not sufficient to increase the incidence of tumors in the urinary bladder to a detectable level (greater than 1%), but that the increase in DNA reactivity combined with increased cell proliferation at the dose of 60 ppm and above produced detectable tumor incidences.

In animal studies utilizing different stimuli for DNA reactivity and increased cell proliferation, an experiment involving the administration of sodium saccharin at 5% of the diet and N-[4-(5-nitro-2-furyl)-2-thiazolyl]-formamide (FANFT) at a dose of 0.005% of the diet, illustrates the interaction[22]. FANFT is a DNA reactive carcinogen specific for the urinary bladder in rats. Sodium saccharin increases cell proliferation and has no effect on DNA reactivity or genotoxicity in general. At these doses, in a standard two year bioassay, there was no increase in tumor incidences, but when they were administered together, there was a detectable incidence of tumors, approximately 30%.

In summary, there are only two fundamental ways by which chemicals can increase the risk of cancer, either DNA reactivity, which increases the rate of the number of errors in the DNA with each replication, or an increase in cell proliferation, which produces an increased number of replications in which spontaneous errors can occur during replication. The two can both occur, which results in synergy.

DNA Reactivity, Immunosuppression and Estrogenic Activity

For the past two decades, there has been an effort to utilize mode of action evaluations for risk assessment of chemicals and then determine if these modes of action have possible human relevance[7–16, 23]. The criteria for evaluation of mode of action have been clearly delineated. The methods used for extrapolating to human relevance both qualitatively and quantitatively have also been delineated and continue to be refined and evolve.

Overall, there are three types of mode of action that clearly are relevant to human cancer risk[1, 5]. These are DNA reactivity, immunosurveillance, and estrogenic stimulation of cell proliferation. These effects can readily be evaluated in short term screens rather than waiting for a two year bioassay to determine carcinogenicity. DNA reactivity can be evaluated utilizing structure activity relationship (SAR) computer programs, by assessment of mutagenicity *in vitro* (Ames assay), and more recently by the utilization of *in vivo* mutagenicity assays[24–33]. If a chemical is DNA reactive, an evaluation utilizing human cells can be performed to demonstrate the relevance to humans, and evaluate metabolic pathways that are necessary to generate the reactive intermediate that will form DNA adducts. Demonstration of DNA reactivity results in presumptive evidence of carcinogenicity in humans. This is not true for other screening tests for genotoxicity, such as micronucleus formation, the Comet assay, and others, which involve indirect damage to DNA and can be greatly influenced by a number of factors, especially cytotoxicity, that do not portend an increase in cancer risk. Especially in *in vitro* studies, many of these genotoxic-

ity assays have been shown to produce false positive results which cannot be extrapolated to the *in vivo* situation in animals, and certainly not to an increase in cancer risk either in animals or in humans.

Immunosuppression is another process that predicts an increased risk of carcinogenesis in humans, and this can be readily evaluated in a variety of both *in vitro* and *in vivo* assays[34]. Hematologic effects and effects on lymphoid organs such as lymph nodes, thymus, spleen, and bone marrow can be demonstrated morphologically in a 90 day study. More specific assays can also be used to determine certain aspects of the immune response.

Individuals that are immunosuppressed are at greatly increased risk of developing cancer[1, 20, 35]. This includes individuals that are born with inherited immunosuppressive disorders, transplant recipients treated with immunosuppressive therapy, patients with a variety of neoplastic and non-neoplastic disorders treated with drugs that are immunosuppressive, and individuals that have AIDS. However, the increased risk of tumors is not uniform for all types of tumors. In reality, the increased risk of cancer in immunosuppressed individuals is related to those malignancies that are produced by infectious diseases, such as B cell lymphoma (EBV), squamous cell carcinoma (HPV), hepatoma (HBV and HCV), and Kaposi's sarcoma (HHV8, also known as Kaposi's sarcoma virus). Thus, the immunosurveillance is for the infectious diseases, not the neoplasms themselves. The infectious diseases can lead to the production of certain malignancies. With respect to human risk, if a chemical is immunosuppressive at levels to which humans are exposed, it will lead to an increased risk of developing these infectious disease-related malignancies.

The relationship of estrogen to the production of certain malignancies, especially breast and endometrium, is well-documented [20, 36, 37]. Other tumors that might be related to estrogen include liver and ovary, although the relationship is not as strong as for breast and endometrium. Screening for an estrogenic effect can be accomplished in a variety of *in vitro* and *in vivo* assays, including estrogen receptor assays and bioassays which include examination of estrogen-dependent tissues such as ovary, uterus, cervix, vagina, and breast[1, 20, 36, 37]. Examination of these tissues is included in routine 90-day studies and could also be included in shorter term studies. Substances with estrogenic activity at doses to which humans are exposed, are likely to pose an increased risk for development of estrogen-related malignancies. The dose and potency of the estrogenic activity are particularly critical in evaluating human risk, but a two year bioassay is not necessary to determine these factors.

Short Term Screen for Carcinogenicity

Currently the standard process for evaluating substances for carcinogenic activity is to perform a dose range finding study, usually 90 days, in the test species, followed by a two year bioassay. If increased incidences of tumors occur in the two year bioassay, further investigative work is

then conducted to determine the mode of action and whether the mode of action is relevant to humans, and to evaluate a more detailed dose response of the key events in the mode of action. Given the vast amount of knowledge that has been gained over the past five decades from the performance of these bioassays and the investigation of the modes of action of a wide variety of chemicals that have been tested, we now know the modes of action in animal models for most tumor types, and furthermore, we have a reasonable basis to judge which of these modes of action are relevant to humans. The proposal was first put forward nearly fifteen years ago to take advantage of this vast knowledge and use it in a more predictive and rational way to evaluate chemicals in short term screening assays instead of in a two year bioassay[1, 5]. The short term screening assays are focused on mode of action and human relevance. What really is needed is a determination as to whether the chemical poses a cancer risk to humans. not an investigation to determine if a chemical poses a cancer hazard in rats or mice. We will present how this process can be applied to an evaluation of liver carcinogenesis and urinary bladder carcinogenesis, and then present an overall approach to the predictive evaluation of cancer risk from chemicals. The role of toxicologic pathology is both essential and noteworthy.

Liver Carcinogenesis

Production of hepatocellular carcinomas (hepatomas) in rodent species was one of the first tumor types to be produced experimentally[5]. This was accomplished by Yoshida in 1932 and involved the administration of an azo dye for production of liver cancer. His seminal observation was followed by further investigations by Kinosita, published in 1937. Extensive investigations on azo dyes and other substances over the past eight decades have provided a good understanding of how chemicals produce liver cancer in rodents[5, 38]. Furthermore, we have also developed a basic understanding of what produces hepatocellular cancer in humans[39, 40]. For liver carcinogenesis, the modes of action can be divided into those that are DNA reactive and those that are non-DNA reactive as described above[5]. Non-DNA reactive chemicals that are carcinogenic for the liver can be divided into those that act through specific receptors versus those that do not. Furthermore, as for all non-DNA reactive modes of action, the increase in cell proliferation can either be due to an increase in cell births or a decrease in cell deaths, which results in an accumulation of more cells. Increased cell births can be produced by cytotoxicity and regeneration or by direct mitogenesis. Decreased cell deaths can be produced by either blocking apoptosis or blocking differentiation (a cell death process). Listed in Table 1 are the various modes of action that have been specifically identified in rodents for hepatocellular carcinogenesis. Examples are known for all of these, but we describe in detail a few of these to illustrate issues that arise with regard to mode of action and extrapolation to human relevance.

Chloroform has been demonstrated repeatedly to pro-

Table 1. Modes of Action for Hepatocellular Carcinogenesis

I. DNA Reactivity
Metabolic activation
II. Increased Cell Proliferation
A. Receptor mediated
1. PPARα (peroxisome proliferation)
2. Enzyme induction (CAR, PXR, AHR)
3. Estrogen
4. Statins
5. Other
B. Non-receptor mediated
1. Cytotoxicity
2. Viral
3. Iron overload
4. Increased apoptosis (e.g. fumonisin B1)
5. Other

Modes of action known to be relevant to humans are indicated in bold type. Modified from Cohen, SM, Toxicol Pathol, 38: 487–501, 2010[5], with permission from Toxicologic Pathology.

duce increased incidences of tumors of the liver and kidney in rats and mice[5, 9, 38, 41, 42]. The mode of action has been delineated and involves metabolic activation to reactive products (phosgene) by cytochrome CYP2E1. This leads to the induction of cytotoxicity in hepatocytes and renal tubule cells, with consequent regenerative proliferation. If this continues for prolonged periods of time, it ultimately leads to an increased incidence of tumors of the liver and kidney.

Exposure to chloroform also occurs in humans. Several decades ago, chloroform was used at relatively high doses as an anesthetic. Occasionally, because controlling exposure was difficult, some patients developed toxicity to the anesthetic chloroform. The toxicity involved liver, and infrequently kidney, similar to what is seen in rats and mice. Furthermore, metabolic activation of chloroform to phosgene occurs in humans by the same cytochrome as in rodents. Thus, there is the potential for chloroform to theoretically increase the incidence of liver or kidney tumors in humans, since the precursor key events are known to occur in humans. However, there are two aspects that preclude the development of tumors in humans that need to be taken in to account in a risk assessment. First, in humans, the exposure is limited, especially if there is any evidence of toxicity, and second, chloroform is no longer used as an anesthetic since there are many better drugs available for this purpose. In the rodent, extensive investigations have demonstrated that the tumorigenic effect only occurs when the dose is sufficient to produce cytotoxicity in the target tissues, liver and kidney. Thus, there is clear evidence for a non-linear, threshold dose response. If the exposure is too low to produce cytotoxicity, there is no increased risk for development of tumors. Humans today are exposed to chloroform at extremely low levels as a by-product of chlorination of drinking water. The exposure in humans is several orders of magnitude below that which is known to produce toxicity in humans. Therefore, based on both time of exposure and dose of exposure, humans are not exposed to sufficient amounts of chloroform in the drinking water or other environmental sources to pro-

duce sustained cytotoxicity. Since there is no risk for increased cell proliferation, there is no increased cancer risk in humans.

Of great importance in investigating liver and kidney tumors produced by chloroform is a detailed understanding of the metabolism and identification of the cytotoxicity and the consequent increased proliferation that occurs in response to the treatment with chloroform. This can be performed in short term studies and involves comprehensive investigations of histopathology, serum enzyme markers for liver toxicity, and serum markers for kidney toxicity. Urinary markers of kidney toxicity also could be evaluated. Very sensitive and rapid techniques are now available to measure the markers for cytotoxicity in both of these tissues. Evidence of increased proliferation can be determined by observation of hyperplasia by routine histopathology or utilization of markers for cell proliferation such as bromodeoxyuridine (BrdU)[43, 44], proliferating cell nuclear antigen (PCNA)[45], and Ki-67[46]. Advantages and disadvantages of these labeling indices for evaluating cell proliferation have previously been described in detail[47, 48].

Another example of chemicals shown to be liver carcinogens in rodents are those known to induce cytochrome P450's, such as phenobarbital and pyrethroid insecticides[49, 50]. These chemicals are non-genotoxic. Following extensive investigations over the past 40 years, the mode of action as to how these chemicals produce liver tumors in rodents has been delineated and includes activation of the CAR receptor and induction of P450 isozymes, with consequent increased hepatocellular proliferation and ultimately tumor formation[5, 38, 51–54]. There are several associated events in the process, including centrilobular hypertrophy and increased liver weight. Humans have the same receptor (CAR) as the rodent, although there appears to be fewer receptors per cell in the human than in the rodent. In addition, activation of the CAR receptor in humans leads to induction of the same P450 isozymes as in the rodent. However, in mice and rats, CAR activation results in an increase in hepatocellular proliferation which is a required key event for the production of tumors. In human hepatocytes, there is no proliferative response. This has been demonstrated *in vitro* in studies involving human liver cells[55], and also *in vivo* utilizing chimeric mice with transplanted human hepatocytes[56]. The human hepatocytes respond to CAR activators such as phenobarbital or permethrin with the expected metabolic responses including induction of P450 isozymes, but there is no increase in human hepatocyte proliferation. Since increased proliferation is a required key event in the mode of action for the production of liver tumors, it is clear that liver tumors will not be produced by this mode of action in humans. Additional evidence supporting a lack of effect in humans by CAR activators are extensive epidemiology investigations of phenobarbital and pyrethroid insecticides[50, 57, 58]. This is particularly relevant for phenobarbital, since patients receive phenobarbital as treatment for epilepsy for many years. The dose administered to humans is similar to the dose to which the rodents are exposed, and the epidemiologic evidence consistently demonstrates the lack of a carcinogenic effect of these agents.

Statins are a third example of a chemical that produces high incidences of liver tumors in rats and mice in the standard two year bioassay[59, 60]. However, the metabolic response to statins is different in rodents than it is in humans. Subsequent extensive epidemiologic investigations involving hundreds of thousands of patients on statins clearly demonstrated that there is no increased or decreased risk of liver cancer or any other types of cancer in patients receiving statins[61–65].

To screen for potential carcinogens in rodent species utilizing a short term assay, there must be evidence that the short term screening assay will provide markers for detection of potential carcinogens. Several years ago, investigators at the National Toxicology Program reviewed the tumor bioassays of more than 500 chemicals and correlated the eventual appearance of liver tumors in rats and/or mice with findings in the 90 day dose range finding study[66]. They demonstrated that all of the potential liver carcinogens showed one or more of the following markers in the 90 day study: hepatocellular necrosis, hepatocellular hypertrophy, hepatocellular cytomegaly, or increased liver weight. Obviously, these are non-specific, and many chemicals which produced these effects, particularly increased liver weight, in a 90 day study did not produce liver tumors in the full two year bioassay. However, the importance for a short term screening assay is that there be no false negatives, and that was found to be the case. All eventual hepatocellular carcinogens produced one or more of these effects in the short term assay.

The proposal is to utilize short term screens to detect potential carcinogens, in this case for the liver, and then to do more detailed mode of action analyses and dose response investigations to provide a more rational risk assessment for humans[5]. In Table 1, the modes of action are identified for hepatocellular carcinogenesis, but highlighted in bold print are those that are actually relevant to humans. Genotoxicity, a known mode of action for certain liver carcinogens such as aflatoxin, is relevant to humans. In addition, it is known that estrogen is related to the rare development of hepatocellular carcinomas in humans, evolving in those circumstances from adenomas. In humans, the most common modes of action for induction of hepatocellular carcinomas involve cytotoxicity, inflammation, and regenerative hepatocellular proliferation, whether due to inherited disorders, iron overload, or viral infection. The modes of action that are not highlighted in this table, such as CAR activation, PPARα activation, or exposure to statins, are not relevant to humans.

Based on our knowledge of hepatocellular carcinogenesis in rodents and in humans, a short term screen is readily achievable (Fig. 1). First, the chemical would be administered for 90 days, with evaluation of the liver for the four markers identified by the NTP (see above) in their screen for rodent hepatocarcinogens. If negative, we can be assured that there is no potential risk for development of liver cancer in humans. If it is positive, then evaluation of the mode of

Rodent Liver Carcinogenesis Screening and Implications for Humans
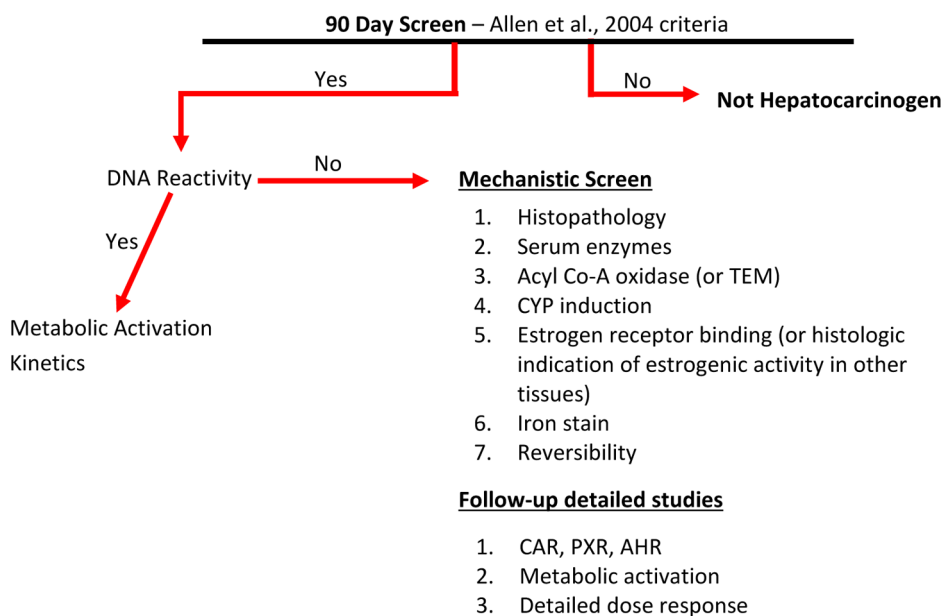

Fig. 1. Proposed sequence of evaluation to screen for potential hepatocarcinogens. The initial screen involves the four criteria proposed by Allen *et al.*[66]. If one or more of these four signals are detected in the 13 wk. screening assay, follow-up mechanistic evaluations are performed to determine the MOA(s) and provide the basis for an assessment of human cancer risk. Modified from Cohen, SM, Toxicol Pathol, 38: 487–501, 2010[5], with permission from Toxicologic Pathology.

action is required to determine whether the chemical produces the effects on the liver by a mode of action that is relevant to human carcinogenesis. Methods that can be used for mode of action analysis are indicated in Fig. 1.

Keep in mind that it is critically important in these short term screenings that they be used to identify potential toxicities that could occur in humans, not simply as dose range finding studies for longer term bioassays. Liver toxicity is a common problem with various pharmaceuticals in development, so it is critical in these animal studies that potential for liver toxicity in general be identified. This is irrespective of any potential for carcinogenesis. Thus, the short term screening is critical not only for identifying potential carcinogens, but more importantly, identifying potential toxicities in humans. If the mode of action is determined to be relevant to humans, a more detailed dose response can then be investigated to determine whether the exposures in humans put them at risk for development of tumors. If the mode of action is not relevant to humans, such as for CAR activators, it is sufficient to conclude that these chemicals will not be carcinogenic for the liver in humans. In addition, if the dose response for a chemical such as chloroform shows that the exposure to humans is significantly below that which will produce the effect on the liver that is necessary for the eventual development of hepatocellular tumors, it can be concluded with confidence that there is no increased risk of carcinogenesis in humans.

All of this information can provide a more rational, mode of action-based risk assessment than is provided by

proceeding to the two year bioassay. For such a proposal to actually be implemented, however, requires not only acceptance by regulatory authorities of the science behind the proposal, but would also require extensive changes in the processes by which chemicals are labeled, particularly in the pharmaceutical industry. A positive finding for one of the short term screening markers cannot be used as the basis for listing on the label that it is a potential carcinogen. If it is not relevant to humans either based on mode of action or on dose, the chemical should not be labeled as a potential carcinogen to the public.

Urinary Bladder Carcinogenesis

A similar approach can be utilized for the urinary bladder. Urinary bladder carcinogenesis has been extensively investigated for the past eight decades, but traces a lineage of scientific investigations back to the observation by Rehn in 1895 when he observed that individuals working in the aniline dye industry had a markedly increased risk of developing bladder cancer[67–69]. It was eventually demonstrated that the increased risk was due to exposure to aromatic amines, which are metabolically activated by N-hydroxylation and subsequent esterification to reactive electrophiles that form DNA adducts and mutation. Several specific chemicals have been identified as human bladder carcinogens, including various aromatic amines, phosphoramide mustards, and arsenic[67–70]. Arsenic, in contrast to the others, is a non-genotoxic carcinogen which produces bladder and other types of

cancer in humans by a process involving cytotoxicity and regenerative proliferation[70].

Screening for potential human bladder carcinogens would involve a similar process (Table 2) as was just illustrated for the liver. Markers for potential urothelial carcinogenesis in rats or mice include evidence of increased cell proliferation[67]. It is usually adequate to use routine light microscopic examination of hematoxylin and eosin stained slides for the presence of hyperplasia. However, a more sensitive evaluation would be determination of a proliferation labeling index, such as BrdU, Ki-67, or PCNA. All potential urothelial carcinogens in rodents (and in humans) show evidence of increased proliferation in a standard 90 day study, whether the ultimate mode of action is due to DNA reactivity (e.g. aromatic amines) or due to increased cell proliferation without genotoxicity (e.g. inorganic arsenic). Again, we will cite some examples to illustrate the process.

Sodium saccharin produces an increased incidence of urinary bladder tumors in rats, particularly males, when administered beginning before weaning and continuing for the full two year bioassay[2, 6, 7, 71, 72]. Administration beginning after weaning does not produce an incidence of tumors adequate for detection in a standard bioassay involving 50–60 animals per group. However, in the so-called two generation study, the incidence is increased sufficiently to be detected in such studies. The dose required to produce any effects by administration of sodium saccharin in the diet are enormous, $\geq 25,000$ ppm. Nevertheless, hyperplasia is present in the urothelium after 4 to 13 weeks of administration, even if it begins after weaning, but most importantly, it turns out that the mode of action is not relevant to humans. The mode of action involves administration of the sodium salt at high doses in the diet which produces an alteration of the urinary milieu that results in formation of calcium phosphate-containing precipitate. This precipitate acts as a cytotoxic agent for the urothelium with consequent regenerative proliferation and ultimately the development of tumors. Various aspects of this mode of action have been extensively investigated and demonstrated in several laboratories. Since the mode of action was clearly not relevant to humans, the International Agency for Research in Cancer (IARC) downgraded its classification of saccharin from 2B to 3 in 1999[2, 71], and the National Toxicology Program removed it from its List of Carcinogens in 2000[72].

Sodium saccharin-induced urinary bladder carcinogenesis is specific for the rat [2, 3, 67, 71, 72]. When administered to mice at high doses, even up to 100,000 ppm of the diet, sodium saccharin produced no effect on the urothelium. The reason for this rat specificity is because mice do not form the precipitate in response to administration of sodium saccharin. In the mouse, the urinary concentrations of calcium, phosphate, and magnesium are approximately 5–10 times lower than in the rat, and are inadequate for formation of the precipitate. Without the precipitate there is no cytotoxicity, no regenerative proliferation, and no formation of tumors. In humans, there is adequate urinary calcium concentration, similar to the rat, but other components of the urine that are

Table 2. Modes of Action for Urothelial Carcinogenesis

DNA Reactivity
Direct Mitogenesis
Cytotoxicity and regenerative cell proliferation
Chemical Toxicity
Formation of urothelial solids
Infection (cystitis)
Obstruction due to neurogenic dysfunction

Modes of action known to be relevant to humans are indicated in bold type.

necessary for the formation of the precipitate do not occur in humans, including protein concentration, overall density (osmolality), and possibly other aspects such as citrate concentration (which chelates calcium and magnesium).

In addition, it became apparent based on extensive investigations from the laboratories of Dr. Nobuyuki Ito and Shoji Fukushima, that it was not the saccharin itself that was producing the effect but sodium salts in general[2, 3, 67, 72]. It was demonstrated that the sodium salts of ascorbate, bicarbonate, glutamate, citrate, chloride, and others produce similar effects in the rat. For these substances, the assumption of species extrapolation and dose extrapolation are both incorrect. It is a high dose phenomenon only, and it is only in the rat.

A related example of urinary bladder carcinogenesis in rodents involves formation of calculi. Calculi can be produced by a variety of substances, such as melamine, uracil, and many others[3, 9, 73]. Clearly, the effect only occurs at high doses, doses sufficiently high to produce precipitation of the material in the urine to form calculi. Calculi, in contrast to the calcium phosphate-containing precipitate produced by sodium salts, produce much greater urothelial damage and much higher incidences of tumors. The effect is a high dose phenomenon only. However, a number of substances that produce calculi in rats and mice resulting in an increased incidence of urinary bladder tumors can also produce calculi in humans[67, 73, 74]. This was clearly demonstrated in China where infants ingested formula contaminated with melamine[75]. Several infants developed urinary tract calculi and six died. Clearly toxicity can occur, so the mode of action for calculi-induced urinary bladder tumors is potentially relevant to humans. However, there are several bases to conclude that the potential for carcinogenesis in humans is significantly lower than in rodents and probably non-existent[3, 9, 73]. This is predominantly due to the anatomic differences between humans and rodents. In rodents, calculi can accumulate in the bladder and remain for the lifetime of the animal. In humans, calculi will produce obstruction, which produces pain and usually hematuria, either of which will lead the affected individual to a physician for removal of the stone. Thus, although stones can form in humans, they will be present for only a brief period of time. There are some individuals that can carry calculi for longer periods of time such as individuals with urinary bladder diverticuli or patients with neurogenic bladder. However, when there

Table 3. Comparison of *In Vivo* Urinary Concentrations after Pulegone Administration and *In Vitro* Cytotoxicity

	In Vivo Urinary Concentration (mM)		*In Vitro* Cytotoxicity (LC$_{50}$ in mM)	
Metabolite	75 mg/kg$^{\alpha}$	150 mg/kg$^{\alpha}$	MYP3 cells	1T1 cells
Pulegone	0.36 ± 0.11	0.46 ± 0.06	0.27	0.57
Piperitenone	0.93 ± 0.28	1.15 ± 0.15	0.5	0.44
Piperitone	0.50 ± 0.12	0.41 ± 0.05	1.16	1.29
Menthofuran	0.11 ± 0.02	0.18 ± 0.03	1.41	3.6
Menthone	ND	ND	4.5	7.25

Note: ND, not detected. $^{\alpha}$Pulegone dose administered to the rat. From DaRocha *et al.*, Toxicol Sci, 128: 1–8, 2012[76], with permission from Toxicological Sciences.

Urothelial Carcinogenesis Screening and Implications for Humans
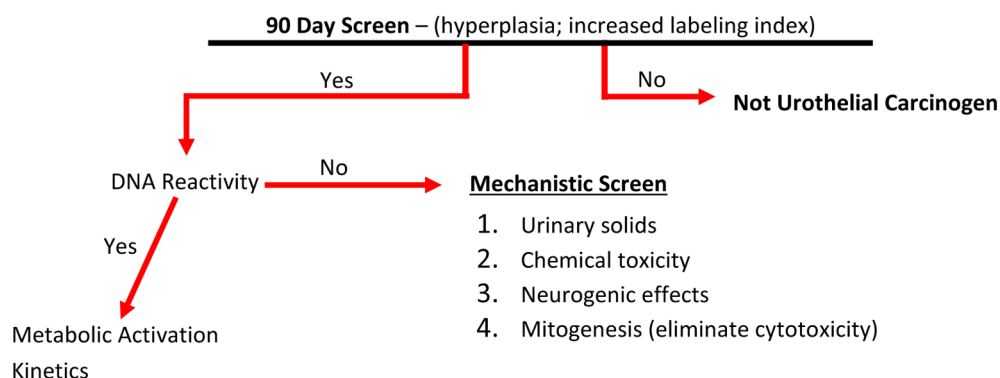
Fig. 2. Proposed sequence of evaluation to screen for potential urothelial carcinogens. The initial screen involves evaluation for hyperplasia or increased labeling index for cell proliferation. If positive, DNA reactivity is evaluated. If that is positive, evaluation for metabolism in humans is assessed. If not DNA reactive, evaluation of the urothelium by light microscopy and possibly scanning electron microscopy is performed. If cytotoxicity, an evaluation of urine for solids is performed along with an assessment of potential cytotoxicity of the chemical and metabolites and corresponding urinary concentrations after administration of carcinogenic dose. If no cytotoxicity, mitogenic activity is presumed.

are long standing calculi in these individuals, there is also bacterial infection. Bacterial cystitis is a known risk factor for the development of bladder tumors, so it is unlikely that the calculi pose any additional risk.

An example of chemically induced urinary bladder cytotoxicity is provided by the natural substance pulegone[76]. Pulegone produced a slightly increased risk of bladder tumors in female rats in the NTP two year bioassay. In short term studies, it produced an increase in hyperplasia and labeling index, due to cytotoxicity of the urothelium with regenerative proliferation. There is no formation of urinary solids, so the toxicity must be produced by the chemical and/or one of its metabolites. The metabolism of pulegone is well-known, and the major urinary metabolites are piperitone and piperitenone. The hepatotoxic metabolite menthofuran also is excreted in the urine but only to a limited extent. By evaluating the urinary concentration of metabolites of the animals administered pulegone and comparing that to the IC50s of the chemicals determined in *in vitro* investigations with urothelial cell lines, it was shown (Table 3) that piperitenone is likely the major contributor to the cytotoxicity, although piperitone and pulegone itself may also contribute to the cytotoxicity. Menthofuran was present at too low of

a concentration to produce cytotoxicity, and menthone was not detected in the urine. The mode of action for pulegone-induced urothelial tumors includes metabolism of pulegone, with excretion and concentration of the metabolites in the urine, which produce urothelial cytotoxicity, consequent regenerative proliferation, and ultimately a low incidence of urothelial tumors. Similar to chloroform for liver and kidney, the dose response requires sufficient chemical to be administered to produce a concentration of metabolites in the urine that will produce cytotoxicity. This does not occur in humans, since the exposure required to produce urinary levels of cytotoxic metabolites are substantially higher than what humans could tolerate.

Similar to what was described above for the liver, a process could be outlined for evaluating the mode of action and potential relevance of rodent bladder carcinogens to humans (Fig. 2). To begin with, the 90 day screen would involve detection of increased proliferation by routine analysis of hematoxylin and eosin stained slides and by the use of a more sensitive proliferation marker such as BrdU, Ki-67, or PCNA labeling index. Similar to the liver, if one of these markers is not present in the 90 day study, there will be no development of bladder tumors in the two year bioassay. If

one of these markers is positive, an investigation of the mode of action and dose response can be performed. The modes of action for urinary bladder carcinogens are listed in Table 2 and include those known for urinary bladder carcinogenesis in humans. Evaluations that can be used to investigate the mode of action and human relevance are urinalysis for solids, culture for infection, and light and scanning electron microscopy for evidence of cytotoxicity. There is clear evidence for DNA reactive carcinogenesis, such as by aromatic amines, and cytotoxicity with consequent regenerative proliferation induced carcinogenesis, such as by Schistosomiasis or inorganic arsenic, as being relevant in humans[68, 69]. Whether or not direct mitogenesis occurs in the bladder is yet to be demonstrated, although nicotine is a possibility in both rodents and humans[77].

Short Term Screen for Carcinogenic Potential

Although a detailed description of the process for the liver and urinary bladder is presented, a similar process could be performed for other tissues[1, 5]. However, other types of screening assays may be required for evaluations in other tissues. Most importantly, it is critical to remember that the primary purpose of the 90 day study is not to evaluate carcinogenesis, it is to evaluate potential toxicity, irrespective of the potential for carcinogenicity.

For some tissues, the rodent model can be a reasonable surrogate for potential toxicity and carcinogenicity in humans, such as for the liver and urinary bladder, and also for the kidney, glandular stomach and large intestine. However, there are several tissues in rodents that are not predictive of carcinogenicity in humans[1, 5]. There are tissues present in rodents that do not occur in humans, including Zymbal's gland, the Harderian gland, and forestomach. Evaluation of these tissues for potential carcinogenicity is irrelevant to humans. Other tissues can show evidence of toxicity, but are not predictive of carcinogenicity in humans. These include the endocrine organs (thyroid, adrenal cortex, adrenal medulla, anterior pituitary, posterior pituitary, parathyroid, gastrointestinal endocrine cells, pancreatic islet cells) and also the different organs sensitive to endocrine stimulation (ovary, testes, endometrium, prostate). Detection of toxicity in these tissues is readily apparent in the 90 day study based on histopathology, and if there are specific concerns, detailed biochemical evaluations can be performed. Nevertheless, these will not provide information regarding potential risk to humans regarding carcinogenesis.

Based on the above discussion, an overall proposal for utilizing the 90 day screening assay for evaluating carcinogenic risk to humans in illustrated in Fig. 3[1, 5]. If a substance is DNA reactive, then evaluation of the metabolism in humans and potential for forming DNA adducts can be readily evaluated. If DNA adduct formation does occur, one must presume that the substance is going to be carcinogenic in humans. If the substance is not DNA reactive, the next step in the process is to evaluate the substance for immunosuppressive activity and estrogenic activity. This can
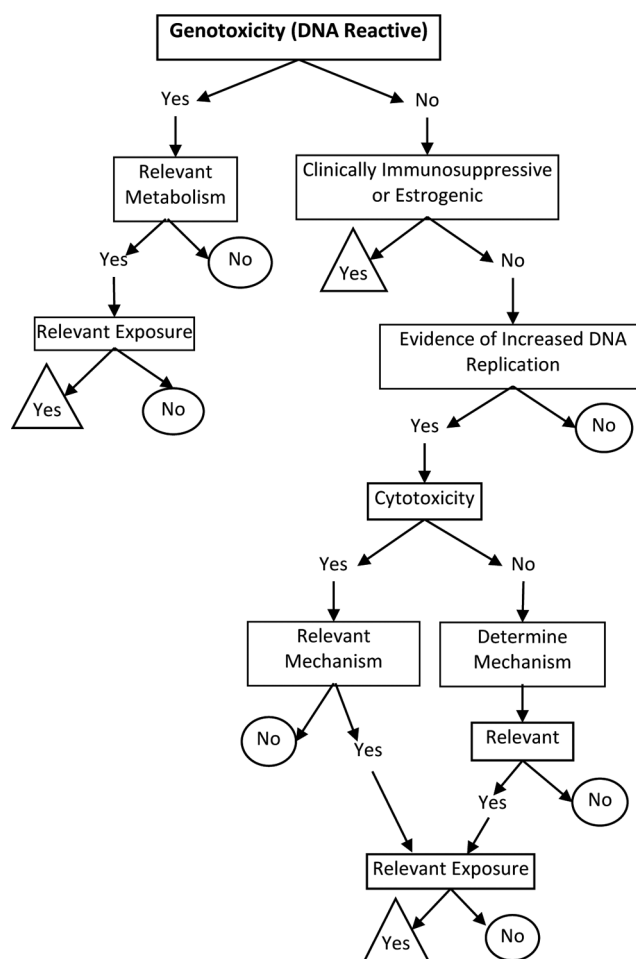

Fig. 3. A proposed guide for evaluating the potential carcinogenicity of chemicals. Each box poses an evaluation to be performed. If the sequence results ultimately in a No that is in a circle, there is no (or negligible) carcinogenic risk in humans. If the sequence results ultimately in a Yes that is in a triangle, it poses a presumptive human carcinogenic risk. From Cohen, SM, Toxicol Sci, 80: 225–229, 2004[1], with permission from Toxicological Sciences.

be readily incorporated into the 90 day bioassay utilizing various receptor assays and immunologic assays. If the substance has either immunosuppressive or estrogenic activity, potential human carcinogenic risk must be assumed, and a dose response and a specific risk assessment will need to be performed with regard to cancer risk. Benefit and risk needs to be weighed, such as in the use of pharmaceuticals for specific disease treatments. If the substance is not DNA reactive, not immunosuppressive, and does not have estrogenic activity that will produce a biologic response *in vivo* at exposure levels for humans, the next step in the process is evaluation of the potential for inducing a proliferative response in the various tissues. Screens for this can be developed for all of the tissues that need to be evaluated, taking into consideration the various discussions above. If the substance shows no evidence of producing an increased proliferative response in any tissue in the 90 day study, it can be

presumed that the substance does not carry a cancer risk for humans. If the substance does produce a proliferative response, evaluation of the mode of action for producing this response and evaluation of the dose response are then investigated to determine human relevance of the mode of action and the dose. Based on these evaluations, one can develop a strong, rationally based risk assessment for the potential of development of cancer in humans, without any need for performing a two year bioassay. In the next several years, various molecular analyses are likely to be developed that can aid in this screening process and in identifying mode of action[78–85]. These could supplement or replace current procedures.

Role of Toxicologic Pathology

As is evident in the above discussion, there is a critical role for toxicologic pathology in these assessments, both with respect to identifying potential toxicities and identifying potential carcinogenic risk. The toxicologic pathologist is involved not only with an evaluation for overall toxicity, but with an evaluation of potential immunologic and endocrine effects and the proliferative effects that are expected for a potential carcinogen. The pathologist would obviously be involved in the detailed investigations into dose response and mode of action analysis. Utilization of routine histopathology is only one part of the overall assessment that can be provided by the toxicologic pathologist. In addition, there are a wide variety of tools available that can be utilized to investigate mode of action, such as immunohistochemistry and molecular analyses. Collaboration with other investigators with expertise in biochemistry, metabolism, and molecular biology is essential. In addition, a pathologist is required for active participation in the design of studies and for selection of tissues to be utilized for these additional investigations.

A toxicologic pathologist also should be actively involved in basic research investigations. During the past two decades there has been an explosion of development of a variety of knock-out and knock-in animal models for investigation of various basic biologic mechanisms and toxicologic investigations. It is critical that pathologists be involved in the evaluation of the phenotype of these models, since individuals without that expertise can frequently misinterpret the morphologic findings. Examples of such misinterpretations are rampant in the literature. As an example, in an investigation to evaluate the potential for troglitazone to produce intestinal tumors in mice, the investigators interpreted the lesions as invasive intestinal adenocarcinomas. However, careful evaluation of the photographs provided in the publication clearly demonstrated that the lesions were actually ulcers with regenerative proliferation, not malignancies[86]. We implore pathologists to become more actively involved in these basic investigations in addition to their role in overall toxicology programs.

In summary, the toxicologic pathologist is critical for the evaluation of potential carcinogenicity and overall toxicity of chemicals. This involves performance of short term assays (≤ 90 days) for toxicity and also provides information for the potential for carcinogenicity. The pathologist needs to be involved with mechanistic evaluation of the toxic endpoints to determine the human relevance and the possible dose response if mode of action for the substance's toxicity is relevant to humans. The pathologist is critical for the evaluation of potential toxicity. In addition, evaluation for the rates of apoptosis and cell proliferation utilizing immunohistochemical assays are particularly useful for both screening purposes and for assessment of mode of action. The pathologist is critical for the selection of specific tissues for molecular analyses, and is the individual best trained for the utilization of immunohistochemical and *in situ* hybridization markers and for the evaluation of these markers in tissues. Identifying the specific cell types involved is essential. In addition, the pathologist should be involved in the selection of tissues for molecular analyses including microdissection.

Toxicologic pathology has continued to expand its armamentarium of tools that are available for investigations in rodents, but also for the important scientific basis for eventually determining the relevance of the mode of action to humans and a detailed dose response.

Disclosure of Potential Conflict of Interest: None

References

1. Cohen SM. Human carcinogenic risk evaluation: an alternative approach to the two-year rodent bioassay. Toxicol Sci. **80**: 225–229. 2004. [Medline] [CrossRef]
2. Cohen SM. Calcium phosphate-containing urinary precipitate in rat urinary bladder carcinogenesis. IARC Sci Publ. **147**: 175–189. 1999. [Medline]
3. IARC Consensus Report. International Agency for Research on Cancer. IARC Scientific Publications. **147**: 1–32. 1999.
4. Williams GM, and Iatropoulos MJ. Evaluation of potential human carcinogenicity of the synthetic monomer ethyl acrylate. Regul Toxicol Pharmacol. **53**: 6–15. 2009. [Medline] [CrossRef]
5. Cohen SM. Evaluation of possible carcinogenic risk to humans based on liver tumors in rodent assays: the two-year bioassay is no longer necessary. Toxicol Pathol. **38**: 487–501. 2010. [Medline] [CrossRef]
6. Box GEP. Science and Statistics. J Am Stat Assoc. **71**: 791–799. 1976. [CrossRef]
7. Sonich-Mullin C, Fielder R, Wiltse J, Baetcke K, Dempsey J, Fenner-Crisp P, Grant D, Hartley M, Knaap A, Kroese D, Mangelsdorf I, Meek E, Rice JM, and Younes M. International Programme on Chemical Safety IPCS conceptual framework for evaluating a mode of action for chemical carcinogenesis. Regul Toxicol Pharmacol. **34**: 146–152. 2001. [Medline] [CrossRef]
8. Cohen SM, Klaunig J, Meek ME, Hill RN, Pastoor T, Lehman-McKeeman L, Bucher J, Longfellow DG, Seed J, Dellarco V, Fenner-Crisp P, and Patton D. Evaluating the human relevance of chemically induced animal tumors.

Toxicol Sci. **78**: 181–186. 2004. [Medline] [CrossRef]

9. Meek ME, Bucher JR, Cohen SM, Dellarco V, Hill RN, Lehman-McKeeman LD, Longfellow DG, Pastoor T, Seed J, and Patton DE. A framework for human relevance analysis of information on carcinogenic modes of action. Crit Rev Toxicol. **33**: 591–653. 2003. [Medline] [CrossRef]

10. Seed J, Carney EW, Corley RA, Crofton KM, DeSesso JM, Foster PM, Kavlock R, Kimmel G, Klaunig J, Meek ME, Preston RJ, Slikker W Jr, Tabacova S, Williams GM, Wiltse J, Zoeller RT, Fenner-Crisp P, and Patton DE. Overview: Using mode of action and life stage information to evaluate the human relevance of animal toxicity data. Crit Rev Toxicol. **35**: 663–672. 2005. [Medline] [CrossRef]

11. Boobis AR, Cohen SM, Dellarco V, McGregor D, Meek ME, Vickers C, Willcocks D, and Farland W. IPCS framework for analyzing the relevance of a cancer mode of action for humans. Crit Rev Toxicol. **36**: 781–792. 2006. [Medline] [CrossRef]

12. Boobis AR, Doe JE, Heinrich-Hirsch B, Meek ME, Munn S, Ruchirawat M, Schlatter J, Seed J, and Vickers C. IPCS framework for analyzing the relevance of a noncancer mode of action for humans. Crit Rev Toxicol. **38**: 87–96. 2008. [Medline] [CrossRef]

13. Meek ME, Boobis A, Cote I, Dellarco V, Fotakis G, Munn S, Seed J, and Vickers C. New developments in the evolution and application of the WHO/IPCS framework on mode of action/species concordance analysis. J Appl Toxicol. **34**: 1–18. 2014. [Medline] [CrossRef]

14. Pastoor TP, Bachman AN, Bell DR, Cohen SM, Dellarco M, Dewhurst IC, Doe JE, Doerrer NG, Embry MR, Hines RN, Moretto A, Phillips RD, Rowlands JC, Tanir JY, Wolf DC, and Boobis ARA. A 21st century roadmap for human health risk assessment. Crit Rev Toxicol. **44**(Suppl 3): 1–5. 2014. [Medline] [CrossRef]

15. Embry MR, Bachman AN, Bell DR, Boobis AR, Cohen SM, Dellarco M, Dewhurst IC, Doerrer NG, Hines RN, Moretto A, Pastoor TP, Phillips RD, Rowlands JC, Tanir JY, Wolf DC, and Doe JE. Risk assessment in the 21st century: roadmap and matrix. Crit Rev Toxicol. **44**(Suppl 3): 6–16. 2014. [Medline] [CrossRef]

16. Simon TW, Simons SS Jr, Preston RJ, Boobis AR, Cohen SM, Doerrer NG, Fenner-Crisp PA, McMullin TS, McQueen CA, Rowlands JC. RISK21 Dose-Response Subteam The use of mode of action information in risk assessment: quantitative key events/dose-response framework for modeling the dose-response for key events. Crit Rev Toxicol. **44**(Suppl 3): 17–43. 2014. [Medline] [CrossRef]

17. Cohen SM, and Ellwein LB. Cell proliferation in carcinogenesis. Science. **249**: 1007–1011. 1990. [Medline] [CrossRef]

18. Cohen SM, and Ellwein LB. Genetic errors, cell proliferation, and carcinogenesis. Cancer Res. **51**: 6493–6505. 1991. [Medline]

19. Cohen SM. Cell proliferation and carcinogenesis. Drug Metab Rev. **30**: 339–357. 1998. [Medline] [CrossRef]

20. Cohen SM, Purtilo DT, and Ellwein LB. Ideas in pathology. Pivotal role of increased cell proliferation in human carcinogenesis. Mod Pathol. **4**: 371–382. 1991. [Medline]

21. Cohen SM, and Ellwein LB. Proliferative and genotoxic cellular effects in 2-acetylaminofluorene bladder and liver carcinogenesis: biological modeling of the ED01 study. Toxicol Appl Pharmacol. **104**: 79–93. 1990. [Medline] [CrossRef]

22. Murasaki G, and Cohen SM. Co-carcinogenicity of sodium saccharin and N-[4-(5-nitro-2-furyl)-2-thiazolyl]formamide for the urinary bladder. Carcinogenesis. **4**: 97–99. 1983. [Medline] [CrossRef]

23. Cohen SM, and Arnold LL. Chemical carcinogenesis. Toxicol Sci. **120**(Suppl 1): S76–S92. 2011. [Medline] [CrossRef]

24. Kirkland DJ, Aardema M, Banduhn N, Carmichael P, Fautz R, Meunier JR, and Pfuhler S. In vitro approaches to develop weight of evidence (WoE) and mode of action (MoA) discussions with positive in vitro genotoxicity results. Mutagenesis. **22**: 161–175. 2007. [Medline] [CrossRef]

25. Kirkland D, Aardema M, Henderson L, and Müller L. Evaluation of the ability of a battery of three in vitro genotoxicity tests to discriminate rodent carcinogens and non-carcinogens I. Sensitivity, specificity and relative predictivity. Mutat Res. **584**: 1–256. 2005. [Medline] [CrossRef]

26. Kirkland D, Aardema M, Müller L, and Makoto H. Evaluation of the ability of a battery of three in vitro genotoxicity tests to discriminate rodent carcinogens and non-carcinogens II. Further analysis of mammalian cell results, relative predictivity and tumour profiles. Mutat Res. **608**: 29–42. 2006. [Medline] [CrossRef]

27. Kirkland DJ, and Müller L. Interpretation of the biological relevance of genotoxicity test results: the importance of thresholds. Mutat Res. **464**: 137–147. 2000. [Medline] [CrossRef]

28. Kirkland D, Pfuhler S, Tweats D, Aardema M, Corvi R, Darroudi F, Elhajouji A, Glatt H, Hastwell P, Hayashi M, Kasper P, Kirchner S, Lynch A, Marzin D, Maurici D, Meunier JR, Müller L, Nohynek G, Parry J, Parry E, Thybaud V, Tice R, van Benthem J, Vanparys P, and White P. How to reduce false positive results when undertaking in vitro genotoxicity testing and thus avoid unnecessary follow-up animal tests: Report of an ECVAM Workshop. Mutat Res. **628**: 31–55. 2007. [Medline] [CrossRef]

29. McKinney JD, Richard A, Waller C, Newman MC, and Gerberick F. The practice of structure activity relationships (SAR) in toxicology. Toxicol Sci. **56**: 8–17. 2000. [Medline] [CrossRef]

30. Rosenkranz, HS, Zhang, YP, Klopman, G. Studies on the potential for genotoxic carcinogenicity of fragrances and other chemicals. Food Chem Toxicol. **36**: 687–696. 1998. [Medline] [CrossRef]

31. Thybaud V, Aardema M, Clements J, Dearfield K, Galloway S, Hayashi M, Jacobson-Kram D, Kirkland D, MacGregor JT, Marzin D, Ohyama W, Schuler M, Suzuki H, and Zeiger E. Expert Working Group on Hazard Identification and Risk Assessment in Relation to In Vitro Testing Strategy for genotoxicity testing: hazard identification and risk assessment in relation to in vitro testing. Mutat Res. **627**: 41–58. 2007. [Medline] [CrossRef]

32. Zeiger E. History and rationale of genetic toxicity testing: an impersonal, and sometimes personal, view. Environ Mol Mutagen. **44**: 363–371. 2004. [Medline] [CrossRef]

33. Zeiger E, Ashby J, Bakale G, Enslein K, Klopman G, and Rosenkranz HS. Prediction of Salmonella mutagenicity. Mutagenesis. **11**: 471–484. 1996. [Medline] [CrossRef]

34. Kaminski NE, Kaplan BLF, and Holsapple MP. Toxic responses of the immune system. In: Klaassen, CD, Casarett and Doull's Toxicology, 7th ed. McGraw Hill, New York. 485–556. 2008.

35. Penn I. Post-transplant malignancy: the role of immunosup-

pression. Drug Saf. **23**: 101–113. 2000. [Medline] [Cross-Ref]

36. Preston-Martin S, Pike MC, Ross RK, Jones PA, and Henderson BE. Increased cell division as a cause of human cancer. Cancer Res. **50**: 7415–7421. 1990. [Medline]

37. IARC Hormonal contraception and post-menopausal hormonal therapy. In IARC Monographs, vol. 72, Cancers of the Liver and Gallbladder, IARC Press, Lyon. 168–180. 1999.

38. Holsapple MP, Pitot HC, Cohen SM, Boobis AR, Klaunig JE, Pastoor T, Dellarco VL, and Dragan YP. Mode of action in relevance of rodent liver tumors to human cancer risk. Toxicol Sci. **89**: 51–56. 2006. [Medline] [CrossRef]

39. Goodman ZD, and Terraccian LM. Tumours and tumour-like lesions of the liver. In: Pathology of the Liver, (Burt AD, Partmann B, and Ferrell LD (eds). Churchill Livingston, Edinburgh, London. 761–814. 2007.

40. Kowdley KV. Iron, hemochromatosis, and hepatocellular carcinoma. Gastroenterology. **127**(Suppl 1): S79–S86. 2004. [Medline] [CrossRef]

41. Andersen M, Brusick D, Cohen S, Dragan Y, Frederick C, Goodman JI, Hard G, Meek B, and O'Flaherty EJUS. U.S. Environmental Protection Agency's revised cancer guidelines for carcinogen risk assessment. Toxicol Appl Pharmacol. **153**: 133–136. 1998. [Medline] [CrossRef]

42. Andersen ME, Meek ME, Boorman GA, Brusick DJ, Cohen SM, Dragan YP, Frederick CB, Goodman JI, Hard GC, O'Flaherty EJ, and Robinson DE. Lessons learned in applying the U.S. EPA proposed cancer guidelines to specific compounds. Toxicol Sci. **53**: 159–172. 2000. [Medline] [CrossRef]

43. Eldridge SR, Tilbury LF, Goldsworthy TL, and Butterworth BE. Measurement of chemically induced cell proliferation in rodent liver and kidney: a comparison of 5-bromo-2′-deoxyuridine and [3H]thymidine administered by injection or osmotic pump. Carcinogenesis. **11**: 2245–2251. 1990. [Medline] [CrossRef]

44. Gratzner HG. Monoclonal antibody to 5-bromo- and 5-iododeoxyuridine: A new reagent for detection of DNA replication. Science. **218**: 474–475. 1982. [Medline] [CrossRef]

45. Dietrich DR. Toxicological and pathological applications of proliferating cell nuclear antigen (PCNA), a novel endogenous marker for cell proliferation. Crit Rev Toxicol. **23**: 77–109. 1993. [Medline] [CrossRef]

46. Scholzen T, and Gerdes J. The Ki-67 protein: from the known and the unknown. J Cell Physiol. **182**: 311–322. 2000. [Medline] [CrossRef]

47. Nolte T, Kaufmann W, Schorsch F, Soames T, and Weber E. Standardized assessment of cell proliferation: the approach of the RITA-CEPA working group. Exp Toxicol Pathol. **57**: 91–103. 2005. [Medline] [CrossRef]

48. Wood CE, Hukkanen RR, Sura R, Jacobson-Kram D, Nolte T, Odin M, and Cohen SM. Scientific and Regulatory Policy Committee (SRPC) Review: Interpretation and Use of Cell Proliferation Data in Cancer Risk Assessment. Toxicol Pathol. **43**: 760–775. 2015. [Medline] [CrossRef]

49. Whysner J, Ross PM, and Williams GM. Phenobarbital mechanistic data and risk assessment: enzyme induction, enhanced cell proliferation, and tumor promotion. Pharmacol Ther. **71**: 153–191. 1996. [Medline] [CrossRef]

50. Yamada T, Uwagawa S, Okuno Y, Cohen SM, and Kaneko H. Case study: an evaluation of the human relevance of the synthetic pyrethroid metofluthrin-induced liver tumors in rats based on mode of action. Toxicol Sci. **108**: 59–68. 2009. [Medline] [CrossRef]

51. Lambert CB, Spire C, Claude N, and Guillouzo A. Dose- and time-dependent effects of phenobarbital on gene expression profiling in human hepatoma HepaRG cells. Toxicol Appl Pharmacol. **234**: 345–360. 2009. [Medline] [CrossRef]

52. Moore JT, Moore LB, Maglich JM, and Kliewer SA. Functional and structural comparison of PXR and CAR. Biochem Biophys Acta. **1619**, 235–238. 2003.

53. Elcombe CR, Peffer RC, Wolf DC, Bailey J, Bars R, Bell D, Cattley RC, Ferguson SS, Geter D, Goetz A, Goodman JI, Hester S, Jacobs A, Omiecinski CJ, Schoeny R, Xie W, and Lake BG. Mode of action and human relevance analysis for nuclear receptor-mediated liver toxicity: A case study with phenobarbital as a model constitutive androstane receptor (CAR) activator. Crit Rev Toxicol. **44**: 64–82. 2014. [Medline] [CrossRef]

54. Wei P, Zhang J, Egan-Hafley M, Liang S, and Moore DD. The nuclear receptor CAR mediates specific xenobiotic induction of drug metabolism. Nature. **407**: 920–923. 2000.

55. Lake BG. Species differences in the hepatic effects of inducers of CYP2B and CYP4A subfamily forms: relationship to rodent liver tumour formation. Xenobiotica. **39**: 582–596. 2009. [Medline] [CrossRef]

56. Yamada T, Okuda Y, Kushida M, Sumida K, Takeuchi H, Nagahori H, Fukuda T, Lake BG, Cohen SM, and Kawamura S. Human hepatocytes support the hypertrophic but not the hyperplastic response to the murine nongenotoxic hepatocarcinogen sodium phenobarbital in an in vivo study using a chimeric mouse with humanized liver. Toxicol Sci. **142**: 137–157. 2014. [Medline] [CrossRef]

57. Lamminpää A, Pukkala E, Teppo L, and Neuvonen PJ. Cancer incidence among patients using antiepileptic drugs: a long-term follow-up of 28,000 patients. Eur J Clin Pharmacol. **58**: 137–141. 2002. [Medline] [CrossRef]

58. IARC Phenobarbital and its sodium salt. In IARC Monographs, vol. 79, Somne Thyrotropic Agents, pp. 161–288. IARC Press, Lyon, France. 2001.

59. MacDonald JS, Gerson RJ, Kornbrust DJ, Kloss MW, Prahalada S, Berry PH, Alberts AW, and Bokelman DL. Preclinical evaluation of lovastatin. Am J Cardiol. **62**: 16J–27J. 1988. [Medline] [CrossRef]

60. MacDonald JS, and Halleck MM. The toxicology of HMG-CoA reductase inhibitors: prediction of human risk. Toxicol Pathol. **32**(Suppl 2): 26–41. 2004. [Medline] [CrossRef]

61. Bonovas S, Filioussi K, Tsavaris N, and Sitaras NM. Statins and cancer risk: a literature-based meta-analysis and meta-regression analysis of 35 randomized controlled trials. J Clin Oncol. **24**: 4808–4817. 2006. [Medline] [CrossRef]

62. Browning DR, and Martin RM. Statins and risk of cancer: a systematic review and metaanalysis. Int J Cancer. **120**: 833–843. 2007. [Medline] [CrossRef]

63. Dale KM, Coleman CI, Henyan NN, Kluger J, and White CM. Statins and cancer risk: a meta-analysis. JAMA. **295**: 74–80. 2006. [Medline] [CrossRef]

64. Farwell WR, Scranton RE, Lawler EV, Lew RA, Brophy MT, Fiore LD, and Gaziano JM. The association between statins and cancer incidence in a veterans population. J Natl Cancer Inst. **100**: 134–139. 2008. [Medline] [CrossRef]

65. Slater EE, and MacDonald JS. Mechanism of action and biological profile of HMG CoA reductase inhibitors. A new

therapeutic alternative. Drugs. **36**(Suppl 3): 72–82. 1988. [Medline] [CrossRef]

66. Allen DG, Pearse G, Haseman JK, and Maronpot RR. Prediction of rodent carcinogenesis: an evaluation of pre-chronic liver lesions as forecasters of liver tumors in NTP carcinogenicity studies. Toxicol Pathol. **32**: 393–401. 2004. [Medline] [CrossRef]

67. Cohen SM. Urinary bladder carcinogenesis. Toxicol Pathol. **26**: 121–127. 1998. [Medline] [CrossRef]

68. Cohen SM, and Johansson SL. Epidemiology and Etiology of Bladder Cancer. Philadelphia, W.B.Saunders Co.: 421–428. 1992.

69. Cohen SM, Shirai T, and Steineck G. Epidemiology and etiology of premalignant and malignant urothelial changes. Scand J Urol Nephrol Suppl. **34**: 105–115. 2000. [Medline] [CrossRef]

70. Cohen SM, Arnold LL, Beck BD, Lewis AS, and Eldan M. Evaluation of the carcinogenicity of inorganic arsenic. Crit Rev Toxicol. **43**: 711–752. 2013. [Medline] [CrossRef]

71. IARC Saccharin and its salts. IARC Monogr Eval Carcinog Risks Hum. **73**: 517–624. 1999. [Medline]

72. Cohen S, Arnold L, and Emerson J. Safety of saccharin. Agro Food Ind Hi-Tech. **19**: 26–29. 2008.

73. Cohen SM, Johansson SL, Arnold LL, and Lawson TA. Urinary tract calculi and thresholds in carcinogenesis. Food Chem Toxicol. **40**: 793–799. 2002. [Medline] [CrossRef]

74. Hsieh DP, Chiang CF, Chiang PH, and Wen CP. Toxicological analysis points to a lower tolerable daily intake of melamine in food. Regul Toxicol Pharmacol. **55**: 13–16. 2009. [Medline] [CrossRef]

75. Xin H, and Stone R. Tainted milk scandal. Chinese probe unmasks high-tech adulteration with melamine. Science. **322**: 1310–1311. 2008. [Medline] [CrossRef]

76. Da Rocha MS, Dodmane PR, Arnold LL, Pennington KL, Anwar MM, Adams BR, Taylor SV, Wermes C, Adams TB, and Cohen SM. Mode of action of pulegone on the urinary bladder of F344 rats. Toxicol Sci. **128**: 1–8. 2012. [Medline] [CrossRef]

77. Dodmane PR, Arnold LL, Pennington KL, and Cohen SM. Orally administered nicotine induces urothelial hyperplasia in rats and mice. Toxicology. **315**: 49–54. 2014. [Medline] [CrossRef]

78. Ellinger-Ziegelbauer H, Gmuender H, Bandenburg A, and Ahr HJ. Prediction of a carcinogenic potential of rat hepatocarcinogens using toxicogenomics analysis of short-term in vivo studies. Mutat Res. **637**: 23–39. 2008. [Medline] [CrossRef]

79. Ellinger-Ziegelbauer H, Stuart B, Wahle B, Bomann W, and Ahr HJ. Characteristic expression profiles induced by genotoxic carcinogens in rat liver. Toxicol Sci. **77**: 19–34. 2004. [Medline] [CrossRef]

80. Ellinger-Ziegelbauer H, Stuart B, Wahle B, Bomann W, and Ahr HJ. Comparison of the expression profiles induced by genotoxic and nongenotoxic carcinogens in rat liver. Mutat Res. **575**: 61–84. 2005. [Medline] [CrossRef]

81. Fielden MR, Brennan R, and Gollub J. A gene expression biomarker provides early prediction and mechanistic assessment of hepatic tumor induction by nongenotoxic chemicals. Toxicol Sci. **99**: 90–100. 2007. [Medline] [CrossRef]

82. Fielden MR, Nie A, McMillian M, Elangbam CS, Trela BA, Yang Y, Dunn RT 2nd, Dragan Y, Fransson-Stehen R, Bogdanffy M, Adams SP, Foster WR, Chen SJ, Rossi P, Kasper P, Jacobson-Kram D, Tatsuoka KS, Wier PJ, Gollub J, Halbert DN, Roter A, Young JK, Sina JF, Marlowe J, Martus HJ, Aubrecht J, Olaharski AJ, Roome N, Nioi P, Pardo I, Snyder R, Perry R, Lord P, Mattes W, and Car BD. Predictive Safety Testing Consortium Carcinogenicity Working Group Interlaboratory evaluation of genomic signatures for predicting carcinogenicity in the rat. Toxicol Sci. **103**: 28–34. 2008. [Medline] [CrossRef]

83. Knasmüller S, Mersch-Sundermann V, Kevekordes S, Darroudi F, Huber WW, Hoelzl C, Bichler J, and Majer BJ. Use of human-derived liver cell lines for the detection of environmental and dietary genotoxicants; current state of knowledge. Toxicology. **198**: 315–328. 2004. [Medline] [CrossRef]

84. Nie AY, McMillian M, Parker JB, Leone A, Bryant S, Yieh L, Bittner A, Nelson J, Carmen A, Wan J, and Lord PG. Predictive toxicogenomics approaches reveal underlying molecular mechanisms of nongenotoxic carcinogenicity. Mol Carcinog. **45**: 914–933. 2006. [Medline] [CrossRef]

85. Thomas RS, Pluta L, Yang L, and Halsey TA. Application of genomic biomarkers to predict increased lung tumor incidence in 2-year rodent cancer bioassays. Toxicol Sci. **97**: 55–64. 2007. [Medline] [CrossRef]

86. Yang K, Fan KH, Lamprecht SA, Edelmann W, Kopelovich L, Kucherlapati R, and Lipkin M. Peroxisome proliferator-activated receptor gamma agonist troglitazone induces colon tumors in normal C57BL/6J mice and enhances colonic carcinogenesis in Apc1638 N/+ Mlh1+/− double mutant mice. Int J Cancer. **116**: 495–499. 2005. [Medline] [CrossRef]

Original Article

Alteration of microRNA expressions in the pons and medulla in rats after 3,3′-iminodipropionitrile administration

Keiko Ogata[1, 2*], Masahiko Kushida[1], Kaori Miyata[1], Kayo Sumida[1], Shuji Takeda[1], Takeshi Izawa[2], Mitsuru Kuwamura[2], and Jyoji Yamate[2]

[1] Environmental Health Science Laboratory, Sumitomo Chemical Co., Ltd., Osaka 554-8558, Japan
[2] Laboratory of Veterinary Pathology, Division of Veterinary Sciences, Graduate School of Life and Environmental Sciences, Osaka Prefecture University, Osaka 598-8531, Japan

Abstract: Although 3,3′-iminodipropionitrile (IDPN) is widely used as a neurotoxicant to cause axonopathy due to accumulation of neurofilaments in several rodent models, its mechanism of neurotoxicity has not been fully understood. In particular, no information regarding microRNA (miRNA) alteration associated with IDPN is available. This study was conducted to reveal miRNA alteration related to IDPN-induced neurotoxicity. Rats were administered IDPN (20, 50, or 125 mg/kg/day) orally for 3, 7, and 14 days. Histopathological features were investigated using immunohistochemistry for neurofilaments and glial cells, and miRNA alterations were analyzed by microarray and reverse transcription polymerase chain reaction. Nervous symptoms such as ataxic gait and head bobbing were observed from Day 9 at 125 mg/kg. Axonal swelling due to accumulation of neurofilaments was observed especially in the pons, medulla, and spinal cord on Day 7 at 125 mg/kg and on Day 14 at 50 and 125 mg/kg. Furthermore, significant upregulation of miR-547* was observed in the pons and medulla in treated animals only on Day 14 at 125 mg/kg. This is the first report indicating that miR-547* is associated with IDPN-induced neurotoxicity, especially in an advanced stage of axonopathy. (DOI: 10.1293/tox.2016-0019; J Toxicol Pathol 2016; 29: 229–236)

Key words: 3,3′-iminodipropionitrile (IDPN), microRNA, axonal swelling, axonopathy, neurotoxicity

Introduction

3,3′-iminodipropionitrile (IDPN), an industrial intermediate, is known as a potent neurotoxicant. IDPN induces behavioral abnormalities in humans and experimental animals. The behavioral manifestation referred to as "waltzing syndrome," which includes circling, repetitive head movements, and hyperactivity, has been reported in IDPN-treated rodents[1–3]. The neurotoxic effects caused by IDPN include proximal axonal neuropathy in the nervous system characterized by accumulation of neurofilaments[4–7]. Although IDPN has been widely used in neurotoxic models, its mechanism for brain impairment has not been fully understood.

microRNAs (miRNAs) are small noncoding RNAs (−25 nucleotides) that play significant roles in regulating a diversity of cellular and biological processes, including growth, development, differentiation, proliferation, the cell cycle, and cell death[8–10]. Recently, it has been reported that exogenous chemicals can alter miRNA expression profiles in the nervous tissues in association with neurotoxicity[11–17]. However, alteration of miRNA expression caused by IDPN has not been reported. The aim of this work was to investigate miRNA expression alterations that contribute to IDPN-induced neurotoxicity. Using an IDPN-induced rat neurotoxicity model, we observed nervous symptoms and performed histopathological examinations including immunohistochemistry for neurofilaments and glial cells in addition to analysis of miRNA expression alterations in the pons and medulla, which are sites highly susceptible to IDPN, by microarray and RT-PCR (reverse transcription polymerase chain reaction).

Materials and Methods

All experiments were performed in accordance with the Guide for Animal Care and Use of Sumitomo Chemical Co., Ltd.

Animals and housing condition

Seventy-seven male Crl:CD(SD) rats (6 weeks old, specific pathogen free) were purchased from Charles River Laboratories Japan, Inc. (Shiga, Japan), and housed individ-

Table 1. Antibody and Staining Information for Immunohistochemistry

Antibody	Marker	Host	Clone	Dilution	Antigen retrieval	Company
NF 68	68 kDa neurofilament	Mouse	NR4	× 500	Microwave in tris-edta (ph9.0), 20 min	Sigma-Aldrich, St. Louis, MO, USA
Olig2	Oligodendrocyte	Rabbit	poly	× 500	Microwave in citrate buffer (ph6.0), 20 min	Immuno-Biological Laboratories, Gunma, Japan
GFAP	Astrocyte	Rabbit	poly	× 2,000	100 Mg/ml proteinase k, 10 min	Dako, Glostrup, Denmark
Iba1	Microglia	Rabbit	poly	× 500	Microwave in citrate buffer (ph6.0), 20 min	Wako Pure Chemical Industries, Osaka, Japan

ually in aluminum cages in a room kept at 24 ± 2°C and 40 to 70% relative humidity with a 12-hr light–dark cycle. Tap water via automatic stainless steel nozzles and CRF-1 pellet diet (Oriental Yeast Co., Ltd., Tokyo, Japan) were freely available.

Experimental design

After a one-week acclimation period, rats were divided into 4 groups (14 or 21 animals per group). Each group was given repeated administrations of distilled water as the vehicle or IDPN (>98% purity, Wako Pure Chemical Industries, Osaka, Japan) at 20, 50, or 125 mg/kg/day via oral gavage. Observation points were set as 3, 7, and 14 days after administration for each dose group (4, 6, or 7 animals per observation point). Clinical symptoms were observed daily. Examination of auditory response by checking animals' responses to auditory stimuli (metal clicker) and measurement of body weight were performed on Days 3, 7, and 14.

Tissue sampling

After observation periods, animals were anesthetized with isoflurane followed by exsanguination. The nervous tissues (brain, spinal cord, and sciatic nerve) were immediately collected. The brains were weighed and sagittally cut. The left half-brains were fixed in 4% paraformaldehyde phosphate buffer solution for histopathology. The right half-brains were regionally dissected, and the pons and medulla were frozen in liquid nitrogen and preserved at −80°C in a freezer for total RNA (including miRNA) extraction. Two rats from each group were perfused *in situ* (4% paraformaldehyde phosphate buffer solution) under deep anesthesia, and their nervous tissues were removed and immersed in the same solution for histopathology and immunohistochemistry.

Histopathology and immunohistochemistry

Fixed whole brains or half-brains were transversely cut at 4 levels (level 1, forebrain; level 2, center of the cerebrum, including the hippocampus; level 3, cerebellum and pons; level 4, medulla), and spinal cords (cervical, thoracic, and lumbar) and sciatic nerves were embedded in paraffin, sectioned, stained with hematoxylin and eosin (HE), and microscopically examined. Paraffin-embedded perfused brains from animals sacrificed on Day 14 were subjected to immunohistochemistry using anti-glial fibrillary acidic protein (GFAP), anti-ionized calcium-binding adapter mol-

ecule 1 (Iba1), anti-Olig2, and anti-neurofilament 68 (NF-68) antibodies. The staining conditions are listed in Table 1. After incubation with the primary antibodies, sections were treated with peroxidase-conjugated secondary antibody (Histofine Simple Stain MAX-PO, Nichirei, Tokyo, Japan). Signals were visualized with a DAB substrate kit (Nichirei).

miRNA microarray analysis

Total RNA extraction from the pons/medulla (Day 7, control and 125 mg/kg groups; Day 14, control, 50, and 125 mg/kg groups) was carried out in accordance with the protocol for a mirVana miRNA Isolation Kit (Life Technologies, Carlsbad, CA, USA). Each total RNA sample in the control and 125 mg/kg groups on Day 14 was subjected to miRNA microarray analysis using a Rat miRNA Microarray Kit (miRBase Rel.16.0, Agilent Technologies, Santa Clara, CA, USA). The procedure was conducted basically in accordance with the manufacturer's protocol (Version 2.0), and the Feature Extraction software (Version 10.7.3.1, Agilent Technologies) was used to generate a quantitative signal value and a qualitative detection call for each probe on the microarray. The 75th percentile was used for per-sample normalization. Analysis of miRNA-normalized expression data was performed using Welch's *t*-test (two-tailed) to obtain the miRNAs that were significantly altered in comparison with the expressions in control samples.

Real-Time RT-PCR

The levels of miRNA expression in the pons/medulla were analyzed by real-time RT-PCR. Reverse transcription and real-time PCR were performed with a TaqMan MicroRNA Reverse Transcription kit (Life Technologies) and TaqMan Universal PCR Master Mix (Life Technologies), and TaqMan MicroRNA Assays (Life Technologies), which include probes and primers, were used for all target miRNAs (miR-547* and miR-135a) and control miRNAs (U6 ncRNA for the pons/medulla) in accordance with the manufacturer's protocol. Real-time RT-PCR was performed using a PikoReal Real-Time PCR System (Thermo Scientific, Waltham, MA, USA). All reactions were run in duplicate. The data were calculated using the ΔΔCT method, and then fold changes compared with the control group were generated.

Target gene prediction for miR-547*

For prediction of the target genes for miR-547*, the TargetScan Human software (http://www.targetscan.org/)

Table 2. Effects of IDPN Treatment on Body Weights, Brain Weights, Nervous Symptoms, Auditory Response, and Histopathology

Dose (mg/kg)		20			50			125		
Day		3	7	14	3	7	14	3	7	14
No.		7	7	7	7	7	7	7	7	7
Body weight		-	↓2%	-	↓1%	↓1%	-	↓3%	▼10%	↓11%
Brain weight (absolute)		-	-	-	-	-	-	-	-	-
Nervous symptoms										
Ataxic gait		0	0	0	0	0	0	0	0	7[a]
Spasmodic gait		0	0	0	0	0	0	0	0	6[a]
Decreased locomotor activity		0	0	0	0	0	0	0	0	7[a]
Head bobbing		0	0	0	0	0	0	0	0	7[b]
Circling		0	0	0	0	0	0	0	0	6[b]
Auditory response										
Score 0 (normal response)		4	4	6	7	7	7	7	7	3
Score -1 (poor response)		0	0	0	0	0	0	0	0	3
Score -2 (no response)		0	0	0	0	0	0	0	0	1

Dose (mg/kg)		20			50			125		
Day		3	7	14	3	7	14	3	7	14
No.		7	7	7	7	7	7	7	7	7
Cerebellum										
Swelling, axon	±	0	0	0	0	0	0	0	0	4
Pons										
Swelling, axon	±	0	0	0	0	0	1	0	7	0
	+	0	0	0	0	0	0	0	0	7
Medulla oblongata										
Swelling, axon	±	0	0	0	0	0	1	0	7	0
	+	0	0	0	0	0	0	0	0	7
Spinal cord										
Swelling, axon	±	0	0	0	0	0	1	0	7	0
	+	0	0	0	0	0	0	0	0	7

☐ Changes related to IDPN administration. [a] Day 9–14. [b] Day 10–14. Percentage values indicate the percentage change compared with the control values (100%). Numbers indicate the numbers of animals showing each finding. Symbols: -, not changed; ▼, significantly lower than the control values; ↓, lower than the control values; ±, grade = slight; +, grade = mild

was used. The search term "Rno-miR-547-5p" was used to obtain target genes.

Statistical analysis

StatLight (Yukms Co., Ltd., Tokyo, Japan) was used to perform statistical analyses. To test for the homogeneity of variances among the groups, Bartlett's test was used to analyze data for body weight and brain weight for miRNA expression analysis (miR-547* expression on Day 14), and the F-test was used for miRNA expression analysis (miR-547* expression on Day 7 and miR-135a expression on Day 14). Depending on the results of Bartlett's test, parametric or nonparametric Dunnett's multiple comparison (two-tailed) was performed for the difference among the groups using the same software. Depending on the results of the F-test, Student's *t*-test or Aspin-Welch's *t*-test (two-tailed) was performed. Statistical significance was evaluated at $p<0.05$ and $p<0.01$.

Results

General condition, nervous symptoms, and auditory response

Effects of IDPN treatment on body weight and brain weight, nervous symptoms, and auditory response are shown in Table 2. In the IDPN 125 mg/kg group, body weight was significantly decreased on Day 7 and slightly decreased on Day 14. Absolute brain weight was not changed in any group. Nervous symptoms such as ataxic gait, head bobbing, circling, spasmodic gait, and decreased locomotor activity were observed in most animals at 125 mg/kg from Day 9. Decreased auditory response was observed in animals at 125 mg/kg on Day 14.

Histopathology and immunohistochemistry for NF-68, GFAP, Iba1, and Olig2

The results of histopathological examination are also shown in Table 2. Photographs of the pons are shown in Fig. 1 (HE and immunohistochemistry for NF-68) and Fig. 2 (immunohistochemistry for GFAP, Iba1, and Olig2). IDPN caused axonal swelling mainly in the pons, medulla, and spinal cord. These changes were slightly observed in
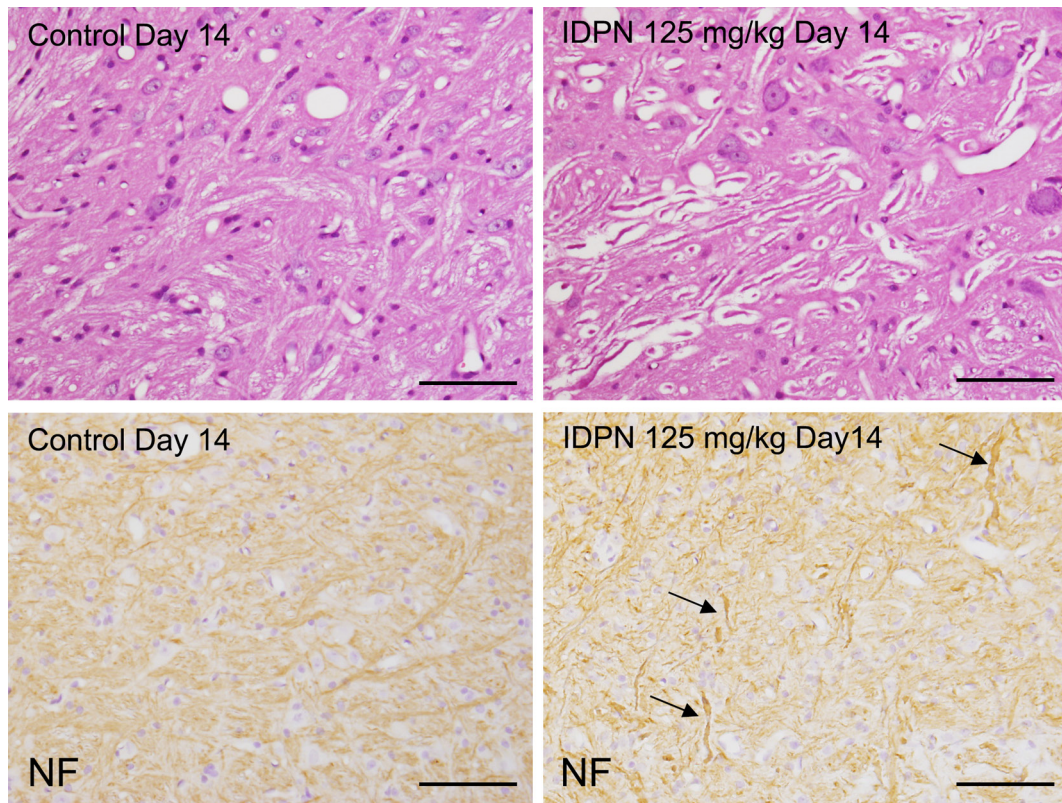
Fig. 1. Microphotographs of the pons in control rats and IDPN 125 mg/kg-treated rats on Day 14. Axonal swellings was noted in IDPN-treated rats. Swollen axons noted in IDPN-treated rats showed positive reactions for anti-neurofilament (NF) immunohistochemistry (arrows). HE, upper row; NF, lower row. Scale bars = 50 μm.
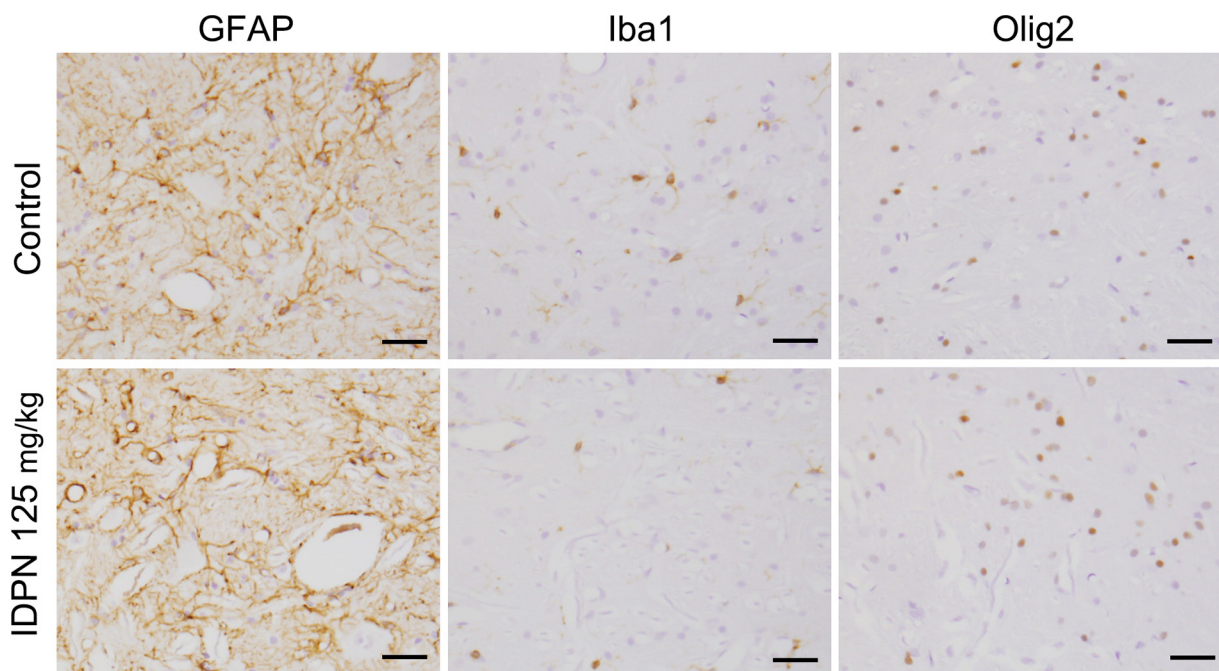

Fig. 2. Microphotographs of immunohistochemistry for GFAP, Iba1, and Olig2 of the pons in control and IDPN 125 mg/kg-treated rats on Day 14. There were no remarkable differences between control and treated rats for any stains. Scale bars = 20 μm.

Table 3. Up-regulated and Down-regulated miRNAs by Microarray Analysis

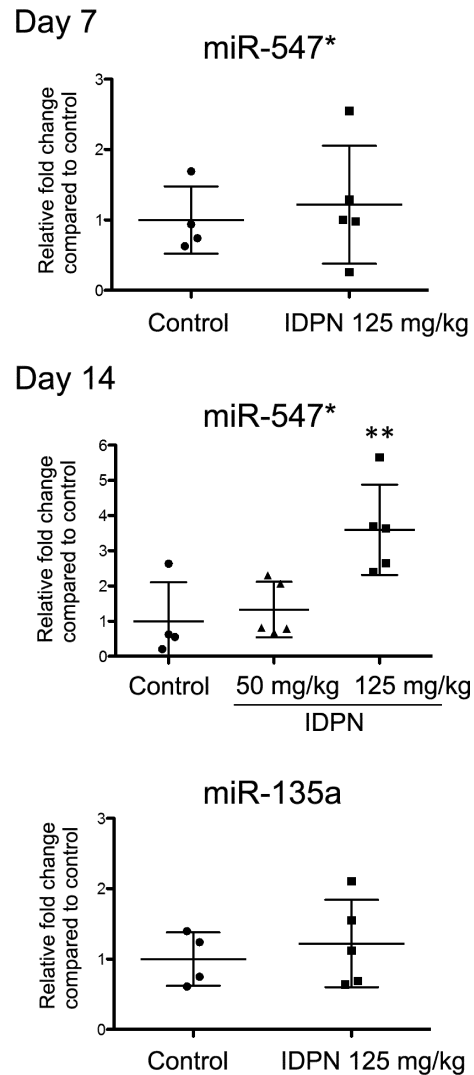| Up-regulated		Down-regulated	
miRNA	fold	miRNA	fold
rno-miR-547*	244.9	rno-let-7c-1*	0.0
rno-miR-3594-3p	135.7	rno-miR-190	0.1
rno-miR-668	117.0	rno-miR-29a*	0.1
rno-miR-487b*	116.7	rno-miR-384-3p	0.2
rno-miR-760-5p	51.3	rno-miR-32	0.3
rno-miR-3550	7.4	rno-let-7a-1*	0.3
rno-miR-540*	5.8	rno-miR-24-2*	0.3
rno-miR-1188-3p	5.4	rno-miR-135a	0.3
rno-let-7i*	5.3	rno-miR-496	0.3
rno-miR-504	5.2	rno-miR-494	0.4
rno-let-7b*	3.3	rno-miR-374	0.4
rno-miR-346	3.1	rno-miR-31*	0.4
rno-miR-207	2.9	rno-miR-126*	0.4
rno-miR-328b-3p	2.8	rno-miR-379*	0.4
rno-let-7d*	2.7	rno-miR-30b-5p	0.4
rno-miR-702-3p	2.7	rno-miR-450a	0.5
rno-miR-485*	2.6	rno-miR-222	0.5
rno-miR-764	2.5	rno-miR-350	0.5
rno-miR-3573-3p	2.5	rno-miR-142-3p	0.5
rno-miR-378*	2.5	rno-miR-365	0.5
rno-miR-466b-2*	2.3	rno-miR-22*	0.5
rno-miR-466c*	2.3		
rno-miR-483	2.3		
rno-miR-347	2.0		

Fig. 3. Real-time PCR analysis for miR-547* and miR-135a expressions in the pons/medulla. miRNA levels were expressed as relative fold changes compared with the control mean levels. Individual data were plotted as points, and mean ± SEM values were expressed as short and long bars. **Significantly different from the control at $p<0.01$ (Dunnett's multiple comparison).

all animals at 125 mg/kg on Day 7, and the severity was increased on Day 14. On Day 14, these findings were also slightly noted in one animal at 50 mg/kg. The same findings were also observed in the cerebellum in animals at 125 mg/kg on Day 14. The swelling of axons was especially noted in vestibular, trigeminal, and reticular formation nuclei of the pons and medulla, and in the ventral horn and funiculus of the spinal cord. No remarkable changes were noted in the other sites in the brain or sciatic nerve. Immunohistochemical stains revealed increased positive reaction for NF-68 in swollen axons, suggesting accumulation of neurofilaments in axons. There were no apparent differences between control and IDPN 125 mg/kg animals in immunoreactivity for glial cells (GFAP, Iba1, and Olig2).

Alterations of miRNA expression in the pons/medulla

Table 3 shows the results of microarray analysis of the pons/medulla. Significantly upregulated or downregulated miRNAs with a fold change of 2.0 or more and 0.5 or less, respectively, were observed. Twenty-four miRNAs were upregulated, and 21 miRNAs were downregulated. miR-547*, miR-3594-3p, miR-668, miR-487b*, and miR-760-5p were drastically upregulated, and let-7c-1*, miR-190, and miR-29a* were drastically downregulated, though expression levels of these miRNA were extremely low in the control animals. Downregulated miRNAs that ranked highly included miR-190, miR-135a, and miR-496, which have been reported to be altered in the nervous system[14, 18–23].

We focused on upregulation of miR-547*, which showed the highest fold change compared with control animals (224.9-fold), and downregulation of miR-135a (0.3-fold), alteration of which has been indicated by several reports in association with the nervous system[14, 18–20].

The results of RT-PCR analysis for miR-547* and miR-135a are shown in Fig. 3. miR-547* was significantly increased at IDPN 125 mg/kg on Day 14 (3.6-fold). The fold change in comparison with control animals was lower in RT-PCR than that in microarray analysis. There were no significant differences at 125 mg/kg on Day 7 or at 50 mg/kg on Day 14. Alteration of the miR-135a expression level was not confirmed by RT-PCR at 125 mg/kg on Day 14. The difference in the results between microarray and RT-PCR analysis was considered to be due to the difference in detection sensitivity. In target gene prediction analysis for miR-547*,

Table 4. Target Genes Having Nervous System-related Gene Ontology Predicted for miR-547* by TargetScan

Human ortholog of target gene	Gene name	Cumulative weighted context++ score	Gene Ontology (GO) associated with nervous system
SNAP23	synaptosomal-associated protein, 23kDa	−0.69	synaptosome, synapse neurotransmitter secretion, nervous system development, brain development, synaptic vesicle, axon, dendrite,
PPT1	palmitoyl-protein thioesterase 1	−0.46	neuronal cell body, negative regulation of neuron apoptosis, synapse, neuron development, regulation of synapse structure and activity
NTNG1	netrin G1	−0.33	nervous system development, axonogenesis

In the top 30 ranking genes ranked by cumulative weighted context++ score, SNAP23 and PPT1 were included. In addition, in the top 100 ranking genes, NTNG1 was included.

genes with nervous system-associated gene ontology, such as SNAP23 (synaptosomal-associated protein, 23 kDa), and PPT1 (palmitoyl-protein thioesterase 1), were found to be involved and to be within the top 30 ranking genes. Within the top 100 ranking genes, NTNG1 (netrin G1) was also included (Table 4).

Discussion

In this study, we revealed alteration of miRNA expressions in the pons/medulla in IDPN-treated rats. Significantly altered miRNAs in the pons/medulla in microarray analysis included drastically upregulated miR-547*, miR-3594-3p, miR-668, miR-487b*, and miR-760-5p and drastically downregulated let-7c-1*, miR-190, and miR-29a*. However, these miRNAs showed extremely low expression levels in the control animals. Therefore, the fold changes in these miRNAs need to be considered carefully. In downregulated miRNAs that ranked highly, nervous system-related alterations were previously reported for miR-190, miR-496, and miR-135a. In particular, nervous system-related alteration of miR-135a has been indicated in association with synaptic depression in spine remodeling, RDX-induced neurotoxicity, corticosteroid dependent stress response, cocaine-induced conditioned place preference, and tumorigenesis[14, 18–20].

In these altered miRNAs, we focused on upregulation of miR-547* and downregulation of miR-135a and performed RT-PCR analysis. Consequently, only upregulation of miR-547* was confirmed by RT-PCR. In the time-course and dose-response analysis, the expression level of miR-547* was only found to be significant at 125 mg/kg on Day 14, at which point nervous symptoms such as ataxic gait, head bobbing, circling, spasmodic gait, and decreased auditory response were most frequently observed, and the severity and incidence of axonal changes, mainly in the medulla, pons, and spinal cord, were increased. Slight axonal changes were also observed at a lower dose (50 mg/kg) on Day 14 and at an earlier time point (on Day 7) at 125 mg/kg; however, they were not accompanied by alteration of miR-547* expression levels. These results suggested that miR-547* is related to an advanced stage of IDPN-induced neurotoxicity rather than an onset phase.

Since little is known about the distribution in tissues and cells and function of miR-547* in any species, the role miR-547* plays in IDPN-induced neurotoxicity remains unclear. However, SNAP23, PPT1, and NTNG1, which are associated with functions of synapses and axons, were included among the potential target genes for miR-547* predicted by TargetScan. Of the three genes, SNAP23 was ranked highest. SNAP23 is a member of the SNAP family that is distributed in both non-neuronal tissues and neuronal tissues, and its roles in membrane trafficking have been indicated[24-34]. Regarding neuronal tissues, SNAP23 is distributed in hippocampal and cortical GABAergic neurons, in glutamatergic and GABAergic synapses of the mature cerebellar cortex, and in astrocytes. Its function in the brain is not fully understood, but it is considered an important protein in the exocytotic machinery in neuronal synapses and astrocytes[24–30]. In this study, there was no difference in SNAP23 mRNA levels in the pons/medulla between control and IDPN 125 mg/kg animals on Day 14 (data not shown). However, it remains unclear whether miR-547* regulates SNAP23 protein expression by translational repression. To clarify this question, analysis of SNAP23 at the protein level will be needed. Moreover, accumulation of neurofilaments was confirmed by immunohistochemistry in our study. Accumulation of neurofilaments has been reported to be caused by a deficit in slow axonal transport of neurofilament proteins[4, 35]. Further study is still needed to determine how miR-547* is involved in regulating synaptic and axonal function in association with axonal impairment caused by IDPN.

The nervous symptoms and histopathological changes in the present study are in general agreement with some reports on the features of IDPN-induced neurotoxicity[1, 3, 4, 6, 7, 36]. Abnormal behaviors and decreased auditory response might be associated with IDPN-induced vestibular and auditory hair cell injuries, as reported in some studies[2, 37–40], although the possibility that decreased auditory response might be caused by weakened condition in animals could not be ruled out. In contrast to our result, it has been reported that IDPN induced sciatic nerve degeneration after 28-day (at 100 mg/kg) or 5-week (at 125 mg/kg) oral administration[5, 7]. Since the observation period in our study was shorter than that of the reported studies, no sciatic nerve de-

generation was detected in the present study. Setting a longer administration period may promote progression of the pathological changes and lead to sciatic nerve degeneration. In addition, glial reactions were not apparent in this study. However, it has been reported that an increase in GFAP concentration in the pons/medulla, midbrain, cerebral cortex, and olfactory bulb was induced by IDPN treatment for 3 days at 400 mg/kg/day with a peak on Day 7 after administration[36, 41]. The differences in dose and period of administration and the difference in GFAP detection methods between this study (immunohistochemistry) and the previous studies (measurement of concentration) were suspected as contributing to the differing results for GFAP. The finding that no apparent glial reactions were seen in this study was considered to be supportive data indicating that miR-547* may regulate genes associated with axonal or synapse function rather than genes associated with other phenomena such as cell death and inflammation.

Regarding the other downregulated miRNAs in microarray in this study, miR-190 and miR-496 have also been reported to be downregulated in relation to the nervous system. *In vivo* and *in vitro* analyses indicates that miR-190 is associated with μ-opioid receptor agonists-modulated stability of dendritic spines via regulation of neurogenic differentiation 1 (NeuroD) activity[22]. miR-190 is also downregulated in the contused cortex after traumatic brain injury in mice[23]. Downregulation of miR-496 has been reported in microarray analysis using fetal mouse brains exposed to ethanol[21]. Further investigation for these miRNAs will be the challenge for the future to clarify the roles of miRNAs that contribute to IDPN-induced neurotoxicity.

In conclusion, miR-547* was considered to be associated with IDPN-induced abnormalities in the pons and medulla. To our knowledge, this is the first report indicating links between upregulation of miR-547* and neurotoxicity of IDPN in rats. Although the potential mechanisms need to be further clarified, miR-547* may provide new useful information regarding the mechanism of IDPN neurotoxicity and the pathogenesis of axonopathy.

Disclosure of Potential Conflicts of Interest: The authors declare that they have no conflict of interest.

References

1. Chou SM, and Hartmann HA. Axonal lesions and waltzing syndrome after idpn administration in rats. with a concept– "axostasis". Acta Neuropathol. **3**: 428–450. 1964. [Medline] [CrossRef]

2. Llorens J, Demêmes D, and Sans A. The behavioral syndrome caused by 3,3′-iminodipropionitrile and related nitriles in the rat is associated with degeneration of the vestibular sensory hair cells. Toxicol Appl Pharmacol. **123**: 199–210. 1993. [Medline] [CrossRef]

3. Okazaki S, Takashima H, Yamaguchi M, Hamamura M, Yamashita K, Okada M, Sunaga M, Tanaka R, Sato S, Umano T, Tsuji R, Yosioka T, and Fujii T. [Neurobehavioral toxicity of acrylamide and IDPN (3,3′-iminodipropionitrile) in rats by 28-day oral administration--problems encountered in collaborative study and a commentary on conducting neurobehavioral testing]. J Toxicol Sci. **28**(Suppl 1): 1–14. 2003; (in Japanese). [Medline]

4. Griffin JW, Hoffman PN, Clark AW, Carroll PT, and Price DL. Slow axonal transport of neurofilament proteins: impairment of beta,beta'-iminodipropionitrile administration. Science. **202**: 633–635. 1978. [Medline] [CrossRef]

5. Schulze GE, and Boysen BG. A neurotoxicity screening battery for use in safety evaluation: effects of acrylamide and 3′,3′-iminodipropionitrile. Fundam Appl Toxicol. **16**: 602–615. 1991. [Medline] [CrossRef]

6. Zhu Q, Lindenbaum M, Levavasseur F, Jacomy H, and Julien JP. Disruption of the NF-H gene increases axonal microtubule content and velocity of neurofilament transport: relief of axonopathy resulting from the toxin beta,beta'-iminodipropionitrile. J Cell Biol. **143**: 183–193. 1998. [Medline] [CrossRef]

7. Yoshioka T, Hamamura M, Yoshimura S, Okazaki Y, Yamaguchi Y, Sunaga M, Hoshuyama S, Iwata H, Okada M, Takei Y, Yamaguchi M, Mitsumori K, Imai K, Narama I, and Okuno Y. Neuropathological evaluation of acrylamide and 3,3′-iminodipropionitrile-induced neurotoxicity in a rat 28-day oral toxicity study-collaborative project for standardization of test procedures and evaluation of neurotoxicity. J Toxicol Pathol. **14**: 279–287. 2001. [CrossRef]

8. Ambros V. The functions of animal microRNAs. Nature. **431**: 350–355. 2004. [Medline] [CrossRef]

9. Miska EA. How microRNAs control cell division, differentiation and death. Curr Opin Genet Dev. **15**: 563–568. 2005. [Medline] [CrossRef]

10. Kloosterman WP, and Plasterk RH. The diverse functions of microRNAs in animal development and disease. Dev Cell. **11**: 441–450. 2006. [Medline] [CrossRef]

11. Kaur P, Armugam A, and Jeyaseelan K. MicroRNAs in Neurotoxicity. J Toxicol. **2012**: 870150. 2012. [Medline]

12. Wang X, Zhou S, Ding X, Zhu G, and Guo J. Effect of triazophos, fipronil and their mixture on miRNA expression in adult zebrafish. J Environ Sci Health B. **45**: 648–657. 2010. [Medline] [CrossRef]

13. Tal TL, and Tanguay RL. Non-coding RNAs--novel targets in neurotoxicity. Neurotoxicology. **33**: 530–544. 2012. [Medline] [CrossRef]

14. Deng Y, Ai J, Guan X, Wang Z, Yan B, Zhang D, Liu C, Wilbanks MS, Escalon BL, Meyers SA, Yang MQ, and Perkins EJ. MicroRNA and messenger RNA profiling reveals new biomarkers and mechanisms for RDX induced neurotoxicity. BMC Genomics. **15**(Suppl 11): S1. 2014. [Medline] [CrossRef]

15. Qi Y, Zhang M, Li H, Frank JA, Dai L, Liu H, and Chen G. MicroRNA-29b regulates ethanol-induced neuronal apoptosis in the developing cerebellum through SP1/RAX/PKR cascade. J Biol Chem. **289**: 10201–10210. 2014. [Medline] [CrossRef]

16. An J, Cai T, Che H, Yu T, Cao Z, Liu X, Zhao F, Jing J, Shen X, Liu M, Du K, Chen J, and Luo W. The changes of miRNA expression in rat hippocampus following chronic

lead exposure. Toxicol Lett. **229**: 158–166. 2014. [Medline] [CrossRef]

17. Ogata K, Sumida K, Miyata K, Kushida M, Kuwamura M, and Yamate J. Circulating miR-9* and miR-384-5p as potential indicators for trimethyltin-induced neurotoxicity. Toxicol Pathol. **43**: 198–208. 2015. [Medline] [CrossRef]

18. Hu Z, Yu D, Gu QH, Yang Y, Tu K, Zhu J, and Li Z. miR-191 and miR-135 are required for long-lasting spine remodelling associated with synaptic long-term depression. Nat Commun. **5**: 3263. 2014. [Medline] [CrossRef]

19. Chen CL, Liu H, and Guan X. Changes in microRNA expression profile in hippocampus during the acquisition and extinction of cocaine-induced conditioned place preference in rats. J Biomed Sci. **20**: 96. 2013. [Medline] [CrossRef]

20. Masliah-Planchon J, Pasmant E, Luscan A, Laurendeau I, Ortonne N, Hivelin M, Varin J, Valeyrie-Allanore L, Dumaine V, Lantieri L, Leroy K, Parfait B, Wolkenstein P, Vidaud M, Vidaud D, and Bièche I. MicroRNAome profiling in benign and malignant neurofibromatosis type 1-associated nerve sheath tumors: evidences of PTEN pathway alterations in early NF1 tumorigenesis. BMC Genomics. **14**: 473. 2013. [Medline] [CrossRef]

21. Wang LL, Zhang Z, Li Q, Yang R, Pei X, Xu Y, Wang J, Zhou SF, and Li Y. Ethanol exposure induces differential microRNA and target gene expression and teratogenic effects which can be suppressed by folic acid supplementation. Hum Reprod. **24**: 562–579. 2009. [Medline] [CrossRef]

22. Zheng H, Law PY, and Loh HH. Non-Coding RNAs Regulating Morphine Function: With Emphasis on the In vivo and In vitro Functions of miR-190. Front Genet. **3**: 113. 2012. [Medline] [CrossRef]

23. Meissner L, Gallozzi M, Balbi M, Schwarzmaier S, Tiedt S, Terpolilli NA, and Plesnila N. Temporal Profile of MicroRNA Expression in Contused Cortex after Traumatic Brain Injury in Mice. J Neurotrauma. **33**: 713–720. 2016. [Medline] [CrossRef]

24. Mandolesi G, Vanni V, Cesa R, Grasselli G, Puglisi F, Cesare P, and Strata P. Distribution of the SNAP25 and SNAP23 synaptosomal-associated protein isoforms in rat cerebellar cortex. Neuroscience. **164**: 1084–1096. 2009. [Medline] [CrossRef]

25. Malarkey EB, and Parpura V. Temporal characteristics of vesicular fusion in astrocytes: examination of synaptobrevin 2-laden vesicles at single vesicle resolution. J Physiol. **589**: 4271–4300. 2011. [Medline] [CrossRef]

26. Bragina L, Candiracci C, Barbaresi P, Giovedì S, Benfenati F, and Conti F. Heterogeneity of glutamatergic and GABAergic release machinery in cerebral cortex. Neuroscience. **146**: 1829–1840. 2007. [Medline] [CrossRef]

27. Stigliani S, Zappettini S, Raiteri L, Passalacqua M, Melloni E, Venturi C, Tacchetti C, Diaspro A, Usai C, and Bonanno G. Glia re-sealed particles freshly prepared from adult rat brain are competent for exocytotic release of glutamate. J Neurochem. **96**: 656–668. 2006. [Medline] [CrossRef]

28. Yamamori S, and Itakura M. [Differential expression and function of SNAP-25 family proteins in the mouse brain]. Seikagaku. **85**: 1016–1020. 2013; (in Japanese). [Medline]

29. Wilhelm A, Volknandt W, Langer D, Nolte C, Kettenmann H, and Zimmermann H. Localization of SNARE proteins

and secretory organelle proteins in astrocytes in vitro and in situ. Neurosci Res. **48**: 249–257. 2004. [Medline] [CrossRef]

30. Verderio C, Pozzi D, Pravettoni E, Inverardi F, Schenk U, Coco S, Proux-Gillardeaux V, Galli T, Rossetto O, Frassoni C, and Matteoli M. SNAP-25 modulation of calcium dynamics underlies differences in GABAergic and glutamatergic responsiveness to depolarization. Neuron. **41**: 599–610. 2004. [Medline] [CrossRef]

31. Weng N, Thomas DD, and Groblewski GE. Pancreatic acinar cells express vesicle-associated membrane protein 2- and 8-specific populations of zymogen granules with distinct and overlapping roles in secretion. J Biol Chem. **282**: 9635–9645. 2007. [Medline] [CrossRef]

32. Stoeckelhuber M, Scherer EQ, Janssen KP, Slotta-Huspenina J, Loeffelbein DJ, Rohleder NH, Nieberler M, Hasler R, and Kesting MR. The human submandibular gland: immunohistochemical analysis of SNAREs and cytoskeletal proteins. J Histochem Cytochem. **60**: 110–120. 2012. [Medline] [CrossRef]

33. Imai A, Nashida T, Yoshie S, and Shimomura H. Intracellular localisation of SNARE proteins in rat parotid acinar cells: SNARE complexes on the apical plasma membrane. Arch Oral Biol. **48**: 597–604. 2003. [Medline] [CrossRef]

34. Low SH, Roche PA, Anderson HA, van Ijzendoorn SC, Zhang M, Mostov KE, and Weimbs T. Targeting of SNAP-23 and SNAP-25 in polarized epithelial cells. J Biol Chem. **273**: 3422–3430. 1998. [Medline] [CrossRef]

35. Fink DJ, Purkiss D, and Mata M. beta,beta'-Iminodipropionitrile impairs retrograde axonal transport. J Neurochem. **47**: 1032–1038. 1986. [Medline] [CrossRef]

36. Llorens J, Crofton KM, and O'Callaghan JP. Administration of 3,3′-iminodipropionitrile to the rat results in region-dependent damage to the central nervous system at levels above the brain stem. J Pharmacol Exp Ther. **265**: 1492–1498. 1993. [Medline]

37. Crofton KM, Janssen R, Prazma J, Pulver S, and Barone S Jr. The ototoxicity of 3,3′-iminodipropionitrile: functional and morphological evidence of cochlear damage. Hear Res. **80**: 129–140. 1994. [Medline] [CrossRef]

38. Llorens J, and Rodríguez-Farré E. Comparison of behavioral, vestibular, and axonal effects of subchronic IDPN in the rat. Neurotoxicol Teratol. **19**: 117–127. 1997. [Medline] [CrossRef]

39. Seoane A, Demêmes D, and Llorens J. Pathology of the rat vestibular sensory epithelia during subchronic 3,3′-iminodipropionitrile exposure: hair cells may not be the primary target of toxicity. Acta Neuropathol. **102**: 339–348. 2001. [Medline]

40. Khan HA, Alhomida AS, and Arif IA. Neurovestibular toxicities of acrylonitrile and iminodipropionitrile in rats: a comparative evaluation of putative mechanisms and target sites. Toxicol Sci. **109**: 124–131. 2009. [Medline] [CrossRef]

41. Seoane A, Espejo M, Pallàs M, Rodríguez-Farré E, Ambrosio S, and Llorens J. Degeneration and gliosis in rat retina and central nervous system following 3,3′-iminodipropionitrile exposure. Brain Res. **833**: 258–271. 1999. [Medline] [CrossRef]

Original Article

4-Methylthio-3-butenyl isothiocyanate (raphasatin) exerts chemopreventive effects against esophageal carcinogenesis in rats

Isamu Suzuki[1, 2], Young-Man Cho[1*], Tadashi Hirata[1, 3], Takeshi Toyoda[1], Jun-ichi Akagi[1], Yasushi Nakamura[4, 5], Eun Young Park[4, 6#], Azusa Sasaki[4], Takako Nakamura[4], Shigehisa Okamoto[7], Koji Shirota[5], Noboru Suetome[5], Akiyoshi Nishikawa[2, 8], and Kumiko Ogawa[1]

[1] Division of Pathology, National Institute of Health Sciences, 1-18-1 Kamiyoga, Setagaya-ku, Tokyo 158-8501, Japan
[2] Pathogenetic Veterinary Science, United Graduate School of Veterinary Sciences, Gifu University, 1-1 Yanagido, Gifu, Gifu 501-1193, Japan
[3] Department of Pharmacology, School of Pharmacy, Showa University, 1-5-8 Hatanodai, Shinagawa-ku, Tokyo 142-8555, Japan
[4] Faculty of Life and Environmental Sciences, Kyoto Prefectural University, 1-5 Shimogamohangi-cho, Sakyo-ku, Kyoto 606-8522, Japan
[5] Kyoto Prefectural Agriculture, Forestry & Fisheries Technology Center, 9 Wakunari, Amarube, Kameoka, Kyoto 621-0806, Japan
[6] Department of Food Science, Korea Christian University, Kkachisan-ro 24-gil, Gangseo-gu 47, Seoul 07661, Republic of Korea
[7] Department of Food Science and Biotechnology, Kagoshima University, 1-21-24 Korimoto, Kagoshima, Kagoshima 890-0065, Japan
[8] Biological Safety Research Center, National Institute of Health Sciences, 1-18-1 Kamiyoga, Setagaya-ku, Tokyo 158-8501, Japan

Abstract: To examine the effects of 4-methylthio-3-butenyl isothiocyanate on esophageal carcinogenesis, male 6-week-old F344 rats were subcutaneously injected with 0.5 mg/kg body weight N-nitrosomethylbenzylamine three times per week for 5 weeks and fed a diet supplemented with 80 ppm 4-methylthio-3-butenyl isothiocyanate, equivalent to 6.05 mg/kg body weight/day for the initiation stage, 4.03 mg/kg body weight/day for the promotion stage, or 4.79 mg/kg body weight/day for all stages. Although the incidence of lesions was not affected by 4-methylthio-3-butenyl isothiocyanate treatment, the multiplicity of squamous cell papilloma in the esophagus was significantly decreased in rats in the 4-methylthio-3-butenyl isothiocyanate initiation stage group (1.13 ± 0.74), 4-methylthio-3-butenyl isothiocyanate promotion stage group (1.47 ± 0.99), and 4-methylthio-3-butenyl isothiocyanate all stage group (1.47 ± 1.13) as compared with rats treated with N-nitrosomethylbenzylamine alone (3.00 ± 1.46). Immunohistochemical analysis revealed that 4-methylthio-3-butenyl isothiocyanate induced apoptosis, suppressed cell proliferation, and increased p21 expression when administered in the promotion phase. These modifying effects were not observed in the rats treated with 4-methylthio-3-butenyl isothiocyanate alone. Our results indicated that 4-methylthio-3-butenyl isothiocyanate may exert chemopreventive effects against N-nitrosomethylbenzylamine-induced esophageal carcinogenesis in rats. (DOI: 10.1293/tox.2016-0037; J Toxicol Pathol 2016; 29: 237–246)

Key words: 4-methylthio-3-butenyl isothiocyanate, raphasatin, esophageal cancer, N-nitrosomethylbenzylamine, chemoprevention

Introduction

Esophageal cancer is the tenth most common cancer and the sixth most common cause of cancer-related deaths worldwide (about 400,000 deaths/year)[1]. In addition, it is one of the most lethal malignancies, with a 5-year survival rate of only 17% in the USA from 1996 to 2004[2, 3]. In Japan,

the 10-year relative survival rate of men with esophageal cancer was reported to be 24.0%; this was lower than those of other digestive tract cancers (gastric cancer, 61.3%; colon cancer, 68.9%) from 2002 to 2006[4]. Therefore, effective chemopreventive approaches against this disease are urgently required.

Esophageal squamous cell carcinoma (ESCC) is one of the most predominant histological types of esophageal cancer. Epidemiological studies have shown that tobacco smoking, excessive alcohol consumption, and eating pickled vegetables are associated with increased risk of ESCC; these habits can lead to the endogenous generation of nitrosamines, a common type of carcinogen[5]. Furthermore, high concentrations of nitrate nitrogen, the precursor of nitrosamine, in drinking water can increase the risk of ESCC[6]. In contrast, the consumption of fruits and vegetables has been

shown to be associated with a reduced risk of ESCC[7, 8]. In these population-based prospective cohort studies, researchers found a dose-dependent decrease in the risk of ESCC associated with a higher intake of total fruits and vegetables. Of the five fruit and vegetable subgroups investigated in the study of Yamaji *et al.*, only individuals consuming cruciferous vegetables had a significantly reduced risk of ESCC on further adjustment for smoking and alcohol consumption status[8]. Among the different types of fruits and vegetables, cruciferous vegetables may provide a good source of effective cancer-preventing compounds[9]. In particular, isothiocyanates (ITCs), one of the constituents in cruciferous vegetables, have been extensively investigated and have attracted considerable attention owing to their promising chemopreventive effects[9].

ITCs have been shown to suppress tumor development in rodent carcinogenesis models of various organs[9–13]. Moreover, phenethyl isothiocyanate (PEITC) has been reported to suppress *N*-nitrosomethylbenzylamine (NMBA)-induced rat esophageal carcinogenesis when rats are treated throughout the experiment[14–16]. 4-Methylthio-3-butenyl isothiocyanate (MTBITC), a component of the daikon (Japanese white radish), was also found to have antimutagenic effects in an *in vitro* study[17] and was shown to suppress pancreatic carcinogenesis in hamsters treated with *N*-nitrosobis(2-oxopropyl)amine (BOP) when given during the initiation stage[18]. MTBITC is a pungent component of the daikon; therefore, heirloom types of daikon (e.g., Karami, Momoyama, and Sabaga), which are more pungent than the conventional type of daikon (Aokubi), are a rich source of MTBITC[19]. Although several *in vitro* studies have shown that MTBITC has chemopreventive properties, such as antiproliferative and pro-apoptotic effects[20–22], few reports have assessed the chemopreventive effects of this compound *in vivo*[18, 23], and it is unclear whether MTBITC exerts chemopreventive effects in esophageal carcinogenesis.

In this study, we aimed to clarify the potential chemopreventive effects of MTBITC in an *in vivo* model of esophageal carcinogenesis. For this purpose, we employed an NMBA-induced rat esophageal carcinogenesis model to allow the initiated cells to develop into preneoplastic/neoplastic lesions from squamous cells rapidly. NMBA is a carcinogenic nitrosamine that is found in the diet in regions where individuals are at high risk of ESCC[24]. The NMBA-induced rat esophageal carcinogenesis model has been extensively used because the relatively short-term (5 weeks) NMBA-treatment protocol results in a 100% tumor incidence within 23 weeks after the first administration of NMBA and allows for evaluation of the effects of compounds administered before, during, and after NMBA treatment[14, 16]. Using this model, we were able to assess the potential influence of MTBITC on the induction and subsequent progression of esophageal neoplasms. In addition, we performed immunohistochemical analysis to assess the mechanisms involved in MTBITC-dependent chemoprevention.

Materials and Methods

Chemicals

MTBITC was extracted and purified from the roots of heirloom varieties of daikon (*Raphanus sativus*) in Kyoto (Momoyama and Sabaga) as previously described[19] and then stored at −80°C until use. The purity of the MTBITC was 98.0%, as estimated by high-performance liquid chromatography (HPLC; Shimadzu, Kyoto, Japan). NMBA (Nard, Osaka, Japan) was dissolved in 20% dimethyl sulfoxide (DMSO; Sigma-Aldrich, St. Louis, MO, USA) in saline and was administered at a volume of 5 mL/kg body weight (BW).

Experimental animals and housing conditions

A total of 95 four-week-old male F344/DuCrlCrlj rats were obtained from Charles River Laboratories Japan (Yokohama, Japan) and acclimated for 1 week prior to testing. The rats were housed in polycarbonate cages (3–4 rats per cage) with softwood chips for bedding in a specific pathogen-free animal facility and maintained under controlled conditions (temperature, 23 ± 2°C; relative humidity, 55 ± 5%; air changes, 12 times/h; and lighting, 12-h light-dark cycle) with free access to the basal diet or test diet and tap water.

Experimental protocol

MTBITC was mixed into a powdered basal diet (CRF-1; Oriental Yeast Co., Ltd., Tokyo, Japan) at 80 ppm based on its ability to suppress pancreatic tumors in the hamsters[18]. The stability of MTBITC in the mixed diet was analyzed by HPLC, and the concentrations of MTBITC in the mixed diet preserved at 4°C for 4 days and 1 week were 96.6% and 90.7%, respectively, whereas those in mixed diets stored at room temperature for 4 days and 1 week were 75.3% and 75.1%, respectively. The MTBITC/diet admixture was prepared once per week and kept at 4°C in a refrigerator, and the contents of the feeding jar were exchanged twice per week.

As shown in Fig. 1, groups 1 (untreated) and 2 (MTBITC-treated) included 10 rats (5 weeks old) each that were fed the basal diet or a diet containing 80 ppm MTBITC without NMBA treatment or DMSO (vehicle) for analysis of the effects of MTBITC alone. Rats in groups 3 (DMSO-treated; n = 15) and 4 (NMBA-treated; n = 15) were fed the basal diet throughout the experiment and treated with DMSO or NMBA, respectively. NMBA was administered subcutaneously 3 times per week for 5 weeks at a dose of 0.5 mg/kg BW as previously described[16]. Groups 5–7 (n = 15 animals each) were given both NMBA and MTBITC as follows: for the initiation stage of treatment, from 1 week before NMBA treatment, rats were simultaneously given a diet mixed with 80 ppm MTBITC for 7 weeks and then the basal diet (group 5; NMBA+MTBITC/basal diet); for the promotion stage of treatment, starting 1 week after the end of NMBA treatment, the animals were continuously fed the MTBITC diet for 19
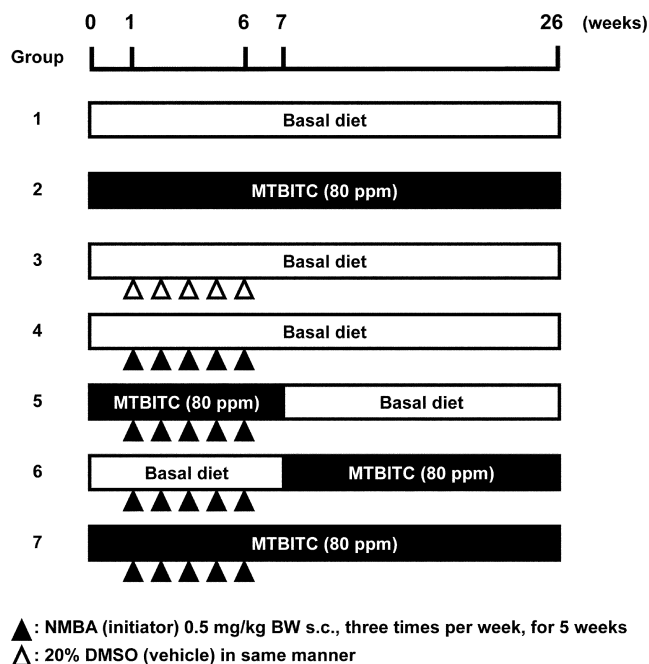
A: NMBA (initiator) 0.5 mg/kg BW s.c., three times per week, for 5 weeks
△: 20% DMSO (vehicle) in same manner

Fig. 1. Experimental design.

weeks (group 6; NMBA/MTBITC); finally, for all stages of treatment, the MTBITC diet was given throughout the experimental period (group 7; NMBA+MTBITC/MTBITC).

The animals were observed daily and weighed once per week during the experimental period. The amounts of supplied and residual diet were weighed twice per week, when the contents of the feeding jars were exchanged, in order to calculate the average daily food consumption and MTBITC intake throughout the treatment period. At experimental week 26, all animals were anesthetized with isoflurane (Mylan Inc., Tokyo, Japan), and blood samples were collected from the abdominal aorta for hematology and serum biochemistry in groups 1 and 2. Other animals were then euthanized by exsanguination from the abdominal aorta. The protocol was approved by the Animal Care and Utilization Committee of the National Institute of Health Sciences (Tokyo).

Hematology and serum biochemistry

To examine whether the dose of MTBITC used in this study itself exerts any effects in rats, hematology and serum biochemistry were analyzed in groups 1 and 2. Hematological examination was performed using a K-4500 automatic hematology analyzer (Sysmex Corp., Kobe, Japan). Aliquots of whole blood samples were mixed with 4 volumes of the supplier's buffer containing 0.5% ethylenediaminetetraacetic acid (EDTA)·2K and applied to the analyzer for the following parameters: white blood cell count (WBC), red blood cell count (RBC), hemoglobin concentration (HGB), hematocrit (HCT), mean corpuscular volume (MCV), mean corpuscular hemoglobin (MCH), mean corpuscular hemoglobin concentration (MCHC), and platelet count (PLT). To

measure the differential leukocyte and reticulocyte counts, aliquots of whole blood samples were mixed with a one-fourth volume of 5.0% EDTA·2K solution. Blood smears were then processed for May-Grunwald Giemsa staining and analyzed with a Microx HEG-50S (Sysmex). Serum biochemistry was analyzed at SRL, Inc. (Tokyo, Japan), using sera frozen after centrifugation of whole blood (1,000 × *g* for 10 min). The following parameters were analyzed: total protein (TP), albumin (Alb), albumin/globulin ratio (A/G), total bilirubin (Bil), glucose, triglyceride (TG), total cholesterol (T-Cho), urea nitrogen (BUN), creatinine (Cre), sodium (Na), chlorine (Cl), potassium (K), calcium (Ca), inorganic phosphorus (IP), aspartate aminotransferase (AST), alanine aminotransferase (ALT), alkaline phosphatase (ALP), and gamma-glutamyl transpeptidase (γ GTP).

Organ weights and histopathological assessment

After necropsy, the esophagus, tongue, and stomach were removed from all rats. In groups 1 and 2, the brain, thymus, lungs, heart, spleen, liver, adrenal glands, kidneys, and testes were weighed, and the skin, mammary glands, femur with marrow, sternum with marrow, mesenteric lymph nodes, salivary glands (sublingual and submandibular), aorta, trachea, small intestine (duodenum, jejunum, and ileum), large intestine (cecum, colon, and rectum), pancreas, urinary bladder, epididymides, seminal vesicles, prostate gland, pituitary gland, thyroid glands, parathyroid glands, spinal cord with vertebrae (cervical, thoracic, and lumbar portions), trigeminal and sciatic nerves, eyes, Harderian glands, femoral skeletal muscle, and nasal cavity were removed to examine whether the dose of MTBITC used in this study itself exerts any effects in rats. To evaluate the chemopreventive effects of MTBITC, the esophagus of each rat was opened longitudinally, and surface nodules greater than 0.5 mm in a single dimension were mapped, counted, and measured. This size is used to ensure detection of proliferative lesions, and it was also applied in previous NMBA-induced esophageal carcinogenesis studies[14, 15]. The esophagus was unbent and fixed on a filter paper to make it flat. The organs were then fixed in 10% buffered formalin for 3 days. Testes and eyes were fixed in Bouin's solution and Davidson's solution, respectively. The nasal cavity, vertebrae, sternum, and femur were treated with a mixture of 10% formic acid and 10% buffered formalin for up to 3 weeks for decalcification. After fixation, the entire length of the esophagus was cut into 2 or 3 sections including all nodules greater than 0.5 mm in diameter. Tissue slices of all organs were routinely processed for paraffin embedding, and sections were prepared and stained with hematoxylin and eosin (HE) for histopathological evaluation. Esophageal lesions were classified into hyperplasia, atypical hyperplasia (i.e., dysplasia), papilloma, and carcinoma of squamous cells based on histopathological features in rats, in accordance with the International Harmonization of Nomenclature and Diagnostic Criteria (INHAND)[25]. Diagnostic features are as follows. Atypical hyperplasia reveals the thickening of squamous epithelium with the presence of abnormal cell shape, size,

or nuclear morphology, and keratinization of cells within deeper layers of mucosa is seen. Papilloma is characterized by branching central fibrovascular stalks that are covered by a variably thick and differentiated squamous epithelium that is often heavily keratinized. Cells comprising a carcinoma show features such as loss of polarity (for example, basal-like tumor cells suddenly forming keratin pearls), an abundance of mitotic figures, cellular and nuclear pleomorphism, and foci of necrosis.

Immunohistochemistry

Esophagus tissues were embedded in paraffin, sectioned to at a thickness of 4-μm, and subjected to immunohistochemistry using a Vectastain Elite ABC Kit (Vector Laboratories Inc., Burlingame, CA, USA) or Histofine Simple Stain Kit (Nichirei Corp, Tokyo, Japan) with 3, 3′-diaminobenzidine/H_2O_2 as a chromogen. The following primary antibodies were used: anti-cleaved caspase-3 rabbit monoclonal antibodies (clone 5A1E, 1:500; Cell Signaling Technology, Inc., Danvers, MA, USA), anti-Ki-67 rabbit monoclonal antibodies (clone SP6, 1:1,000; Abcam, Cambridge, CA, USA), anti-p21 rabbit monoclonal antibodies (clone EPR3993, 1:2,000; Abcam), and anti-p53 mouse monoclonal antibodies (clone PAb 240, 1:2,500; Abcam). Antigen retrieval was performed in an autoclave for 10 min at 121°C in 10 mM citrate buffer (pH 6.0) for Ki-67, p21, and p53 or in a microwave for 10 min at 90°C in Target Retrieval Solution, pH 9 (Dako, Tokyo, Japan), for cleaved caspase-3.

Immunohistochemical analysis was performed for rats in groups 2–7. All immunostained slides were counterstained with hematoxylin for microscopic examination. To compare the effects of MTBITC on early-stage esophageal carcinogenesis, we analyzed normal looking epithelia from rats in groups 2 and 3 or diffuse hyperplastic epithelia (i.e., the majority of the mucosa consisting of squamous cells in increased layers other than focal preneoplastic/neoplastic lesions in NMBA-treated animals) in groups 4–7. The numbers of positive cells were counted in 5 randomly selected areas per epithelium at a magnification of 200× from 10 randomly selected rats per group, and cell numbers were normalized to the unit length of the muscularis mucosae in accordance with Taniai et al.[26].

Statistical analysis

All data were expressed as means ± SDs per group, and the data of groups 3 and 4 were compared with those of the other groups to evaluate the effects of MTBITC on NMBA-induced rat esophageal carcinogenesis. For comparison of numerical data between multiple groups, Bartlett's test for equal variance was used to determine whether variances were homogenous between the groups. If a significant difference in variance was not observed, one-way analysis of variance (ANOVA) was performed. If significant differences were found, Dunnett's multiple comparison tests (for multiplicity data) or Tukey-Kramer's multiple range tests (for other data) were performed for comparisons between the groups. If a significant difference was found using Bartlett's test, Kruskal-Wallis tests were performed. If significant differences were found, Steel tests (for multiplicity data) or Steel-Dwass tests (for other data) were applied.

The significance of differences in data for hematology, serum biochemistry, and organ weights (both absolute and relative weights) between groups 1 and 2 was analyzed with Student-Welch tests. For histopathological findings, Fisher's exact probability tests were performed. Differences with *P* values of less than 0.05 were considered statistically significant.

Results

One rat in group 3 became emaciated due to malocclusion and was excluded from the study. No treatment-related clinical signs or deaths were detected during the 26-week study period. The treatments did not affect body weight. Analysis of food consumption revealed that rats in groups 2, 5, 6, and 7 consumed 4.64, 6.05, 4.03, and 4.79 mg MTBITC/kg BW/day, respectively (Table 1).

No MTBITC-related changes were observed in hematological parameters, serum biochemistry, organ weights, and histopathological features in groups 1 and 2, except for incidental and spontaneous changes (data not shown). A significant low value for lung weight was observed in group 2, but it was thought to be incidental, since the difference was minimal and no significant histopathological change was observed.

The incidence and multiplicity data for macroscopic esophageal nodules greater than 0.5 mm in diameter in each group are summarized in Table 2. The nodules were diagnosed as squamous cell hyperplasia, atypical hyperplasia, papilloma, or carcinoma, as described later. No statistically significant differences in the incidence of nodules were detected among groups 4–7. In contrast, the multiplicities of nodules in groups 5–7 were significantly lower than that in group 4 (*P*<0.01).

The incidence and multiplicity data of esophageal preneoplastic/neoplastic lesions, as identified by histological assessment, are shown in Table 3, and the representative appearance of each lesion is shown in Fig. 2. There were no significant differences in the incidences of lesions among groups 4–7. However, the multiplicity data for atypical hyperplasia (*P*<0.05 in groups 5 and 7) and for papilloma (*P*<0.01 in groups 5–7) were significantly decreased compared with those in group 4. As for carcinoma, the animals in groups 6 and 7 revealed a tendency to exhibit slightly lower incidence and multiplicity data than those in group 4, without statistical significance. Moreover, focal hyperplasia and papilloma of squamous cells in the tongue was sporadically detected in rats in groups 4–7; however, there were no significant differences in the incidence and multiplicity data (data not shown). Additionally, no changes were observed in the stomach in all groups of rats.

The results of the immunohistochemical analysis are graphically summarized in Fig. 3. The numbers of epithelial cells positive for cleaved caspase-3, the activated form of

Table 1. Body Weight, Food Consumption, and Intake of MTBITC

Group	No. of animals	Body weight (g)		Food consumption (g/rat/day)	Intake of MTBITC (mg/kg BW/day)
		Initial	Final		
1. Untreated	10	84.1 ± 6.7	364 ± 14.6	15.4	0
2. MTBITC-treated	10	84.2 ± 6.5	369 ± 28.0	16.3	4.64
3. DMSO-treated	14	84.5 ± 5.4	378 ± 14.3	16.5	0
4. NMBA-treated	15	84.0 ± 5.4	361 ± 21.9	15.8	0
5. NMBA+MTBITC/basal diet	15	84.0 ± 5.3	360 ± 23.3	15.7	6.05
6. NMBA/MTBITC	15	83.9 ± 5.3	364 ± 21.4	16.1	4.03
7. NMBA+MTBITC/MTBITC	15	83.9 ± 5.2	364 ± 27.5	16.7	4.79

Body weight values represent the mean ± SD.

Table 2. Incidence and Multiplicity Data for Macroscopic Esophageal Nodules

Group	No. of animals	Incidence (%)	Multiplicity (no./rat)
1. Untreated	10	0	
2. MTBITC-treated	10	0	
3. DMSO-treated	14	0	
4. NMBA-treated	15	15 (100)	4.53 ± 1.77
5. NMBA+MTBITC/basal diet	15	13 (87)	1.67 ± 0.98**
6. NMBA/MTBITC	15	12 (80)	1.73 ± 1.10**
7. NMBA+MTBITC/MTBITC	15	12 (80)	1.87 ± 1.19**

Multiplicity values represent the mean ± SD. ** $P<0.01$ versus the NMBA-treated group.

Table 3. Incidence and Multiplicity Data for Esophageal Preneoplastic/Neoplastic Lesions

Group	No. of animals	Incidence (%)			Multiplicity (no./rat)		
		Atypical hyperplasia	Papilloma	Carcinoma	Atypical hyperplasia	Papilloma	Carcinoma
1. Untreated	10	0	0	0			
2. MTBITC-treated	10	0	0	0			
3. DMSO-treated	14	0	0	0			
4. NMBA-treated	15	14 (93)	15 (100)	9 (60)	2.73 ± 1.58	3.00 ± 1.46	0.67 ± 0.62
5. NMBA+MTBITC/basal diet	15	14 (93)	12 (80)	8 (53)	1.67 ± 1.23*	1.13 ± 0.74**	0.60 ± 0.63
6. NMBA/MTBITC	15	14 (93)	12 (80)	6 (40)	1.80 ± 1.15	1.47 ± 0.99**	0.47 ± 0.64
7. NMBA+MTBITC/MTBITC	15	11 (73)	12 (80)	6 (40)	1.53 ± 1.36*	1.47 ± 1.13**	0.47 ± 0.64

Multiplicity values represent the mean ± SD. * $P<0.05$ versus the NMBA-treated group. ** $P<0.01$ versus the NMBA-treated group.

caspase-3 involved in apoptotic signaling, were significantly higher in groups 5–7 than in group 3 ($P<0.01$). The animals in group 4 also showed a tendency to exhibit a higher number of positive cells than the animals in group 3; however, this difference was not statistically significant. Moreover, the numbers of positive cells in groups 6 and 7 were significantly increased as compared with those in group 4 ($P<0.05$).

We next examined cell proliferation by analysis of Ki-67, an established cell proliferation marker. The numbers of Ki-67-positive cells in groups 4 and 5 were significantly increased as compared with that in group 3 ($P<0.01$). In contrast, groups 6 and 7 exhibited no obvious differences in the numbers of positive cells compared with that in group 3. Moreover, groups 6 and 7 showed significant decreases in the numbers of positive cells compared with that in group 4 ($P<0.01$).

There were no obvious differences in the number of cells positive for p21, a potent cyclin-dependent kinase (CDK) inhibitor, in groups 3–5. However, the numbers of p21-positive cells were significantly increased in groups 6 and 7 as compared with those in groups 3 ($P<0.01$) and 4 ($P<0.01$ versus group 6 and $P<0.05$ versus group 7).

The numbers of cells positive for p53, a well-studied tumor suppressor, were significantly increased in groups 4–7, i.e., all the NMBA-treated groups, compared with that in group 3 ($P<0.01$). However, there were no obvious immunoreactive differences between group 4 and groups 5–7.

As for all examined markers, the animals in the group 2 exhibited no obvious differences in the immunoreactive cell populations compared with those in group 3.
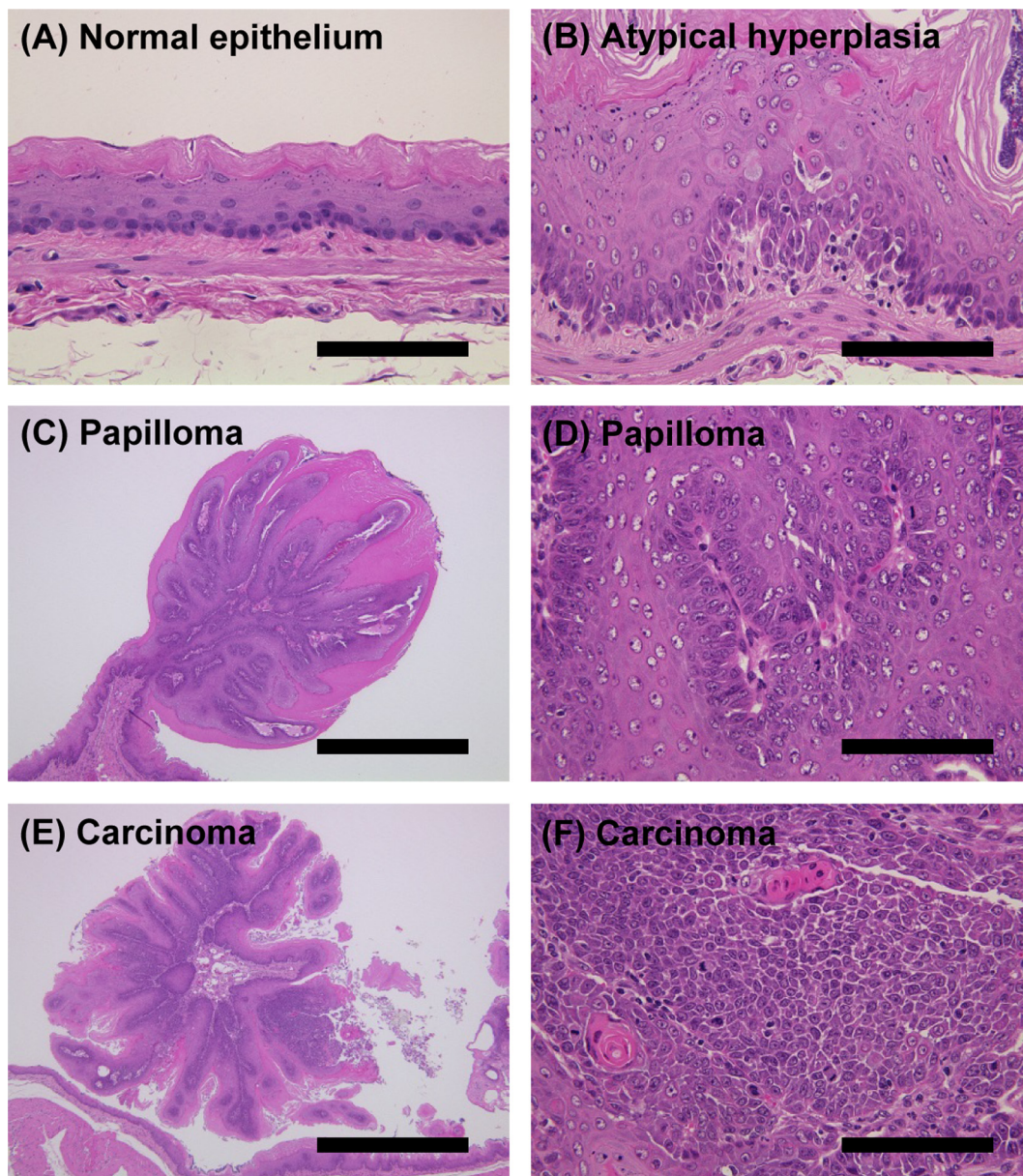
Fig. 2. Representative appearances of esophageal lesions. Normal epithelium (A) in rats in the DMSO-treated group, and squamous cell atypical hyperplasia (B), papilloma (C, D), and carcinoma (E, F) in rats in the NMBA-treated group (HE staining). Atypical hyperplasia exhibits thickening of the squamous epithelium along with the presence of an abnormal cell shape, size, or nuclear morphology, and keratinization of cells within deeper layers of the mucosa is seen. Papilloma is characterized by branching central fibrovascular stalks that are covered by a variably thick and differentiated squamous epithelium that is often heavily keratinized. Cells comprising a carcinoma show features such as loss of polarity (for example, basal-like tumor cells suddenly form keratin pearls), an abundance of mitotic figures, cellular and nuclear pleomorphism, and foci of necrosis. Bars = 100 μm (A, B, D, F) or 1,000 μm (C, E).

Discussion

In the present study, we showed that 26 weeks of dietary administration of 80 ppm MTBITC (equivalent to 4.64 mg/kg BW/day) alone did not have any effects in male F344 rats. Importantly, MTBITC treatment clearly inhibited NM-BA-induced esophageal carcinogenesis when administered during the initiation and/or promotion phase, causing induction of apoptosis and inhibition of cell proliferation in the promotion phase.

Few *in vivo* studies have reported the effects of MT-BITC on cancer[18, 23], and the current study is the first report demonstrating the chemopreventive effects of MTBITC on esophageal tumorigenesis in rats. Several other ITCs have also been shown to inhibit carcinogen-induced lung, colonic, pancreatic, and esophageal tumorigenesis[10–16], and the characteristics of these ITCs differ[21, 27], which may contribute to the observed variations in carcinogenesis. For ex-

(A) cleaved caspase-3

(B) Ki-67

(C) p21
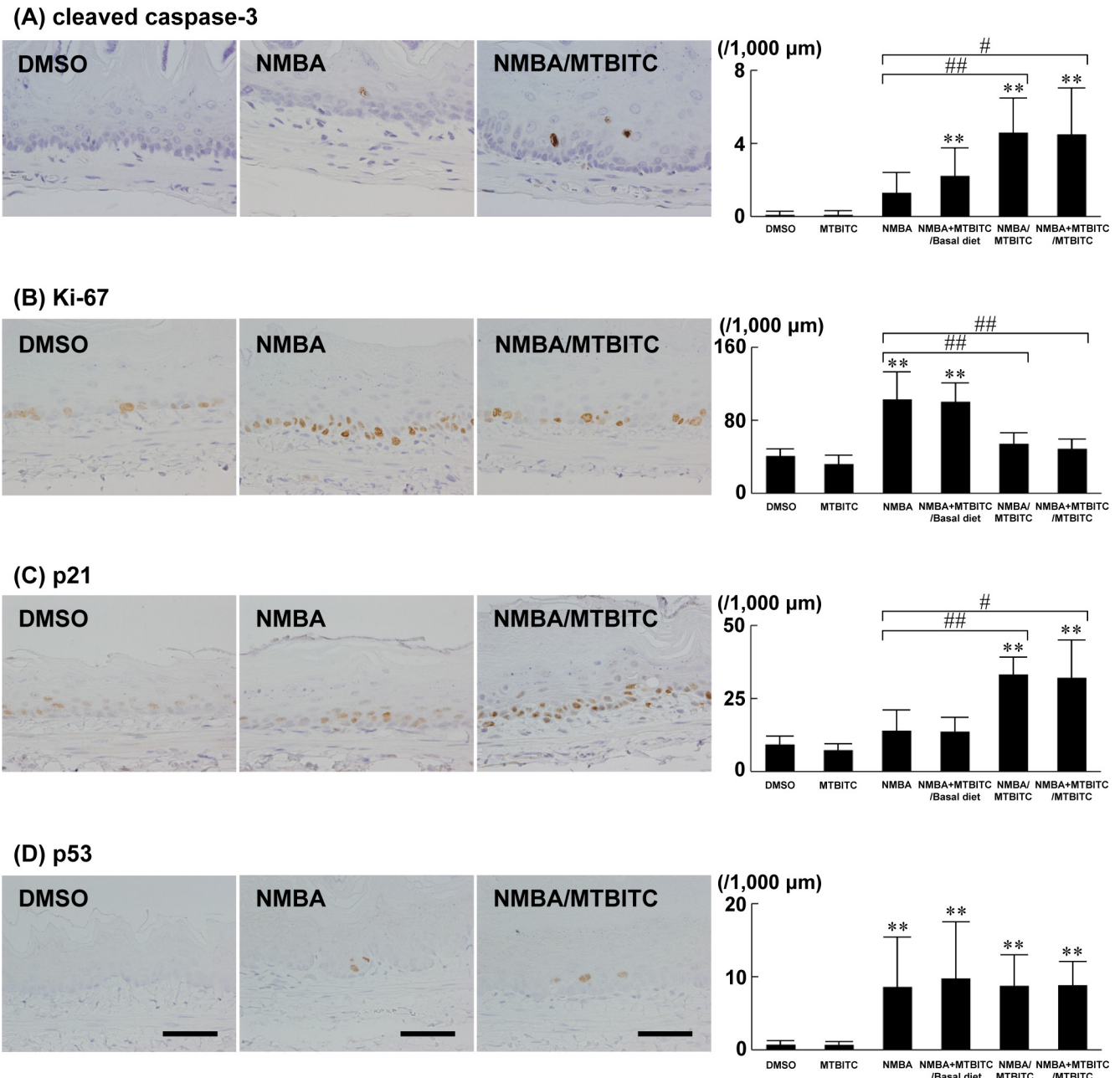
(D) p53

Fig. 3. Distribution of cleaved caspase-3-, Ki-67-, p21-, and p53-positive cells in the esophageal epithelium. Photomicrographs show the cellular distributions of markers in the DMSO-treated, NMBA-treated, and NMBA/MTBITC groups. The graphs show positive cells per unit muscularis mucosae length (1,000 μm) of the epithelium in the DMSO-treated, MTBITC-treated, NMBA-treated, NMBA+MTBITC/basal diet, NMBA/MTBITC, and NMBA+MTBITC/MTBITC groups. Values represent the mean + SD. (A) Cleaved caspase-3, (B) Ki-67, (C) p21, and (D) p53. Bars = 50 μm. ** $P<0.01$ versus the DMSO-treated group. # $P<0.05$ versus the NMBA-treated group. ## $P<0.01$ versus the NMBA-treated group.

ample, unlike dietary administration of 80 ppm MTBITC in the present experiment, 500 ppm of PEITC fails to exert chemopreventive effects on NMBA-induced tumorigenesis in the rat esophagus when administered during the promotion stage[14]. In contrast, 80 ppm MTBITC, benzyl isothiocyanate, or sulforaphane (SFN), a type of ITC, prevents BOP-induced pancreatic carcinogenesis in hamsters when administered during the initiation stage but not during the promotion stage[13, 18]. These reports, combined with our current findings, indicate that the chemopreventive effects of ITCs may differ depending on the target organ and/or the target molecules of the carcinogen.

In the present study, we also investigated the effects of MTBITC on cell proliferation and apoptosis in the esophageal epithelium of NMBA-treated rats. We found that cleaved caspase-3-positive cells were significantly in-

creased in animals treated with MTBITC during the promotion stage, as compared with that in animals treated with NMBA alone, indicating that MTBITC treatment increased apoptosis. MTBITC has been reported to induce apoptosis in HeLa (human cervical epithelial carcinoma), A549 (human alveolar basal epithelial carcinoma), MCF-7 (human mammary epithelial carcinoma), and PC-3 (human prostate epithelial carcinoma) cell lines[20]. Specifically, MTBITC was shown to upregulate the expression of Bax and caspase-3, two pro-apoptotic genes, and downregulate the expression of Bcl-2 and Bcl-xl, two anti-apoptotic genes. In terms of cell proliferation, we found that the numbers of Ki-67-positive cells were significantly increased in animals treated with NMBA alone or with MTBITC during the initiation stage as compared with that in animals treated with DMSO. Preneoplastic cells are generally known to have higher proliferative activity than normal cells[28, 29], and similar high proliferative activity was previously observed in a rat NMBA carcinogenesis model identical to the model used in this study[30]. However, the numbers of Ki-67-positive cells were significantly decreased in animals treated with MTBITC during the promotion stage as compared with that in animals treated with NMBA alone, indicating that MTBITC treatment decreased cell proliferation in the esophagus in rats treated with NMBA.

We also investigated the expression of p21 in the rat esophageal epithelium to determine the effects of MTBITC on the cell cycle checkpoint in this model. p21 is a potent CDK inhibitor that blocks cell cycle progression at the G_1, G_2, and/or G_0 phase[31]. In the present study, we found that animals treated with MTBITC during the promotion stage showed higher numbers of p21-positive cells than animals treated with NMBA alone. Several studies have shown that ITCs upregulate the expression of p21 and suppress the expression of cyclins and CDKs, resulting in induction of cell cycle arrest by PEITC in MCF-7 and MDA-MB-231 cells (derived from human breast adenocarcinomas) and by SFN in LNCaP and PC-3 cells (derived from human prostate adenocarcinomas)[32, 33]. SNF has been known to induce apoptosis derived from reactive oxygen species[34] and to elevate the transcription of p21 through the inhibition of histone deacetylase (HDAC) activity[33] in human prostate adenocarcinoma cells. Furthermore, MTBITC shares a similar chemical structure with SFN; therefore, MTBITC might have similar activity regarding ROS induction and HDAC inhibition. Further investigation is needed to clarify this. Consequently, our results suggest that MTBITC treatment may suppress cell proliferation through increased expression of p21, at least in part, in the rat esophageal epithelium.

Interestingly, rats in all NMBA-treated groups showed increased numbers of p53-positive cells in the esophagus compared with that in the DMSO-treated group, regardless of the presence of MTBITC treatment. p53 is a short-lived protein in normal tissues; however, mutant p53 protein has an extended half-life and is often highly expressed in tumor cells[35]. Mutations in the *p53* gene have been observed in NMBA-induced esophageal tumors in rats[36] and in esoph-

ageal tumors in humans[37]. Thus, the increased number of p53-positive cells may be explained by NMBA treatment, and MTBITC may not have affected the expression of p53 in the esophagus of NMBA-treated rats. However, we did not investigate mutations in the *p53* gene directly in our study.

Compared with the esophagus in the vehicle control group, administration of MTBITC alone did not alter these factors on the esophagus epithelium, suggesting that MTBITC may have selectively affected the NMBA-treated esophageal cells, while the normal esophageal cells were left unaffected. Selective targeting and negligible toxicity in normal cells are important prerequisites for probable chemopreventive compounds. Similarly, ITCs, including MTBITC, have been reported to induce cell cycle arrest and apoptosis in preneoplastic/neoplastic cells but not in normal cells in *in vitro* studies[20, 32, 33]. This might be due to a fact that ITCs could target a particular molecular event present in hyperplastic and cancer cells but absent in normal cells, for example, higher cell proliferative activity[28, 29].

MTBITC has been shown to inhibit genotoxicity *in vitro* and *in vivo*[17, 23] and to induce several types of antioxidative enzymes, including quinone reductase, NAD(P)H:quinone oxidoreductase, heme oxygenase-1, thioredoxin reductase, and glutathione S-transferase in HepG2 (human hepatocellular carcinoma) cells or hepatocytes of rats and mice[21, 22]. Moreover, induction of antioxidative enzymes is transcriptionally regulated through the antioxidant response element (ARE), and activation of gene transcription through the ARE is mediated primarily by nuclear factor E2-related factor 2 (Nrf2)[38]. Indeed, several types of ITCs, including MTBITC, activate Nrf2 in primary cultures of rat hepatocytes[21]. Furthermore, several ITCs have been reported to inhibit the induction of cytochrome P450 (CYP) enzymes. CYP enzymes are generally known to activate certain carcinogens, and simultaneous administration of PEITC has been reported to inhibit NMBA-induced esophageal carcinogenesis in rats through its ability to reduce the metabolism of NMBA and to inhibit the DNA adduct formation induced by NMBA metabolites[15]. PEITC also inhibits CYP1A2, CYP2E1, and CYP3A in rat liver microsomes[39]. In addition, MTBITC inhibits CYP3A2 in primary cultures of rat hepatocytes[21]. Based on these reports, MTBITC treatment during the initiation phase may affect the Nrf2-ARE pathway and the inhibition of CYP enzymes in the rat esophagus. Further studies are needed to confirm this hypothesis.

In conclusion, we showed for the first time that treatment with approximately 4–6 mg MTBITC/kg BW/day suppressed NMBA-induced esophageal tumorigenesis when administered during the initiation and/or promotion stages. Converting this dose based on body surface area as described in the FDA guidance[40], the human equivalent dose would be 0.65–0.98 mg/kg BW/day. The above effects were related to the induction of apoptosis and the suppression of cell proliferation in NMBA-treated esophageal cells with elevated p21 expression. On the other hand, these changes were not observed in the animals treated with MTBITC alone, suggesting the specificity of MTBITC to NMBA-

initiated cells but not to the normal esophageal epithelium. Based on the previously reported concentration of MTBITC in heirloom daikon varieties such as Karami, Momoyama, and Sabaga (421, 276, 227 μmol/100 g, respectively)[19], the estimated daily dose of MTBITC in this study was equal to about 60–160 g heirloom daikon in humans (60 kg BW); therefore, it is feasible to consume a sufficient amount of heirloom daikon containing MTBITC to achieve chemoprevention for esophageal cancer. Further studies of the efficacy of MTBITC will provide additional insights into the health benefits of daikon.

Disclosure of Potential Conflicts of Interest: Isamu Suzuki is an employee of BoZo Research Center Inc., Shizuoka, Japan, and Tadashi Hirata is an employee of Japan Tobacco Inc., Kanagawa, Japan. The authors declare that they have no conflicts of interest.

References

1. Ferlay J, Soerjomataram I, Ervik M, Dikshit R, Eser S, Mathers C, Rebelo M, Parkin DM, Forman D, and Bray F. GLOBOCAN 2012 v1.0, cancer incidence and mortality worldwide: IARC CancerBase No. 11. International Agency for Research on Cancer. 2013, http://globocan.iarc.fr./Pages/fact_sheets_cancer.aspx.
2. Enzinger PC, and Mayer RJ. Esophageal cancer. N Engl J Med. **349**: 2241–2252. 2003. [Medline] [CrossRef]
3. Jemal A, Siegel R, Ward E, Hao Y, Xu J, and Thun MJ. Cancer statistics, 2009. CA Cancer J Clin. **59**: 225–249. 2009. [Medline] [CrossRef]
4. Ito Y, Miyashiro I, Ito H, Hosono S, Chihara D, Nakata-Yamada K, Nakayama M, Matsuzaka M, Hattori M, Sugiyama H, Oze I, Tanaka R, Nomura E, Nishino Y, Matsuda T, Ioka A, Tsukuma H, Nakayama T. J-CANSIS Research Group Long-term survival and conditional survival of cancer patients in Japan using population-based cancer registry data. Cancer Sci. **105**: 1480–1486. 2014. [Medline] [CrossRef]
5. Kamangar F, Chow WH, Abnet CC, and Dawsey SM. Environmental causes of esophageal cancer. Gastroenterol Clin North Am. **38**: 27–57, vii. 2009. [Medline] [CrossRef]
6. Zhang N, Yu C, Wen D, Chen J, Ling Y, Terajima K, Akazawa K, Shan B, and Wang S. Association of nitrogen compounds in drinking water with incidence of esophageal squamous cell carcinoma in Shexian, China. Tohoku J Exp Med. **226**: 11–17. 2012. [Medline] [CrossRef]
7. Freedman ND, Park Y, Subar AF, Hollenbeck AR, Leitzmann MF, Schatzkin A, and Abnet CC. Fruit and vegetable intake and esophageal cancer in a large prospective cohort study. Int J Cancer. **121**: 2753–2760. 2007. [Medline]
[CrossRef]
8. Yamaji T, Inoue M, Sasazuki S, Iwasaki M, Kurahashi N, Shimazu T, and Tsugane S. Japan Public Health Center-based Prospective Study Group Fruit and vegetable consumption and squamous cell carcinoma of the esophagus in Japan: the JPHC study. Int J Cancer. **123**: 1935–1940. 2008. [Medline] [CrossRef]
9. IARC Cruciferous Vegetables, Isothiocyanates and Indoles. IARC Handbooks of Cancer Prevention, Vol. 9. Lyon. 2004.
10. Chung FL, Conaway CC, Rao CV, and Reddy BS. Chemoprevention of colonic aberrant crypt foci in Fischer rats by sulforaphane and phenethyl isothiocyanate. Carcinogenesis. **21**: 2287–2291. 2000. [Medline] [CrossRef]
11. Yang YM, Conaway CC, Chiao JW, Wang CX, Amin S, Whysner J, Dai W, Reinhardt J, and Chung FL. Inhibition of benzo(*a*)pyrene-induced lung tumorigenesis in A/J mice by dietary *N*-acetylcysteine conjugates of benzyl and phenethyl isothiocyanates during the postinitiation phase is associated with activation of mitogen-activated protein kinases and p53 activity and induction of apoptosis. Cancer Res. **62**: 2–7. 2002. [Medline]
12. Nishikawa A, Furukawa F, Kasahara K, Tanakamaru Z, Miyauchi M, Nakamura H, Ikeda T, Imazawa T, and Hirose M. Failure of phenethyl isothiocyanate to inhibit hamster tumorigenesis induced by *N*-nitrosobis(2-oxopropyl)amine when given during the post-initiation phase. Cancer Lett. **141**: 109–115. 1999. [Medline] [CrossRef]
13. Kuroiwa Y, Nishikawa A, Kitamura Y, Kanki K, Ishii Y, Umemura T, and Hirose M. Protective effects of benzyl isothiocyanate and sulforaphane but not resveratrol against initiation of pancreatic carcinogenesis in hamsters. Cancer Lett. **241**: 275–280. 2006. [Medline] [CrossRef]
14. Siglin JC, Barch DH, and Stoner GD. Effects of dietary phenethyl isothiocyanate, ellagic acid, sulindac and calcium on the induction and progression of *N*-nitrosomethylbenzylamine-induced esophageal carcinogenesis in rats. Carcinogenesis. **16**: 1101–1106. 1995. [Medline] [CrossRef]
15. Stoner GD, Morrissey DT, Heur YH, Daniel EM, Galati AJ, and Wagner SA. Inhibitory effects of phenethyl isothiocyanate on *N*-nitrosobenzylmethylamine carcinogenesis in the rat esophagus. Cancer Res. **51**: 2063–2068. 1991. [Medline]
16. Stoner GD, and Gupta A. Etiology and chemoprevention of esophageal squamous cell carcinoma. Carcinogenesis. **22**: 1737–1746. 2001. [Medline] [CrossRef]
17. Nakamura Y, Iwahashi T, Tanaka A, Koutani J, Matsuo T, Okamoto S, Sato K, and Ohtsuki K. 4-(Methylthio)-3-butenyl isothiocyanate, a principal antimutagen in daikon (*Raphanus sativus*; Japanese white radish). J Agric Food Chem. **49**: 5755–5760. 2001. [Medline] [CrossRef]
18. Okamura T, Umemura T, Inoue T, Tasaki M, Ishii Y, Nakamura Y, Park EY, Sato K, Matsuo T, Okamoto S, Nishikawa A, and Ogawa K. Chemopreventive effects of 4-methylthio-3-butenyl Isothiocyanate (Raphasatin) but not curcumin against pancreatic carcinogenesis in hamsters. J Agric Food Chem. **61**: 2103–2108. 2013. [Medline] [CrossRef]
19. Nakamura Y, Nakamura K, Asai Y, Wada T, Tanaka K, Matsuo T, Okamoto S, Meijer J, Kitamura Y, Nishikawa A, Park EY, Sato K, and Ohtsuki K. Comparison of the glucosinolate-myrosinase systems among daikon (*Raphanus sativus*, Japanese white radish) varieties. J Agric Food Chem. **56**: 2702–2707. 2008. [Medline] [CrossRef]
20. Beevi SS, Mangamoori LN, Subathra M, and Edula JR.

Hexane extract of *Raphanus sativus* L. roots inhibits cell proliferation and induces apoptosis in human cancer cells by modulating genes related to apoptotic pathway. Plant Foods Hum Nutr. **65**: 200–209. 2010. [Medline] [CrossRef]

21. La Marca M, Beffy P, Della Croce C, Gervasi PG, Iori R, Puccinelli E, and Longo V. Structural influence of isothiocyanates on expression of cytochrome P450, phase II enzymes, and activation of Nrf2 in primary rat hepatocytes. Food Chem Toxicol. **50**: 2822–2830. 2012. [Medline] [CrossRef]

22. Scholl C, Eshelman BD, Barnes DM, and Hanlon PR. Raphasatin is a more potent inducer of the detoxification enzymes than its degradation products. J Food Sci. **76**: C504–C511. 2011. [Medline] [CrossRef]

23. Ben Salah-Abbès J, Abbès S, Ouanes Z, Abdel-Wahhab MA, Bacha H, and Oueslati R. Isothiocyanate from the Tunisian radish (*Raphanus sativus*) prevents genotoxicity of Zearalenone *in vivo* and *in vitro*. Mutat Res. **677**: 59–65. 2009. [Medline] [CrossRef]

24. Lu SH, Chui SX, Yang WX, Hu XN, Guo LP, and Li FM. Relevance of *N*-nitrosamines to oesophageal cancer in China. IARC Sci Publ. **105**: 11–17. 1991. [Medline]

25. Nolte T, Brander-Weber P, Dangler C, Deschl U, Elwell MR, Greaves P, Hailey R, Leach MW, Pandiri AR, Rogers A, Shackelford CC, Spencer A, Tanaka T, and Ward JM. Nonproliferative and proliferative lesions of the gastrointestinal tract, pancreas and salivary glands of the rat and mouse. J Toxicol Pathol. **29**(Suppl): 1S–125S. 2016. [Medline] [CrossRef]

26. Taniai E, Yafune A, Kimura M, Morita R, Nakane F, Suzuki K, Mitsumori K, and Shibutani M. Fluctuations in cell proliferation, apoptosis, and cell cycle regulation at the early stage of tumor promotion in rat two-stage carcinogenesis models. J Toxicol Sci. **37**: 1113–1126. 2012. [Medline] [CrossRef]

27. Akagi K, Sano M, Ogawa K, Hirose M, Goshima H, and Shirai T. Involvement of toxicity as an early event in urinary bladder carcinogenesis induced by phenethyl isothiocyanate, benzyl isothiocyanate, and analogues in F344 rats. Toxicol Pathol. **31**: 388–396. 2003. [Medline] [CrossRef]

28. Foster JR. Cell death and cell proliferation in the control of normal and neoplastic tissue growth. Toxicol Pathol. **28**: 441–446. 2000. [Medline] [CrossRef]

29. Ogawa K. Molecular pathology of early stage chemically induced hepatocarcinogenesis. Pathol Int. **59**: 605–622. 2009. [Medline] [CrossRef]

30. Lechner JF, Wang LS, Rocha CM, Larue B, Henry C, McIntyre CM, Riedl KM, Schwartz SJ, and Stoner GD. Drinking water with red beetroot food color antagonizes esophageal carcinogenesis in *N*-nitrosomethylbenzylamine-treated rats. J Med Food. **13**: 733–739. 2010. [Medline] [CrossRef]

31. Dutto I, Tillhon M, Cazzalini O, Stivala LA, and Prosperi E. Biology of the cell cycle inhibitor p21(CDKN1A): molecular mechanisms and relevance in chemical toxicology. Arch Toxicol. **89**: 155–178. 2015. [Medline] [CrossRef]

32. Sarkars R, Mukherjee S, and Roy M. Targeting heat shock proteins by phenethyl isothiocyanate results in cell-cycle arrest and apoptosis of human breast cancer cells. Nutr Cancer. **65**: 480–493. 2013. [Medline] [CrossRef]

33. Clarke JD, Hsu A, Yu Z, Dashwood RH, and Ho E. Differential effects of sulforaphane on histone deacetylases, cell cycle arrest and apoptosis in normal prostate cells versus hyperplastic and cancerous prostate cells. Mol Nutr Food Res. **55**: 999–1009. 2011. [Medline] [CrossRef]

34. Singh SV, Srivastava SK, Choi S, Lew KL, Antosiewicz J, Xiao D, Zeng Y, Watkins SC, Johnson CS, Trump DL, Lee YJ, Xiao H, and Herman-Antosiewicz A. Sulforaphane-induced cell death in human prostate cancer cells is initiated by reactive oxygen species. J Biol Chem. **280**: 19911–19924. 2005. [Medline] [CrossRef]

35. Evke E, Minbay FZ, Temel SG, and Kahveci Z. Immunohistochemical detection of p53 protein in basal cell skin cancer after microwave-assisted antigen retrieval. J Mol Histol. **40**: 13–21. 2009. [Medline] [CrossRef]

36. Wang D, Weghorst CM, Calvert RJ, and Stoner GD. Mutation in the *p53* tumor suppressor gene in rat esophageal papillomas induced by *N*-nitrosomethylbenzylamine. Carcinogenesis. **17**: 625–630. 1996. [Medline] [CrossRef]

37. Greenblatt MS, Bennett WP, Hollstein M, and Harris CC. Mutations in the *p53* tumor suppressor gene: clues to cancer etiology and molecular pathogenesis. Cancer Res. **54**: 4855–4878. 1994. [Medline]

38. Nguyen T, Nioi P, and Pickett CB. The Nrf2-antioxidant response element signaling pathway and its activation by oxidative stress. J Biol Chem. **284**: 13291–13295. 2009. [Medline] [CrossRef]

39. Yang CS, Smith TJ, and Hong JY. Cytochrome P-450 enzymes as targets for chemoprevention against chemical carcinogenesis and toxicity: opportunities and limitations. Cancer Res. **54**(Suppl): 1982s–1986s. 1994. [Medline]

40. FDA Estimating the maximum safe starting dose in initial clinical trials for therapeutics in adult healthy volunteers. Guidance for industry, Rockville. 2005. http://www.fda.gov/downloads/Drugs/guidancecomplianceregulatoryinformation/Guidances/UCM078932.pdf.

Original Article

Quercetin inhibited cadmium-induced autophagy in the mouse kidney via inhibition of oxidative stress

Yuan Yuan[1], Shixun Ma[2], Yongmei Qi[3], Xue Wei[3], Hui Cai[4*], Li Dong[5], Yufeng Lu[6], Yupeng Zhang[7], and Qingjin Guo[7]

[1] Department of Intensive Medicine, Gansu Provincial Hospital, 204 West Donggang Rd, Lanzhou, Gansu Province, 730000, China
[2] Department of General Surgery 1, Gansu Provincial Hospital, 204 West Donggang Rd, Lanzhou, Gansu Province, 730000, China
[3] Gansu Key Laboratory of Biomonitoring and Bioremediation for Environmental Pollution, School of Life Sciences, Lanzhou University, 222 South Tianshui Rd, Lanzhou, Gansu Province, 730000, China
[4] Medical Department, Gansu Provincial Hospital, 204 West Donggang Rd, Lanzhou, Gansu Province, 730000, China
[5] Department of Centrol Laboratory, Gansu Provincial Hospital, 204 West Donggang Rd, Lanzhou, Gansu Province, 730000, China
[6] Department of Obstetrics, Gansu Provincial Hospital, 204 West Donggang Rd, Lanzhou, Gansu Province, 730000, China
[7] Department of Oncological Surgery, Ningxia Medical University, 1160 South Shengli Rd, Yinchuan, Ningxia Province, 750000, China

Abstract: The objective of the current study was to explore the inhibitory effects of quercetin on cadmium-induced autophagy in mouse kidneys. Mice were intraperitoneally injected with cadmium and quercetin once daily for 3 days. The LC3-II/β-actin ratio was used as the autophagy marker, and autophagy was observed by transmission electron microscopy. Oxidative stress was investigated in terms of reactive oxygen species, total antioxidant capacity, and malondialdehyde. Cadmium significantly induced typical autophagosome formation, increased the LC3-II/β-actin ratio, reactive oxygen species level, and malondialdehyde content, and decreased total antioxidant capacity. Interestingly, quercetin markedly decreased the cadmium-induced LC3-II/β-actin ratio, reactive oxygen species levels, and malondialdehyde content, and simultaneously increased total antioxidant capacity. Cadmium can inhibit total antioxidant capacity, produce a large amount of reactive oxygen species, lead to oxidative stress, and promote lipid peroxidation, eventually inducing autophagy in mouse kidneys. Quercetin could inhibit cadmium-induced autophagy via inhibition of oxidative stress. This study may provide a theoretical basis for the treatment of cadmium injury. (DOI: 10.1293/tox.2016-0026; J Toxicol Pathol 2016; 29: 247–252)

Key words: quercetin, cadmium, autophagy, inhibition, mouse kidney

Introduction

Cadmium (Cd) is one of the most common toxic heavy metals[1]. It can harm human beings in various ways, and hence, prevention and treatment for Cd poisoning is of great significance[2, 3].

Autophagy is a conserved metabolic pathway in which cellular components can be degraded and reused by eukaryotic cells[4]. Microtubule-associated protein light chain 3 (LC3) is considered to be a characteristic protein of autophagy[3]. When autophagy is initiated, LC3 is enzymolysized into the cytosolic type (LC3-I), which then combines with phosphatidylethanolamine (PE) to transform into the membrane type (LC3-II)[5]. The level of autophagy can be estimated by detecting the LC3-II/β-actin ratio using western blotting[6]. Transmission electron microscopy is one of the best approaches to provide direct evidence for autophagy[2, 7]. On the other hand, autophagy is also morphologically defined, especially by transmission electron microscopy, as massive autophagic vacuolization of the cytoplasm (autophagosome)[8].

Recent studies showed that Cd can affect the body's (or cell's) antioxidant system[4], change the activity of antioxidant enzymes, and make the body (or cell) to produce a large amount of ROS, thus leading to oxidative stress[3, 9–11]. In addition, Cd can induce ROS-mediated autophagy of kidney cells via a series of pathways[2] and can induce mitophagy through the ROS-mediated PTEN-induced putative kinase 1/ Parkin (PINK1/Parkin) pathway in the kidneys of mice[1, 2].

Quercetin (3,3′,4',5,7-pentahydroxyavone) (Qu) and its derivatives are the most widely distributed plant kingdom flavonoids, which act as antioxidants by scavenging free radicals[12, 13]. Qu exerts its antioxidant effect by scavenging free radicals directly[12–15], and it is a renoprotective drug in Traditional Chinese Medicine (TCM). However, it is unknown whether Qu can inhibit Cd-induced autophagy in the

mouse kidney, and the underlying molecular mechanisms for such an effect have not been explored and reported.

Our study investigated how Qu inhibits Cd-induced autophagy in mouse kidneys.

Materials and Methods

Chemicals

Qu (99% purity) was purchased from Aladdin Chemical Reagent Plant (Shanghai, China). CdCl2 (99% purity) and dimethyl sulfoxide (DMSO) (99% purity) were obtained from Tianjin Chemical Reagent Plant (Tianjin, China). Sodium chloride injection (0.9%, NS) was purchased from Guangdong Otsuka Plant (Guangdong, China). A total antioxidant ability detection kit (FRAP method), BCA protein assay kit, and lipid peroxidation (MDA) detection kits were obtained from Beyotime Biotechnology Co. Ltd. (Jiangsu, China).

Animals

One-month-old male Kunming mice, weighing 22.0 ± 2.0 g were obtained from the Experimental Animal Research Center of Lanzhou University (Lanzhou, China). The mice were acclimated in the laboratory for one week before the experiments, maintained at a room temperature of 22–24°C with alternating 12 hour light/dark cycles, offered water and food ad libitum, and provided with adequate levels of lighting and humidity.

In the preliminary experiments, the mice were intraperitoneally injected with different concentrations of Cd (0.20, 0.40, 0.60, and 0.80 mg/kg bw/day) once daily for 1, 2, 3, and 5 days, and the LC3-II/β-actin ratio was determined. We found that autophagy was most obviously induced after 0.40 mg/kg bw/day Cd exposure for 3 days, and hence, 0.40 mg/kg bw/day Cd was selected for the following experiments.

Qu was initially dissolved in DMSO to make a 200 mg/kg stock solution (pure), diluted to twice the required concentration with pure DMSO, blended with the same volume of NS or 0.8 mg/kg Cd before use, and finally used after cooling to room temperature.

Mice were randomly divided into a control group, Cd-treated group, and co-treated groups (treated with 0, 5, 15, 25, 50, 75, and 100 mg/kg bw/day Qu and 0.4 mg/kg bw/day Cd), each of which contained 8 mice. The mice were intraperitoneally injected with NS, 0.40 mg/kg bw/day Cd, and different concentrations of mixed solutions of Qu and Cd in the same proportion (5 µl/g bw/day) once daily for 3 days. The detailed scheme of mouse treatments is described in Table 1.

The physical condition of the animals was monitored for 25 minutes three times per day. All mice showed good activity levels and feeding, with no obvious change in body weight, and did not exhibit any special symptoms.

On the 4th day, all mice were intraperitoneally injected with xylazine (100 mg/kg bw). After anesthesia, the chest and abdomen were opened, and the heart was perfused with

Table1. The Detailed Scheme of Mouse Treatments

Groups	Treatments
Control group	0.9% sodium chloride injection (NS)
Cd-treated group	0.40 mg/kg bw/day Cd
Co-treated groups	0 mg/kg bw/day Qu and 0.4 mg/kg bw/day Cd
	5 mg/kg bw/day Qu and 0.4 mg/kg bw/day Cd
	15 mg/kg bw/day Qu and 0.4 mg/kg bw/day Cd
	25 mg/kg bw/day Qu and 0.4 mg/kg bw/day Cd
	50 mg/kg bw/day Qu and 0.4 mg/kg bw/day Cd
	75 mg/kg bw/day Qu and 0.4 mg/kg bw/day Cd
	100 mg/kg bw/day Qu and 0.4 mg/kg bw/day Cd

10 mL of PBS buffer (cold at 4°C, pH 7.4). The kidney was removed and fascia was peeled[13]. All experiments were performed in accordance the Guidelines for Care and Use of Animals at Lanzhou University.

Transmission electron microscopy

Tissues from the kidney cortex of the control and Cd-treated group of mice were cut into $0.3 \times 0.3 \times 0.3$ cm³ blocks and fixed with 1 ml of 2.5% glutaraldehyde. The fixative was replaced with fresh liquid every 24 h until the samples were sent to the electron microscope facility of Lanzhou University. The samples were then postfixed in OsO4, dehydrated in ethanol and acetone, and embedded in resin. Ultrathin sections (60–70 nm) were cut and mounted on pioloform-coated copper grids (Plano). Sections were stained with lead citrate and uranyl acetate and viewed with a transmission electron microscope (JEOL JEM-1230, JEOL Ltd., Japan) operated at 80 kV. Micrographs were taken using a Gatan Erlangshen ES500W camera.

Measurement of ROS

The renal cortex tissues were collected in 1.5 mL centrifuge tubes, and finely cut. PBS (cold at 4°C, pH 7.4) was added to the samples, filtered with 200-mesh stainless steel mesh, centrifuged at 500 rpm for 8 min, and then washed twice with PBS. The cells were counted and adjusted to 1×10^6 cells/mL in each tube, and 1 mL of 10 µM 2,7-dichloro-dihydrofluorescein diacetate (DCFH-DA) was added. Then the contents within each tube were mixed, and the tubes were incubated at 37°C for 30 min. The samples were then centrifuged at 1,000 rpm for 5 min, washed three times, and filtered with a 200-mesh nylon membrane into a flow tube. ROS were analyzed using flow cytometry (FCM) (BD Biosciences, Franklin Lakes, NJ, USA) at the excitation and emission settings for FITC (excitation 488 nm, emission 525 nm). At least 5,000 cells were detected, and all of the above operations were carried out on ice. The incubation process required dark conditions and was completed within 4 h.

Preparation of tissue homogenates

A suitable amount of the kidney cortex tissues (about 200 mg from each group) was transferred into 1.5 mL centrifuge tubes to make tissue homogenates. The samples were frozen by immersion in liquid nitrogen for 30 s and

then mashed. This was followed by the addition of 1 mL 1× PBS buffer and 10 μL 0.1 mM PMSF solution, mixing of the contents within each tube, and pulverization with a SCIENTZ-IID ultrasonic cell crushing apparatus (total time, 10 min; open, 5 s; close, 5 s; power, 25%). The samples were centrifuged at 12,000 *g* for 10 min at 4°C, and the supernatant was collected; the precipitate was discarded. The tissue homogenates were diluted 20-fold, and the protein concentration was detected with a bicinchoninnc acid (BCA) protein assay kit. The prepared tissue homogenates were used to detect the total protein concentration, total antioxidant capacity (T-AOC), and MDA and for western blotting (all of the operations were carried out on ice).

Western blotting

Electrophoresis protein samples and tissue homogenates were prepared at appropriate sample volumes based on the protein concentration. Protein samples were separated by SDS-PAGE (15% gel; 60 V for 30 min and then 120 V for 90 min). The protein was transferred onto 0.22-μm polyvinylidene fluoride (PVDF) membranes (electric current 200 mA, 90 min), which were blocked with 5% skimmed milk powder solution (27°C, 60 min). The PVDF membranes were cut into two parts; one part was used for incubation (4°C, overnight) with anti-LC3 (1:2,000, mouse monoclonal, Sigma-Aldrich, St. Louis, MO, USA), and the other one was use for incubation (4°C, overnight) with anti-β-actin (1:2,000, rabbit polyclonal, Sigma-Aldrich). The membranes were washed three times with Tris Buffered Saline with Tween-20 (TBST) buffer and then incubated with horseradish peroxidase (HRP)-conjugated secondary antibodies (27°C, 60 min), anti-mouse (1:20,000, goat polyclonal, ZhongShan Golden Bridge Biotechnology, Beijing, China) or anti-rabbit (1:20,000, goat polyclonal, ZhongShan Golden Bridge Biotechnology), and LC3 and β-actin were detected with the Immobilon Western Chemiluminescent HRP Substrate (Millipore, Billerica, MA, USA).

Detection kits

Detection of total protein concentration, MDA, and T-AOC was carried out according to the manufacturer's instructions. The standard curves were prepared, and then the concentrations of the substances in the test samples were measured and presented as the content of the samples.

Statistical analysis

The results were processed with the Excel 2003, Origin 75, FlowJo 7.6, ImageJ, and iSee software. Data were expressed as mean ± SD values (n = 8). Statistical comparisons were made using one-way analysis of variance (ANOVA) followed by the least significant difference (LSD) post hoc test. All statistical analyses were performed using the SPSS 17.0. Differences were considered significant at $P<0.05$ and highly significant at $P<0.01$[1].

Results

Cd induced autophagy in the mouse kidney

To quantify autophagy progression, we detected conversion of the cellular protein LC3-I to LC3-II (autophagy marker). In preliminary experiments, mice were intraperitoneally injected with different concentrations of Cd (0.20, 0.40, 0.60, and 0.80 mg/kg bw/day) once daily for 1, 2, 3, and 5 days. Compared with control exposure, exposure to 0.20, 0.40, 0.60, and 0.80 mg/kg bw/day Cd for 3 days markedly elevated the LC3-II/β-actin ratio 1.35-, 1.47-, 1.31-, and 1.27-fold in the kidneys of mice ($P<0.05$ except for 0.40 mg/kg bw/day Cd, in which case $P<0.01$), respectively (Fig. 1A). Therefore, 0.40 mg/kg bw/day Cd was selected for the following experiments.

Compared with control exposure, exposure to 0.4 mg/kg bw/day Cd induced typical double-membrane and lamellar autophagosomes in the epithelia of proximal tubules after 3 days of treatment (Fig. 1B). Multiple typical autophagosomes were found in the perinuclear area, and the mitochondria were contained in autophagic vacuoles.

Qu inhibited Cd-induced autophagy in the mouse kidney

Mice were injected with NS or Cd (0.40 mg/kg bw/day) alone or in combination with Qu (0, 5, 15, 25, 50, 75, and 100 mg/kg bw/day) for 3 days, and then the LC3-I, LC3-II, and β-actin levels were determined by western blotting. Compared with control exposure, 0.40 mg/kg bw/day Cd exposure for 3 days markedly elevated the LC3-II/β-actin ratio in the kidneys of mice ($P<0.01$). There was no significant difference in the LC3-II/β-actin ratio in the kidneys ($P>0.05$) between the Cd-treated group and the mice co-treated with Qu (0 mg/kg bw/day). Among the Qu co-treated groups, the groups treated with 5, 15, 25, 50, 75, and 100 mg/kg bw/day Qu for 3 days showed markedly reduced LC3-II/β-actin ratios (1.15-, 1.24-, 1.47-, 1.43-, 1.41-, and 1.26-fold), in the kidneys ($P<0.01$ except for 5 mg/kg bw/day Qu exposure, in which case $P<0.05$) respectively (Fig. 2).

Qu inhibited Cd-induced autophagy in mouse kidney cells via inhibition of oxidative stress

The mice were injected with NS or Cd (0.40 mg/kg bw/day), alone or in combination with Qu (0, 5, 15, 25, 50, 75, and 100 mg/kg bw/day), for 3 days, and then the T-AOC and MDA were determined with detection kits. The levels of ROS in the mouse kidney were determined by FCM.

Compared with control exposure, 0.40 mg/kg bw/day Cd exposure for 3 days markedly reduced the T-AOC in the kidneys of mice ($P<0.01$). Compared with the Cd-treated group, the mice in the Qu (0 mg/kg bw/day) co-treated group showed no significant difference ($P>0.05$) in the T-AOC in the kidneys. Among the Qu co-treated groups, the groups treated with 5, 15, 25, 50, 75, and 100 mg/kg bw/day Qu for 3 days showed an obvious improvement in the T-AOC in the kidneys of mice ($P<0.01$ except for 5 mg/kg bw/day Qu exposure, in which case $P<0.05$) (Fig. 3A).
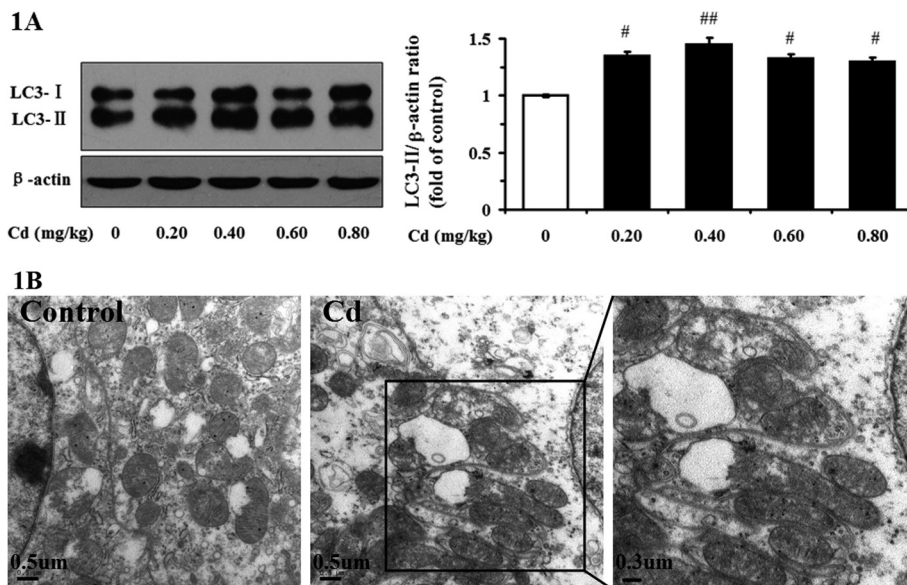
1A

1B

Fig. 1. Cd induced autophagy in the mouse kidney. The mice were received either NS (control, 0 mg/kg bw/day) or a daily intraperitoneal injection of Cd (0.20, 0.40, 0.60, and 0.80 mg/kg bw/day) once daily for 3 days. (1A) LC3-I, LC3-II, and β-actin levels were detected by western blotting. (1B) (Cd 0.40 mg/kg bw/day) Transmission electron microscopy showed double-membrane and lamellar mitophagosomes in the epithelia of proximal tubules. Data are presented as mean ± SD values (n = 8). #, ##Significantly different from the control group at P<0.05 and P<0.01, respectively.
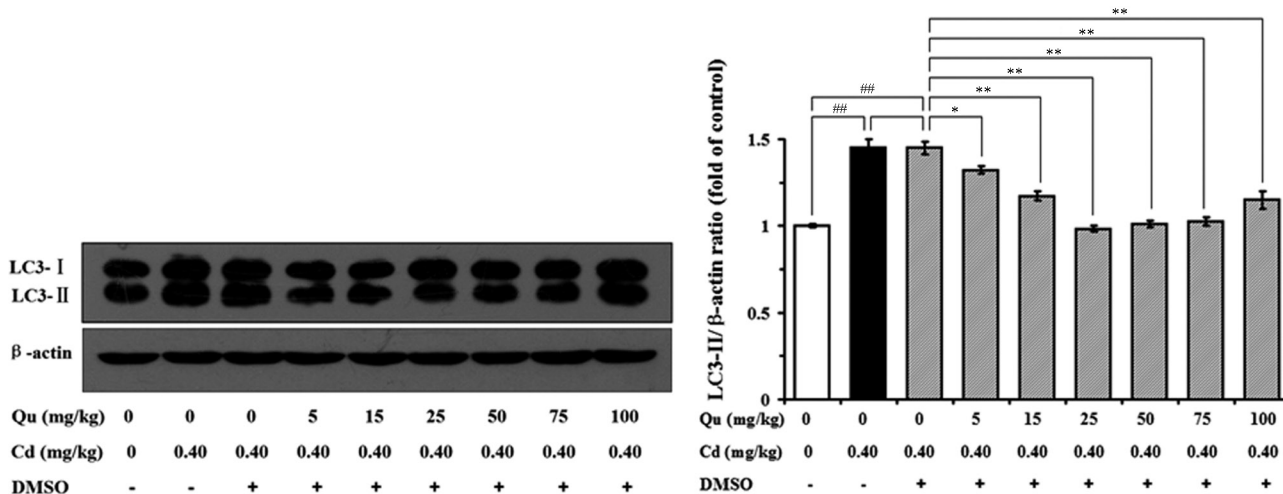
Fig. 2. Qu inhibited Cd-induced autophagy in the mouse kidney. The mice were injected with NS or Cd (0.40 mg/kg bw/day) alone or in combination with Qu (0, 5, 15, 25, 50, 75, and 100 mg/kg bw/day) once daily for 3 days, and then the LC3-I and LC3-II levels were detected by western blotting. Data are presented as mean ± SD values (n = 8). #, ##Significantly different from the control group at P<0.05 and P<0.01, respectively. *, **Significantly different from the Qu (0 mg/kg bw/day) co-treated group at P<0.05 and P<0.01, respectively.

Compared with control exposure, 0.40 mg/kg bw/day Cd exposure for 3 days markedly elevated the MDA levels in the kidneys of mice (P<0.01). Compared with the Cd-treated group, the mice in the Qu (0 mg/kg bw/day) co-treated group showed no significant difference (P>0.05) in the MDA levels in the kidneys. Among the Qu co-treated groups, the groups treated with 5, 15, 25, 50, 75, and 100 mg/kg bw/day Qu for 3 days showed markedly reduced the MDA levels in the kidneys (P<0.01) (Fig. 3B).

It was also found that, 0.40 mg/kg bw/day Cd exposure for 3 days markedly elevated the levels of ROS in the kidneys of mice (P<0.01). There was no significant difference in ROS levels in the kidneys of mice between the Cd-treated group and Qu (0 mg/kg bw/day) co-treated groups (P>0.05). Among the Qu co-treated groups, the groups treated with 5, 15, 25, 50, 75, and 100 mg/kg bw/day Qu for 3 days showed markedly reduced ROS levels in the kidneys (P<0.01) (Fig. 3C).
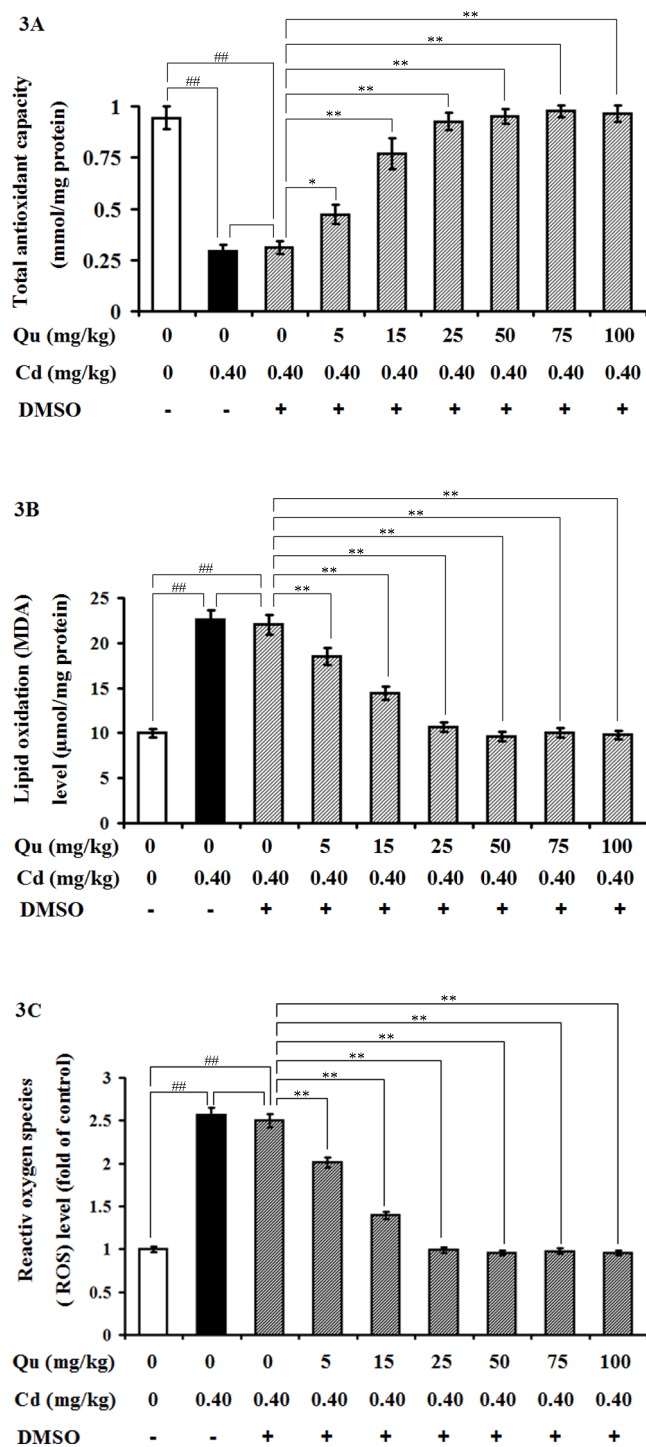
Fig. 3. Qu inhibited Cd-induced autophagy in mouse kidney cells via inhibition of oxidative stress. The mice were injected with Cd (0.40 mg/kg bw/day) alone or in combination with Qu (0, 5, 15, 25, 50, 75, and 100 mg/kg bw/day) once daily for 3 days, and then the total antioxidant capacity (3A) and lipid oxidation levels (MDA) (3B) were detected with detection kits. The levels of ROS (3C) in the mouse kidney were detected by flow cytometry (FCM). Data are presented as mean ± SD values (n = 8). [#, ##]Significantly different from the control group at P<0.05 and P<0.01, respectively. [*, **]Significantly different from the Qu (0 mg/kg bw/day) co-treated group at P<0.05 and P<0.01, respectively.

Discussion

Acute or chronic exposure to Cd can damage many organs, with the kidney being the most sensitive and vulnerable one[16, 17]. Previous studies have shown that Cd can cause damage to renal tubular epithelial cells[18]. Specifically, Cd could trigger cellular damages such as necrosis, apoptosis, and autophagy[19]. Relatively high concentrations of Cd can induce apoptosis and necrosis in general, while low concentration can cause autophagy[2, 12].

Autophagy is an adaptive mechanism that responds to changing environmental stimuli, such as starvation and oxidative stress. Therefore, signal transduction can promote cell survival[20]. Under cellular homeostasis conditions, autophagy plays a housekeeping role in the circulation of cytoplasmic components and protein[21]. Under stress conditions, cells remove harmful particles and protein aggregates through autophagy to prevent cell death[22]. However, autophagic cell death can occur when a large number of cells are destroyed and cleared[12]. Autophagy is related to numerous physiological and pathological processes, including cell survival, cell death, cell metabolism, development, infection, immunity, and aging[11, 23, 24]. It has also been found to be closely involved in the etiology of many important human diseases, including cancer, neurodegenerative diseases, and metabolic disorders[5, 22].

In this study, mice were intraperitoneally injected with Cd (5 µl/g bw/day) for 3 days to establish a Cd-induced mouse kidney autophagy model successfully (Fig. 1 and Fig. 2). Moreover, 0.40 mg/kg Cd induced autophagy most obviously (P<0.01). DMSO was used to dissolve quercetin, and 7 concentrations of quercetin (0, 5, 15, 25, 50. 75 and 100 mg/kg) were chosen for the experiments. DMSO was selected to dissolve Qu because there was no difference in LC3-II/β-actin ratio between the Cd-treated group and a Qu (0 mg/kg bw/day) co-treated group (50% DMSO did not affect the LC3-II/β-actin ratio). When the concentration of Qu was more than 100 mg/kg, Qu could not dissolve in 50% DMSO. In the co-treatment group, each concentration of Qu was combined with 0.4 mg/kg Cd and intraperitoneally injected into the mice for 3 days. We found that 5 to 100 mg/kg Qu inhibited Cd-induced autophagy in mouse kidney cells (P<0.05) and that the inhibitory effect of quercetin at the dose of 25 mg/kg was highly significant (P<0.01, Fig. 2).

The results showed that Cd significantly induced typical autophagosome formation (Fig 1B), increased the LC3-II/β-actin ratio (Fig. 1A and Fig. 2), enhanced ROS levels (Fig. 3C) and MDA content (Fig. 3B), and decreased the T-AOC (Fig. 3A). Qu markedly decreased the Cd-induced LC3-II/β-actin ratio (Fig. 2), ROS levels (Fig. 3C), and MDA content (Fig. 3B), but it simultaneously increased the T-AOC (Fig. 3A).

The results indicated that Cd inhibited the T-AOC of mouse kidneys, induced production of a large amount of ROS, leading to oxidative stress, and promoted intracellular lipid oxidation, eventually leading to autophagy in mouse kidney cells. Qu might reduce the generation of ROS in cells to inhibit oxidative stress and inhibit intracellular lipid oxi-

dation, ultimately inhibiting the autophagy of mouse kidney cells induced by cadmium via an increase in the T-AOC of the mouse kidney.

Taken together, the findings suggest that Qu may play a protective role in Cd-induced mouse kidney injury through its antioxidant activity. This study provides a theoretical basis for treatment of Cd injury. Qu may have some protective effects on the kidney by decreasing Cd-induced injury and may have certain social and economic benefits.

Disclosure of Potential Conflicts of Interest: The authors declare that there are no conflicts of interest.

References

1. Wei X, Qi Y, Zhang X, Qiu Q, Gu X, Tao C, Huang D, and Zhang Y. Cadmium induces mitophagy through ROS-mediated PINK1/Parkin pathway. Toxicol Mech Methods. **24**: 504–511. 2014. [Medline] [CrossRef]

2. Chargui A, Zekri S, Jacquillet G, Rubera I, Ilie M, Belaid A, Duranton C, Tauc M, Hofman P, Poujeol P, El May MV, and Mograbi B. Cadmium-induced autophagy in rat kidney: an early biomarker of subtoxic exposure. Toxicol Sci. **121**: 31–42. 2011. [Medline] [CrossRef]

3. Wei X, Qi Y, Zhang X, Gu X, Cai H, Yang J, and Zhang Y. ROS act as an upstream signal to mediate cadmium-induced mitophagy in mouse brain. Neurotoxicology. **46**: 19–24. 2015. [Medline] [CrossRef]

4. Chiarelli R, and Roccheri MC. Heavy metals and metalloids as autophagy inducing agents: focus on cadmium and arsenic. Cells. **1**: 597–616. 2012. [Medline] [CrossRef]

5. Debnath J, Baehrecke EH, and Kroemer G. Does autophagy contribute to cell death? Autophagy. **1**: 66–74. 2005. [Medline] [CrossRef]

6. Huber TB, Edelstein CL, Hartleben B, Inoki K, Jiang M, Koya D, Kume S, Lieberthal W, Pallet N, Quiroga A, Ravichandran K, Susztak K, Yoshida S, and Dong Z. Emerging role of autophagy in kidney function, diseases and aging. Autophagy. **8**: 1009–1031. 2012. [Medline] [CrossRef]

7. Toyokuni S. Molecular mechanisms of oxidative stress-induced carcinogenesis: from epidemiology to oxygenomics. IUBMB Life. **60**: 441–447. 2008. [Medline] [CrossRef]

8. Son YO, Wang X, Hitron JA, Zhang Z, Cheng S, Budhraja A, Ding S, Lee JC, and Shi X. Cadmium induces autophagy through ROS-dependent activation of the LKB1-AMPK signaling in skin epidermal cells. Toxicol Appl Pharmacol. **255**: 287–296. 2011. [Medline] [CrossRef]

9. Cuypers A, Plusquin M, Remans T, Jozefczak M, Keunen E, Gielen H, Opdenakker K, Nair AR, Munters E, Artois TJ, Nawrot T, Vangronsveld J, and Smeets K. Cadmium stress: an oxidative challenge. Biometals. **23**: 927–940. 2010. [Medline] [CrossRef]

10. Gibellini L, Pinti M, Nasi M, Montagna JP, De Biasi S, Roat E, Bertoncelli L, Cooper EL, and Cossarizza A. Quercetin and cancer chemoprevention. Evid Based Complement Alternat Med. **2011**: 591356. 2011. [Medline] [CrossRef]

11. Boots AW, Drent M, de Boer VC, Bast A, and Haenen GR. Quercetin reduces markers of oxidative stress and inflammation in sarcoidosis. Clin Nutr. **30**: 506–512. 2011. [Medline] [CrossRef]

12. Ishisaka A, Ichikawa S, Sakakibara H, Piskula MK, Nakamura T, Kato Y, Ito M, Miyamoto K, Tsuji A, Kawai Y, and Terao J. Accumulation of orally administered quercetin in brain tissue and its antioxidative effects in rats. Free Radic Biol Med. **51**: 1329–1336. 2011. [Medline] [CrossRef]

13. Wang K, Liu R, Li J, Mao J, Lei Y, Wu J, Zeng J, Zhang T, Wu H, Chen L, Huang C, and Wei Y. Quercetin induces protective autophagy in gastric cancer cells: involvement of Akt-mTOR- and hypoxia-induced factor 1α-mediated signaling. Autophagy. **7**: 966–978. 2011. [Medline] [CrossRef]

14. Zhong J, Guo D, Chen CB, Wang W, Schuster M, Loibner H, Penninger JM, Scholey JW, Kassiri Z, and Oudit GY. Prevention of angiotensin II-mediated renal oxidative stress, inflammation, and fibrosis by angiotensin-converting enzyme 2. Hypertension. **57**: 314–322. 2011. [Medline] [CrossRef]

15. Jing Y, Liu LZ, Jiang Y, Zhu Y, Guo NL, Barnett J, Rojanasakul Y, Agani F, and Jiang BH. Cadmium increases HIF-1 and VEGF expression through ROS, ERK, and AKT signaling pathways and induces malignant transformation of human bronchial epithelial cells. Toxicol Sci. **125**: 10–19. 2012. [Medline] [CrossRef]

16. Forbes JM, Coughlan MT, and Cooper ME. Oxidative stress as a major culprit in kidney disease in diabetes. Diabetes. **57**: 1446–1454. 2008. [Medline] [CrossRef]

17. Manu KA, Shanmugam MK, Ramachandran L, Li F, Siveen KS, Chinnathambi A, Zayed ME, Alharbi SA, Arfuso F, Kumar AP, Ahn KS, and Sethi G. Isorhamnetin augments the anti-tumor effect of capeciatbine through the negative regulation of NF-κB signaling cascade in gastric cancer. Cancer Lett. **363**: 28–36. 2015. [Medline] [CrossRef]

18. Karimi MM, Sani MJ, Mahmudabadi AZ, Jafarisani A, and Khatibi SR. Effect of acute toxicity of cadmium in mice kidney cells. Iran J Toxicol. **6**: 691–698. 2012.

19. Golab F, Kadkhodaee M, Zahmatkesh M, Hedayati M, Arab H, Schuster R, Zahedi K, Lentsch AB, and Soleimani M. Ischemic and non-ischemic acute kidney injury cause hepatic damage. Kidney Int. **75**: 783–792. 2009. [Medline] [CrossRef]

20. Prozialeck WC, and Edwards JR. Mechanisms of cadmium-induced proximal tubule injury: new insights with implications for biomonitoring and therapeutic interventions. J Pharmacol Exp Ther. **343**: 2–12. 2012. [Medline] [CrossRef]

21. Chaabane W, User SD, El-Gazzah M, Jaksik R, Sajjadi E, Rzeszowska-Wolny J, and Los MJ. Autophagy, apoptosis, mitoptosis and necrosis: interdependence between those pathways and effects on cancer. Arch Immunol Ther Exp (Warsz). **61**: 43–58. 2013. [Medline] [CrossRef]

22. Cagnol S, and Chambard JC. ERK and cell death: mechanisms of ERK-induced cell death--apoptosis, autophagy and senescence. FEBS J. **277**: 2–21. 2010. [Medline] [CrossRef]

23. Circu ML, and Aw TY. Glutathione and modulation of cell apoptosis. Biochim Biophys Acta. **1823**: 1767–1777. 2012. [Medline] [CrossRef]

24. Chuang SY, Lin CH, and Fang JY. Natural compounds and aging: between autophagy and inflammasome. BioMed Res Int. **2014**: 297293. 2014. [Medline] [CrossRef]

Original Article

Celecoxib alleviates oxaliplatin-induced hyperalgesia through inhibition of spinal ERK1/2 signaling

Hongping Chen[1, 2], Qinghua Wang[1], Danni Shi[1], Dongbo Yao[1], Lei Zhang[1], Junping Xiong[3], and Baohua Xu[4*]

[1] Department of Histology and Embryology, Medical College, Nanchang University, Bayi Road 461, Nanchang 330006, China
[2] Jiangxi Province Key Laboratory of Tumor Pathogen's and Molecular Pathology, Bayi Road 461, Nanchang 330006, China
[3] Department of Human Anatomy, Medical College, Nanchang University, Bayi Road 461, Nanchang 330006, China
[4] Department of Animal Science, Medical College, Nanchang University, Bayi Road 461, Nanchang 330006, China

Abstract: Numerous pieces of evidence have revealed that oxaliplatin (OXA) evokes mechanical and cold hypersensitivity. However, the mechanism underlying these bothersome side effects needs to be further investigated. It is well known that cyclooxygenase-2 (COX-2) and extracellular signal-regulated kinases (ERK1/2) signaling play crucial roles in several pain states. Our previous data showed that Akt2 in the dorsal root ganglion (DRG) participated in the regulation of OXA-induced neuropathic pain. But it is still unclear whether spinal ERK1/2 signaling is involved in the regulation of OXA-induced hyperalgesia, and the linkage between COX-2 and ERK1/2 signaling in mediating OXA-induced hyperalgesia also remains unclear. In this research, we investigated the possible mechanism of celecoxib, a COX-2 inhibitor, in OXA-induced neuropathic pain. Our results show that single dose of OXA (12 mg/kg) significantly attenuated both the tail withdrawal latency (TWL) and mechanical withdrawal threshold (MWT) at days 4 after the OXA treatment. Administration of celecoxib (30 mg/kg/day) for 4 and 6 days inhibited the decrease in TWL and MWT, and each was significantly higher than that of the OXA+vehicle group and was equivalent to that of the vehicles group. OXA increased the expression of cyclooxygenase-2 (COX-2) mRNA and phosphorylated extracellular signal-regulated kinase1/2 (pERK1/2) protein in the lumbar 4-5 (L4-5) spinal cord dorsal horn neurons. Administration of celecoxib for 7 days suppressed the increase in expression of COX-2 and pERK1/2 induced by OXA. Our findings suggested that COX-2 and ERK1/2 signaling in spinal cord contributed to the OXA-induced neuropathic pain. (DOI: 10.1293/tox.2016-0032; J Toxicol Pathol 2016; 29: 253–259)

Key words: oxaliplatin, cyclooxygenase-2, pERK1/2, neuropathic pain, celecoxib

Introduction

Oxaliplatin (OXA), a third-generation platinum-based chemotherapy agent, is considered a central component in the treatment of advanced colorectal cancer[1]. OXA treatment has prolonged the lives of many people diagnosed in advanced stages of the colorectal cancer. Despite its efficacy, there are numerous adverse effects associated with OXA. Neurotoxicity is a common adverse effect of oxaliplatin that usually presents as peripheral neuropathy. The development of a neuropathic syndrome impairs quality of life and potentially results in chemotherapy dose reductions and/or early discontinuation[2, 3]. There are 2 forms of OXA-induced neurotoxicity: acute neuropathy and chronic

neuropathy. The acute form occurs in >90% of patients and may begin during the infusion or within hours of completion. Chronic neuropathy is cumulative and is most commonly seen in patients who have received doses of 540 mg/m^{2} or more[4].

Accumulating studies have reported the important role of OXA in inducing cold and mechanical allodynia. Many studies have focused on the side effects of OXA in the dorsal root ganglion (DRG), which contains the cell bodies of the primary sensory neurons responsible for transduction and modulation of sensory information and transmission of it to the spinal cord[5, 6]. Our previous research also indicate that celecoxib alleviates OXA-induced neuropathic pain through inhibiting of the PI3K/Akt2 pathway in the mouse DRG[7]. Recently, an increasing number of data suggested that spinal pathological responses are evoked by OXA, contributing to hyperalgesia. OXA contributes to neuropathic pain through the activation of glias[8, 9]. OXA-induced mechanical allodynia is associated with spinal NMDA receptor subunit NR2B upregulation, while selective NR2B antagonists Ro25-6981 and ifenprodil attenuate the OXA-induced pain behaviors[10]. Milnacipran, a serotonin–noradrenaline reuptake inhibitor,

is effective against OXA-induced mechanical allodynia, and the anti-allodynic effect is mainly mediated by actions on the spinal cord[11]. Moreover, bee venom acupuncture treatment alleviates OXA-induced acute cold allodynia in rats via activation of the serotonergic system, especially spinal 5-HT3 receptors[12].

It is well known that cyclooxygenase-2 (COX-2) and extracellular signal-regulated kinases (ERK1/2) signaling play crucial roles in several pain states[13, 14]. In the present study, we explored the expression levels of COX-2 and ERK1/2 in L4-5 segments of the spinal cord, from which the hind limb receives innervations, of OXA-treated mice. The roles of the COX-2 inhibitor celecoxib in OXA-induced pain behaviors and its underlying mechanisms were also investigated. It is hoped than our novel understanding of OXA-induced neurotoxicity in cancer therapy will provide a new therapeutic strategy to prevent hyperalgesia.

Materials and Methods

Animals

Adult Male C57BL/6J mice (10 weeks old; 49–51 passages from the original colony) were provided by the Center of Laboratory Animal Science of Nanchang University. The mice were fed a standard laboratory diet under controlled temperature and a 12-h light/dark cycle at 20–22°C. All experimental procedures were approved by the Institutional Animal Care and Use Committee of the Medical College of Nanchang University and were performed in accordance with the principles outlined in the National Institutes of Health Guide for the Care and Use of Laboratory Animals.

Experimental protocols

Mice were randomly divided into 3 groups, with 10 mice in each group: a vehicles group, an OXA+vehicle group, and an OXA+celecoxib (30 mg/kg/day) group. In the OXA+vehicle group and the OXA+celecoxib group, the mice were injected intraperitoneally with single doses of 12 mg/kg body weight of OXA (Qilu Pharmaceutical Co., Ltd, Jinan, China) dissolved in 5% glucose solution on day 0 (d0). Celecoxib was dissolved in 0.5% methylcellulose vehicle (Sigma-Aldrich, St Louis, MO, USA) and was delivered twice daily by oral gavage for 7 days, beginning on d1. The same volume of 5% glucose solution was intraperitoneally injected in the vehicles group. The mice in the vehicles and the OXA+vehicle groups were delivered the same volume of 0.5% methylcellulose according to the procedure for the OXA+celecoxib group. The dosage of celecoxib (30 mg/kg/day) was chosen according to a previous report[7]. This dose of celecoxib was an effective level against the neuropathic pain-induced by OXA. The pain behaviors were tested once every 2 days from d0 before OXA administration to d8. They were tested every day beginning 24h after first dose of celecoxib.

OXA treatment is a well characterized model used for studying neuropathic pain. Based on the OXA concentration used, there are generally two ways to induce hyperalgesia: long-term treatment with a low dose of OXA for [15, 16] and short-term treatment with high dose of OXA[7, 17]. In this study, the dosage of OXA was chosen according to a previous report[6]. A single dose of a high concentration of OXA was used to induce hyperalgesia. In brief, single doses of 12 mg/kg body weight of OXA were injected intraperitoneally. At d8, all the mice were deeply anesthetized with pentobarbital sodium (100 mg/kg sodium pentobarbital, i.p.) and sacrificed by decapitation.

Cold-sensitivity detection

The behavioral signs of cold allodynia were measured by a tail immersion test in cold water. Each mouse was lightly immobilized in a plastic holder, and its tail was dipped in cold water. The tail was immersed in 4°C water, and then the tail withdrawal latency (TWL) was counted. The tail immersion test was repeated 3 times at 5 min intervals. The average latency was taken as a measure for the severity of cold allodynia. All behavioral tests were performed blind.

Mechanical-sensitivity detection

Mechanical allodynia measurement was carried out as previously described[18]. In brief, the mechanical withdrawal threshold (MWT) was determined to evaluate mechanical hyperalgesia using calibrated von Frey filaments (BME-403, Institute of Biomedical Engineering, Tianjin, China). The measurement was repeated 3 times at 30 s intervals. The average was taken as the mechanical withdrawal threshold. All behavioral tests were performed blind.

Real-time PCR quantification

The whole spinal cord was collected by pressure expulsion with ice cold saline. The dorsal and ventral parts of the L4-5 spinal cord were dissected on an ice cooled glass dish. Total RNA from L4-5 spinal cord dorsal segments was isolated using TRIzol (Invitrogen, Carlsbad, CA, USA) according to the manufacturer's protocol. Reverse transcription was performed using 1,000 ng total RNA as a template and a Applied Biosystems Reverse Transcription Kit (Applied Biosystems, Foster City, CA, USA). Real-time quantitative PCR for COX-2 was performed using an ABI 7500 Real-Time PCR System (Applied Biosystems, Foster City, CA, USA). The expression level of COX-2 was normalized to GAPDH. The probe was purchased from Applied Biosystems. All assays were performed in triplicate. The average fold change relative to the vehicles group was calculated in each group.

Immunohistochemistry

Spinal cord segments of L4-5 were analyzed from 6 mice in each group. The formalin-fixed, paraffin-embedded tissues were cut, and sections (5 μm thick) were used for immunohistochemistry (IHC) detection. Six nonadjacent sections from each specimen of the L4-5 spinal cord were selected. IHC was carried out as previously described[19], using primary antibodies against pERK1/2 (1:100; Santa Cruz Biotechnology, Dallas, TX, USA). A rabbit kit (PV-6001,
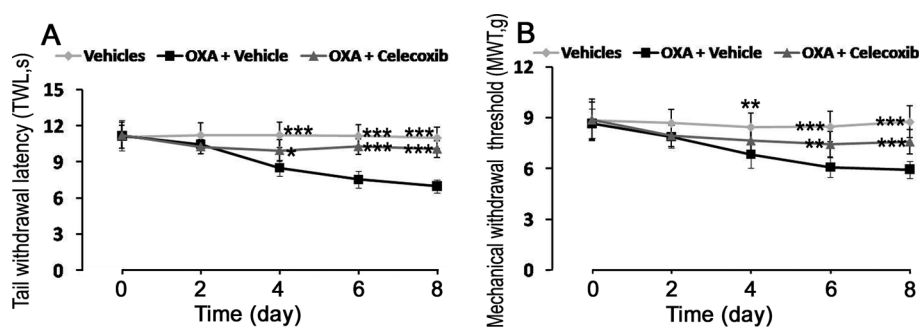
Fig. 1. Effects of celecoxib on OXA-induced cold and mechanical hypersensitivity. (A) Celecoxib attenuated the cold hypersensitivity induced by OXA. (B) Celecoxib attenuated the mechanical hypersensitivity induced by OXA. Data are showed as the mean ± SD (n = 10). *$P<0.05$; **$P<0.01$; and ***$P<0.001$ (all vs the OXA+vehicle group).

ZSGB-BIO, Beijing, China) was used as a secondary antibody according to the maufacture's instructions. Protein localization was detected following incubation with diaminobenzidine and H_2O_2 for 2 min. Finally, sections were dehydrated in graded alcohols and mounted with neutral balsam. The numbers of pERK1/2-positive neurons from one side of spinal cord dorsal horn of each mouse were counted. Data from 6 sections of the same mouse were averaged.

Western blot

L4-5 spinal cord dorsal segments were homogenized in radioimmunoprecipitation assay (RIPA) buffer. Samples of 30 µg of total protein were separated by 10% SDS-polyacrylamide gel electrophoresis and transferred onto a polyvinylidene difluoride membrane. After incubation with primary antibody pERK1/2 (1:1,000; Santa Cruz Biotechnology, Dallas, TX, USA) or total extracellular signal-regulated kinase1/2 (tERK,1:1,000; Cell Signaling Technology, Danvers, MA, USA), the membrane was incubated with peroxidase conjugated secondary antibodies (Cell Signaling Technology, Danvers, MA, USA). Immunodetection was completed using Pierce-enhanced chemiluminescence substrate (Thermo Scientific, Waltham, MA, USA), and the membrane was then exposed to X-ray film. The average fold change relative to the vehicles group was calculated in each group.

Statistical analysis

Data are shown as the mean ± SD. Comparisons of means between two groups were carried out using a *t*-test. Statistical comparisons were performed by analysis of variance (ANOVA) with Dunnett's test for multiple comparisons. A value of $P<0.05$ was considered to be significant.

Results

Celecoxib attenuated the cold and mechanical hypersensitivity induced by OXA

The TWL and MWT were measured to evaluate the effects of celecoxib on pain behaviors of OXA-treated mice. The results showed that both the TWL and MWT thresholds significantly decreased in the OXA+vehicle group (8.50 s and 6.83 g, respectively) when compared with the vehicles group (11.22 s and 8.46 g, respectively) at d4 and remained at low levels. At d8, the TWL and MWT thresholds (6.97 s and 5.93 g, respectively) were still lower when compared with those of the vehicles group (Fig. 1). Celecoxib significantly increased the TWL threshold (from 8.50 s to 9.95 s) beginning at d4. At d6, The TWL threshold continued to increase. Celecoxib significantly upregulated the MWT threshold (from 6.07 g to 7.45 g) beginning at d6. At d8, both the TWL and MWT thresholds still were upregulated by celecoxib (Fig. 1). The results suggested that celecoxib alleviated the OXA-induced pain behaviors.

Celecoxib decreased pERK1/2-positive neurons in the L4-5 spinal cord dorsal horn

The immunoreactivity of pERK1/2 was detected using immunohistochemistry. The results showed that OXA increased the number of pERK1/2-positive neurons from 8.67 to 30.67 neurons and that administration of celecoxib efficiently decreased the number of pERK1/2-positive neurons from 30.67 to 15.17 neurons (Fig. 2). The results imply that ERK1/2 signaling may be involved in the regulation of OXA-induced hypersensitivity.

Celecoxib suppressed the OXA-induced COX-2 mRNA expression

COX-2 mRNA was detected by real-time PCR. COX-2 mRNA expression was significantly upregulated (2.10 folds) in the OXA+vehicle group as compared with the vehicles group. Administration of celecoxib significantly suppressed the expression of COX-2 mRNA compared with the OXA+vehicle group (Fig. 3).

Celecoxib downregulated the level of OXA-induced pERK1/2 protein

To investigate the potential mechanism of celecoxib in reversing of OXA-induced hyperalgesia in term of protein level, the pERK1/2 protein was measured by Western blot. The level pERK1/2 protein significantly increased to 261% in the OXA+vehicle group as compared with the vehicles
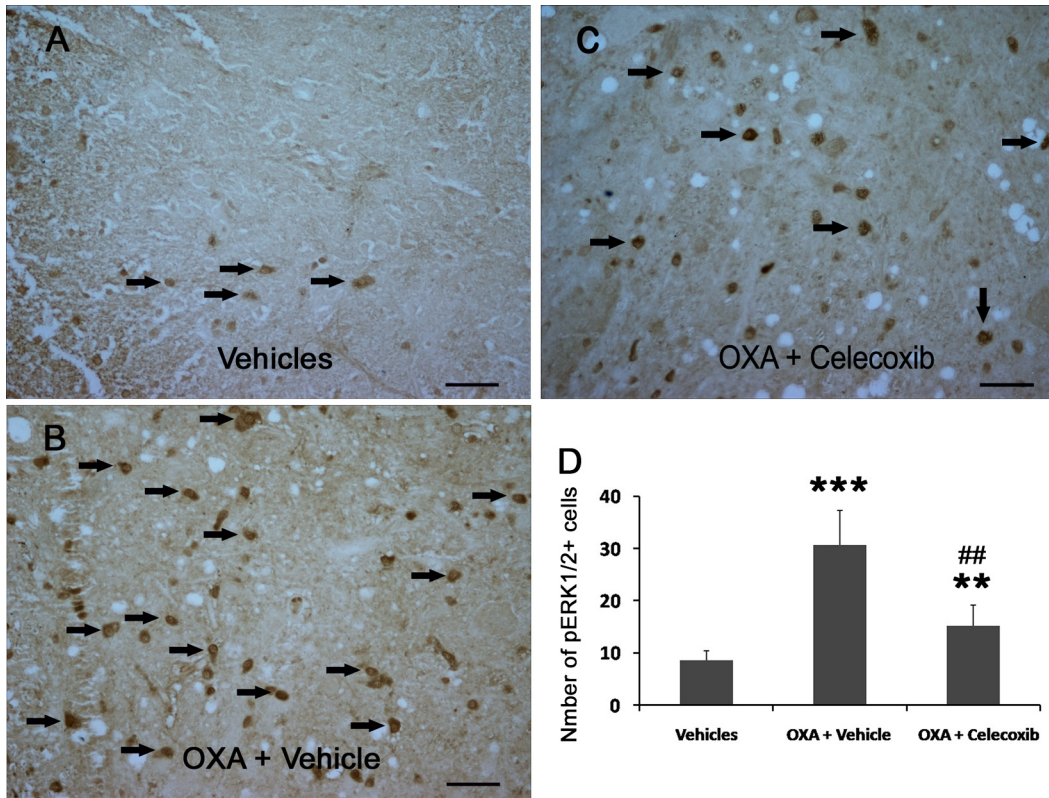
Fig. 2. Celecoxib decreased pERK1/2-positive neurons in the L4-5 spinal cord dorsal horn of OXA-treated mice. (A–C) pERK1/2 immunoreactivities (brown) were detected. Arrowheads indicate representative pERK1/2-positive neurons. Scale bar is 40 μm. (D) The numbers of pERK1/2-positive neurons on one side of the L4-5 spinal cord dorsal horn. Data are shown as the mean ± SD (n = 6). **$P<0.01$; ***$P<0.001$ (both vs the vehicles group). ##$P<0.01$ (vs the OXA+vehicle group).
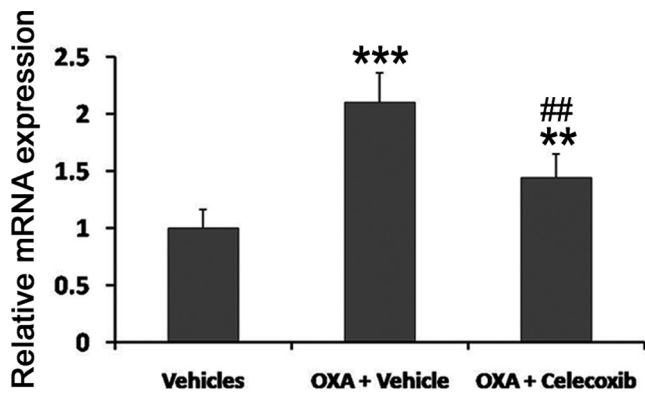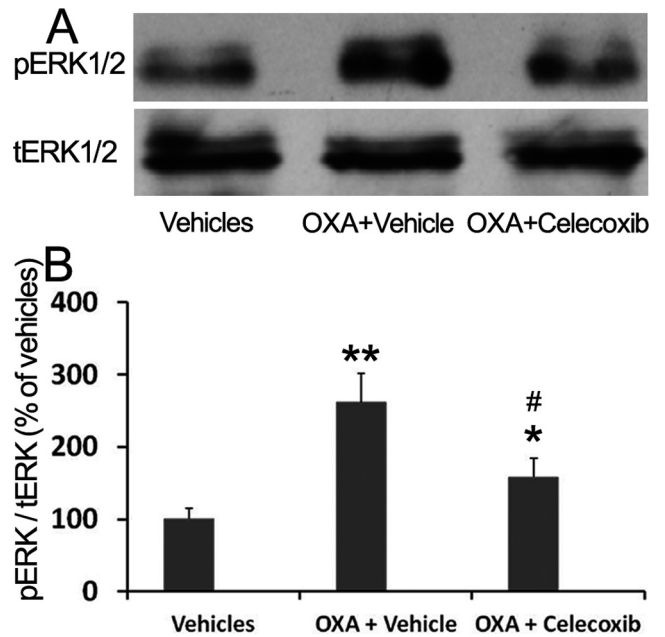

Fig. 3. OXA increased the COX-2 mRNA in L4-5 spinal cord dorsal horn. COX-2 mRNA was detected by real-time PCR. Data are shown as the mean ± SD (n = 6). **$P<0.01$; ***$P<0.001$ (both vs the vehicles group). ##$P<0.01$ (vs the OXA+vehicle group).

Fig. 4. Celecoxib decreased the expression of pERK1/2 protein in the L4-5 spinal cord dorsal horn of OXA-treated mice. pERK1/2 protein was measured by Western blot. Data are shown as the mean ± SD (n = 4). *$P<0.05$; **$P<0.01$ (both vs the vehicles group). #$P<0.05$ (vs the OXA+vehicle group).

group. Administration of celecoxib significantly decreased pERK1/2 protein expression (Fig. 4). These data further illustrated that the spinal COX-2 and pERK1/2 pathway mediated OXA-induced hypersensitivity.

Discussion

The present study demonstrated the following novel findings: (1) Administration of oxaliplatin (OXA) increased spinal cyclooxygenase-2 (COX-2) mRNA and ERK1/2 protein. (2) Celecoxib suppressed the COX-2 and ERK1/2 pathway in the spinal cord of OXA-treated mice. (3) Celecoxib alleviated OXA-induced hyperalgesia through inhibition of spinal pERK1/2 protein. These results reveal a critical role of spinal COX-2 and ERK1/2 signaling in OXA-induced neuropathic pain.

Neuropathic pain, arising from lesions to peripheral nerves, is present in many neurological diseases and occurs in patients with diabetes, cancer, and AIDS. Moreover, it is frequently induced by chemotherapy[20]. It is caused by an injury to the peripheral or central nervous system. Characteristic features of neuropathic pain are hyperalgesia, allodynia, and spontaneous pain. Numerous pieces of evidence have shown that upregulation of spinal pain mediators and related receptors contributes to neuropathic pain[21, 22].

Nonsteroidal anti-inflammatory drugs (NSAIDs) are strong cyclooxygenase (COX) inhibitors that are widely used in the management of acute and inflammatory pain. Two isoforms of COX, COX-1 and COX-2, are targets of NSAIDs. A variety of studies have shown that COX-2 inhibitors play a pivotal role in neuropathic pain. Ibuprofen attenuates hyperalgesia following chronic constriction injury by suppressing the expression of P2X3 receptors in the DRG[23]. Celecoxib produces an antihyperalgesic and antiallodynic effect in diabetic rats[24]. Furthermore, spinal COX-2 contributes to neuropathic pain. Spinal nerve ligation causes mechanical allodynia, which is accompanied by increased expression of spinal COX-2 immunoreactivity[25]. Intrathecal administrations of the COX-2 inhibitors attenuate streptozotocin-induced mechanical hyperalgesia through inhibition of spinal COX-2 protein[13]. It has been revealed that the COX-2 inhibitor celecoxib can inhibit tumor growth and enhance the anti-tumor effect of OXA through their synergistic role in inhibiting different targets[26].

However, the effects of spinal COX-2 on OXA-induced neuropathic pain are poorly understood. In the present investigation, we found that administration of celecoxib could alleviate both mechanical and cold hypersensitivity induced by OXA through inhibition of spinal COX-2 mRNA. Our findings may provide a clinically useful evidence for the dual roles of celecoxib in cancer therapy: enhancing the anti-tumor effect of OXA and alleviating OXA-induced hyperalgesia.

Chemotherapy-induced peripheral neuropathy could trigger the pathophysiological changes in the spinal cord, as evidenced by neuroinflammatory processes including the release of pro-inflammatory cytokines[27]. OXA increases production of pro-inflammatory and neuroexcitatory cytokines (TNF, IL-1b) in the dorsal horn of the spinal cord[28]. COX-2, an inflammatory mediator, increases in the spinal cord dorsal horn neurons following L5 spinal nerve ligation[25]. Our previous data show that OXA can increase the expression of COX-2 in the DRG[7]. In the present study, we also found that OXA increased the COX-2 mRNA expression in the spinal dorsal horn. However, administration of 2.4 mg/kg OXA for 5 consecutive days every week for 3 weeks slightly increased the expression of COX-2 protein, with no significant difference in the rat spinal cord[15]. Therefore, OXA increased the spinal COX-2 level in a dose-dependent manner. The mechanisms of the OXA-induced increase in COX-2 mRNA are still not clear and need to be further investigated.

The mitogen-activated protein kinase (MAPK) cascade is a highly conserved module that is involved in various pathological functions, including neuropathic pain[29, 30]. At least four members of the MAPK family, ERK1/2, JNK, p38, and ERK5, have been identified[31]. The role of spinal ERKs in nociception had been explored in the recent years. It is reported that the immunoreactivity of pERK1/2 can be used as a quantitative marker for sensitization or inhibition in the pain pathway at the spinal level[14].

It has been revealed that COX-2 is involved in the regulation of MAP kinase signaling. The p-ERK Level is downregulated after celecoxib treatment in the cirrhotic liver model of rats[32]. The COX-2 inhibitor parecoxib exerts its analgesic effect on surgical pain through inhibition of neuronal ERK activation in the spinal cord[33]. In the present study, we investigated the role of spinal ERK1/2 signaling in OXA-induced neuropathic pain. OXA increased the expression of pERK1/2 in the spinal dorsal horn neurons while celecoxib alleviated the OXA-induced hyperalgesia accompanied by the downregulation of pERK1/2. Thus, spinal ERK1/2 plays a vital role in OXA-induced neuropathic pain.

In conclusion, our study was the first to show that COX-2 and pERK1/2 were increased within the spinal cord after administration of OXA. A COX-2 inhibitor alleviated the neuropathic pain caused by OXA through inhibition of COX-2 and pERK1/2. These data illustrated that OXA can induce neuropathic pain, and this role of OXA was mediated by the COX-2 and pERK1/2 pathway.

Disclosure of Potential Conflicts of Interest: We have no conflicts of interest.

References

1. Petrioli R, Licchetta A, Roviello G, Pascucci A, Francini E, Bargagli G, Conca R, Miano ST, Marzocca G, and Francini G. Multidisciplinary Oncology Group On Gastrointestinal Tumors CEA and CA19.9 as early predictors of progression in advanced/metastatic colorectal cancer patients receiving oxaliplatin-based chemotherapy and bevacizumab. Cancer Invest. **30**: 65–71. 2012. [Medline] [CrossRef]

2. Xiao WH, and Bennett GJ. Effects of mitochondrial poisons on the neuropathic pain produced by the chemotherapeutic agents, paclitaxel and oxaliplatin. Pain. **153**: 704–709. 2012. [Medline] [CrossRef]

3. Brouwers EE, Huitema AD, Boogerd W, Beijnen JH, and Schellens JH. Persistent neuropathy after treatment with cisplatin and oxaliplatin. Acta Oncol. **48**: 832–841. 2009. [Medline] [CrossRef]

4. Cersosimo RJ. Oxaliplatin-associated neuropathy: a review. Ann Pharmacother. **39**: 128–135. 2005. [Medline] [CrossRef]

5. Mi Y, Zhang X, Zhang F, Qi J, Gao H, Huang D, Li L, Zhang H, and Du X. The role of potassium channel activation in celecoxib-induced analgesic action. PLoS One. **8**: e54797. 2013. [Medline] [CrossRef]

6. Chen H, Wang Q, Lei Q, Zhang L, and Kang L. Ontogenic expression profiles and oxaliplatin regulation of leptin expression in mice dorsal root ganglion. Neuroreport. **26**: 870–876. 2015. [Medline] [CrossRef]

7. Jiang SP, Zhang ZD, Kang LM, Wang QH, Zhang L, and Chen HP. Celecoxib reverts oxaliplatin-induced neuropathic pain through inhibiting PI3K/Akt2 pathway in the mouse dorsal root ganglion. Exp Neurol. **275**: 11–16. 2016. [Medline] [CrossRef]

8. Di Cesare Mannelli L, Pacini A, Bonaccini L, Zanardelli M, Mello T, and Ghelardini C. Morphologic features and glial activation in rat oxaliplatin-dependent neuropathic pain. J Pain. **14**: 1585–1600. 2013. [Medline] [CrossRef]

9. Di Cesare Mannelli L, Pacini A, Micheli L, Tani A, Zanardelli M, and Ghelardini C. Glial role in oxaliplatin-induced neuropathic pain. Exp Neurol. **261**: 22–33. 2014. [Medline] [CrossRef]

10. Mihara Y, Egashira N, Sada H, Kawashiri T, Ushio S, Yano T, Ikesue H, and Oishi R. Involvement of spinal NR2B-containing NMDA receptors in oxaliplatin-induced mechanical allodynia in rats. Mol Pain. **7**: 8. 2011. [Medline] [CrossRef]

11. Andoh T, Kitamura R, and Kuraishi Y. Milnacipran inhibits oxaliplatin-induced mechanical allodynia through spinal action in mice. Biol Pharm Bull. **38**: 151–154. 2015. [Medline] [CrossRef]

12. Lee JH, Li DX, Yoon H, Go D, Quan FS, Min BI, and Kim SK. Serotonergic mechanism of the relieving effect of bee venom acupuncture on oxaliplatin-induced neuropathic cold allodynia in rats. BMC Complement Altern Med. **14**: 471. 2014. [Medline] [CrossRef]

13. Matsunaga A, Kawamoto M, Shiraishi S, Yasuda T, Kajiyama S, Kurita S, and Yuge O. Intrathecally administered COX-2 but not COX-1 or COX-3 inhibitors attenuate streptozotocin-induced mechanical hyperalgesia in rats. Eur J Pharmacol. **554**: 12–17. 2007. [Medline] [CrossRef]

14. Donnerer J, and Liebmann I. pERK1/2 immunofluorescence in rat dorsal horn and paraventricular nucleus neurons as a marker for sensitization and inhibition in the pain pathway. Tissue Cell. **47**: 55–60. 2015. [Medline] [CrossRef]

15. Di Cesare Mannelli L, Pacini A, Corti F, Boccella S, Luongo L, Esposito E, Cuzzocrea S, Maione S, Calignano A, and Ghelardini C. Antineuropathic profile of N-palmitoylethanolamine in a rat model of oxaliplatin-induced neurotoxicity. PLoS One. **10**: e0128080. 2015. [Medline] [CrossRef]

16. Renn CL, Carozzi VA, Rhee P, Gallop D, Dorsey SG, and Cavaletti G. Multimodal assessment of painful peripheral neuropathy induced by chronic oxaliplatin-based chemotherapy in mice. Mol Pain. **7**: 29. 2011. [Medline] [CrossRef]

17. Ohsawa M, Otake S, Murakami T, Yamamoto S, Makino T, and Ono H. Gabapentin prevents oxaliplatin-induced mechanical hyperalgesia in mice. J Pharmacol Sci. **125**: 292–299. 2014. [Medline] [CrossRef]

18. Li X, Kang L, Li G, Zeng H, Zhang L, Ling X, Dong H, Liang S, and Chen H. Intrathecal leptin inhibits expression of the P2X2/3 receptors and alleviates neuropathic pain induced by chronic constriction sciatic nerve injury. Mol Pain. **9**: 65. 2013. [Medline] [CrossRef]

19. Chen HP, Zhou W, Kang LM, Yan H, Zhang L, Xu BH, and Cai WH. Intrathecal miR-96 inhibits Nav1.3 expression and alleviates neuropathic pain in rat following chronic construction injury. Neurochem Res. **39**: 76–83. 2014. [Medline] [CrossRef]

20. Cavaletti G. Chemotherapy-induced peripheral neurotoxicity (CIPN): what we need and what we know. J Peripher Nerv Syst. **19**: 66–76. 2014. [Medline] [CrossRef]

21. Barragán-Iglesias P, Pineda-Farias JB, Cervantes-Durán C, Bravo-Hernández M, Rocha-González HI, Murbartián J, and Granados-Soto V. Role of spinal P2Y6 and P2Y11 receptors in neuropathic pain in rats: possible involvement of glial cells. Mol Pain. **10**: 29. 2014. [Medline] [CrossRef]

22. Lim G, Wang S, Zhang Y, Tian Y, and Mao J. Spinal leptin contributes to the pathogenesis of neuropathic pain in rodents. J Clin Invest. **119**: 295–304. 2009. [Medline]

23. Wang Y, Zhang X, Guo QL, Zou WY, Huang CS, and Yan JQ. Cyclooxygenase inhibitors suppress the expression of P2X(3) receptors in the DRG and attenuate hyperalgesia following chronic constriction injury in rats. Neurosci Lett. **478**: 77–81. 2010. [Medline] [CrossRef]

24. Juárez-Rojop IE, Morales-Hernández PE, Tovilla-Zárate CA, Bermúdez-Ocaña DY, Torres-Lopez JE, Ble-Castillo JL, Díaz-Zagoya JC, and Granados-Soto V. Celecoxib reduces hyperalgesia and tactile allodynia in diabetic rats. Pharmacol Rep. **67**: 545–552. 2015. [Medline] [CrossRef]

25. Lau YM, Wong SC, Tsang SW, Lau WK, Lu AP, and Zhang H. Cellular sources of cyclooxygenase-1 and -2 up-regulation in the spinal dorsal horn after spinal nerve ligation. Neuropathol Appl Neurobiol. **40**: 452–463. 2014. [Medline] [CrossRef]

26. Zhao S, Cai J, Bian H, Gui L, and Zhao F. Synergistic inhibition effect of tumor growth by using celecoxib in combination with oxaliplatin. Cancer Invest. **27**: 636–640. 2009. [Medline] [CrossRef]

27. Zhang H, Yoon SY, Zhang H, and Dougherty PM. Evidence that spinal astrocytes but not microglia contribute to the pathogenesis of Paclitaxel-induced painful neuropathy. J Pain. **13**: 293–303. 2012. [Medline] [CrossRef]

28. Janes K, Wahlman C, Little JW, Doyle T, Tosh DK, Jacobson KA, and Salvemini D. Spinal neuroimmune activa-

tion is independent of T-cell infiltration and attenuated by A3 adenosine receptor agonists in a model of oxaliplatin-induced peripheral neuropathy. Brain Behav Immun. **44**: 91–99. 2015. [Medline] [CrossRef]

29. Crown ED. The role of mitogen activated protein kinase signaling in microglia and neurons in the initiation and maintenance of chronic pain. Exp Neurol. **234**: 330–339. 2012. [Medline] [CrossRef]

30. Stenberg L, Kanje M, Mårtensson L, and Dahlin LB. Injury-induced activation of ERK 1/2 in the sciatic nerve of healthy and diabetic rats. Neuroreport. **22**: 73–77. 2011. [Medline] [CrossRef]

31. Nishimoto S, and Nishida E. MAPK signalling: ERK5 versus ERK1/2. EMBO Rep. **7**: 782–786. 2006. [Medline] [CrossRef]

32. Gao JH, Wen SL, Yang WJ, Lu YY, Tong H, Huang ZY, Liu ZX, and Tang CW. Celecoxib ameliorates portal hypertension of the cirrhotic rats through the dual inhibitory effects on the intrahepatic fibrosis and angiogenesis. PLoS One. **8**: e69309. 2013. [Medline] [CrossRef]

33. Guo YJ, Shi XD, Fu D, Yang Y, Wang YP, and Dai RP. Analgesic effects of the COX-2 inhibitor parecoxib on surgical pain through suppression of spinal ERK signaling. Exp Ther Med. **6**: 275–279. 2013. [Medline]

Case Report

Acute alloxan toxicity causes granulomatous tubulointerstitial nephritis with severe mineralization

Lianshan Zhang[1], Yui Terayama[2], Taiki Nishimoto[3], Yasushi Kodama[3], and Kiyokazu Ozaki[2]*

[1] Department of Pathology, Hebei Medical University, 361 Zhongshan East Road, Shijiazhuang 050017, China

[2] Laboratory of Pathology, Faculty of Pharmaceutical Sciences, Setsunan University, 45-1 Nagaotoge-cho, Hirakata, Osaka 573-0101, Japan

[3] Laboratory of Clinicopathological Therapeutics, Faculty of Pharmaceutical Sciences, Hiroshima International University, 5-1-1 Hirokoshinkai, Kure, Hiroshima 737-0112, Japan

Abstract: Alloxan had been recognized as having a direct nephrotoxic effect different from its diabetogenic action. We encountered previously unreported granulomatous tubulointerstitial nephritis with severe luminal and interstitial mineralization in one diabetic rat after one week of alloxan administration. Histopathologically, many dilated and occluded proximal and distal tubules were segmentally observed in the cortex and outer medulla. The tubular lumen contained minerals and cell debris. Tubular epithelial cells were degenerated and piled up, and they protruded into the lumen, where they enveloped minerals. Mineralization was observed mainly in the tubular lumen, and to some extent in the subepithelium and interstitium. The mineralization beneath the tubular epithelium was often continuous from the subepithelium to the interstitium. In these lesions, the tubular basement membrane was disrupted by mineralization, and a granuloma with multinuclear foreign-body giant cells was formed in the interstitial areas. (DOI: 10.1293/tox.2016-0017; J Toxicol Pathol 2016; 29: 261–264)

Key words: alloxan, tubular necrosis, mineralization, granuloma, rat

The alloxan-induced type 1 diabetic rat is one of the most commonly used experimental animal models of diabetes. Prior to inducing a prolonged diabetic state, alloxan causes acute tubulointerstitial nephritis, consequently leading to nephrotoxicity and animal deaths[1–3]. There are only a few reports on severe luminal and interstitial mineralization induced by alloxan[2]. Herein, we report a case of granulomatous tubulointerstitial nephritis with severe luminal and interstitial mineralization in an alloxan-induced rat and describe its pathological features.

Six-week-old Wistar/Crlj male rats were purchased from Charles River Laboratories Japan, Inc., and reared in a barrier-sustained animal room maintained at a temperature of 23 ± 2°C and a relative humidity of 55 ± 10% with 12-h light/dark cycles and ventilation at least 10 times/h with high-efficiency particulate air-filtered fresh air. Twelve rats were administered a single dose of alloxan (50 mg/kg) by intravenous injection at 7 weeks of age. Rats other than the case showed no apparent clinical symptoms or renal

histological changes except the diabetic condition, and all rats were sacrificed at 7 days after alloxan administration. One rat experienced a gradual reduction in body weight accompanied by both a reduction in food intake and urine volume following alloxan injection. Its kidneys were fixed in 10% phosphate-buffered formalin, dehydrated, and then embedded in paraffin. Sections (4 μm thick) were stained with hematoxylin and eosin, PAS reaction, and Von Kossa's method. For immunohistochemical examination, the sections were deparaffinized in xylene and rehydrated through graded ethanol series. The rehydrated sections were microwaved in 10 mM citrate buffer (pH 6.0) for 10 min at 98°C to retrieve the antigen. Solutions and washes were prepared between the various steps using 0.05 M Tris buffered saline (TBS, pH 7.6) with 0.01% Tween 20. Nonspecific endogenous peroxidase activity was blocked by exposure to 0.03% hydrogen peroxide in 100% methanol for 5 min, and masking was conducted with 1% goat or horse normal serum in Tris buffered saline for 5 min at room temperature. Incubation was carried out overnight at 4°C with anti-aquaporin 1 (AQP1) rabbit polyclonal antibody (diluted 1:500, AB2219, Millipore, Billerica, MA, USA), anti-sodium/potassium ATPase subunit alpha 1 (Na/K pump) mouse monoclonal antibody (diluted 1:1,000, 05-369, Millipore) and anti-Iba1 rabbit polyclonal antibody (diluted 1:500, 019-19741, Wako Pure Chemical Industries, Osaka, Japan). These slides were subsequently rinsed with TBS plus Tween 20, treated for 30 min at room temperature with biotinylated secondary

antibody (Vectastain Elite kit, PK6102, PK6101, Vector Laboratories, Burlingame, CA, USA), rinsed with TBS plus Tween 20, incubated for 30 min at room temperature with Vectastain Elite ABC reagent (Vectastain Elite kit, PK6102, PK6101, Vector Laboratories), rinsed with TBS plus Tween 20, incubated in diaminobenzidine solution containing 0.01% hydrogen peroxide for the peroxidase coloring reaction, and counterstained with Mayer's hematoxylin.

Grossly, both the kidneys were enlarged. Other organs and tissues had no gross findings. Histologically, both the kidneys showed similar lesions. Many dilated and occluded tubules were segmentally observed in the cortex and outer medulla (Fig. 1). Degeneration and necrosis of tubular epithelial cells were seen along with tubular obstruction due to cell debris and mineralization (Fig. 2). Dilated regenerated tubules were lined with flattened and attenuated epithelia in basophilic cytoplasm. These tubular epithelial cells often piled up, formed small cell clusters, and protruded into the lumen. In some tubules, protruded tubular epithelial cells enveloped minerals (Fig. 3). The mineralization was confirmed as calcium salts using Von Kossa's method (Fig. 4) and was observed in the tubular lumen, subepithelium, and interstitium (Fig. 2), but apparent mineralization of the arterial wall was not seen. The mineralization beneath the tubular epithelium was often continuous from the subepithelium to the interstitium. In these lesions, the tubular basement membrane was sometimes disrupted by mineralization (Fig. 5), and multinuclear foreign-body giant cells and macrophages often infiltrated (Fig. 2). Multinuclear foreign-body giant cells were usually located around minerals, and they often contained minerals in their cytoplasm (Fig. 2). Double staining with PAS and Iba1 confirmed that Iba1-positive macrophages infiltrated from the interstitium to the subepithelial mineralization area, penetrating the basal lamina (Fig. 6). Many degenerated and regenerated tubules did not have a brush border, but some dilated and degenerated tubules did. Both the Na/K pump-positive distal tubules and AQP1-positive proximal tubules (Fig. 7) showed degenerative changes. However, severely damaged tubules did not express either AQP1 or the Na/K pump.

The nephrotoxic effect of alloxan had been recognized long before its diabetogenic action was identified[1–3]. Renal changes included extensive swelling and vacuolar degeneration of tubular cells, necrosis of tubular cells, tubular dilation, and cellular infiltrates resembling granulomas in the interstitium from the third day to fourteenth day following alloxan administration[2]. Renal damage may lead to uremia and death. In this report, the histologic changes observed in an alloxan-induced diabetic rat resembled those in previous reports[2], and they were likely due to the nephrotoxicity of alloxan.

Unlike previous reports, to the best of our knowledge, severe mineralization was not found in the rat with alloxan-induced nephrotoxicity. In the present case, mineralization of calcium salts located in the tubular lumen and beneath the tubular epithelium resulted in the formation of granulomas in the interstitial and tubular regions. As the continuity of mineralization between the tubule and the interstitium was apparent, it is possible that translocation of minerals from the tubular lumen to the interstitium occurred, a process that has been well demonstrated for calcium oxalate (CaOx) crystals (crystalline nephritis)[4–8]. The crystals of CaOx generally form in the renal tubules. If crystals come in contact with renal epithelial cells, they are endocytosed and moved to lysosomes for removal or moved from the luminal to the basolateral side between the cells and the basement membrane[4–8]. They are subsequently transported to the renal interstitium, where macrophages eliminate them while inducing an inflammatory and foreign body reaction[4]. In our case, the features of the protruded granuloma with mineralization and the continuity of mineralization between the tubule and the interstitium resembled a granuloma with crystals in crystalline nephritis. Thus, the unique pathologic features of our case may also be caused by the translocation of minerals from the tubular lumen to the interstitium. However, it is well-known that mineralization occurs in tubules, the tubular lumen, and the interstitium of the kidney as dystrophic calcification in rats including those of the Wister strain[9]. In addition, although apparent mineralization of the arterial wall was not seen, metastatic calcification as a result of systemic calcium/phosphorus imbalance may occur in the kidney. Thus, the possibility that mineralization simultaneously occurred in the tubules, tubular lumen, and interstitium as a dystrophic or metastatic calcification cannot be ruled out. Further study will be needed to clarify the mechanism of mineralization.

Alloxan is a small molecule that resembles glucose, binds the GLUT-2 glucose transporter, and can enter cells via the GLUT2 glucose transporter[10, 11]. It generates superoxide and hydroxyl radicals; since beta cells have relatively weak defenses against oxidative stress, they are especially sensitive to free radical-mediated damage by alloxan and undergo necrotic cell death within 48 hours postinjection[12]. The GLUT2 glucose transporter is expressed in beta cells, hepatocytes, renal tubular cells, and small intestinal epithelial cells[12]. This transporter of renal tubules is mainly located at the basolateral membrane of proximal tubular epithelial cells. If alloxan induced tubular damage via GLUT2, only the proximal tubule would be damaged. However, in our case, both the Na/K pump-positive distal tubules and the AQP1-positive proximal tubules showed degenerative changes. Thus, the renal toxicity of alloxan may involve other mechanisms independent of the GLUT2 glucose transporter.
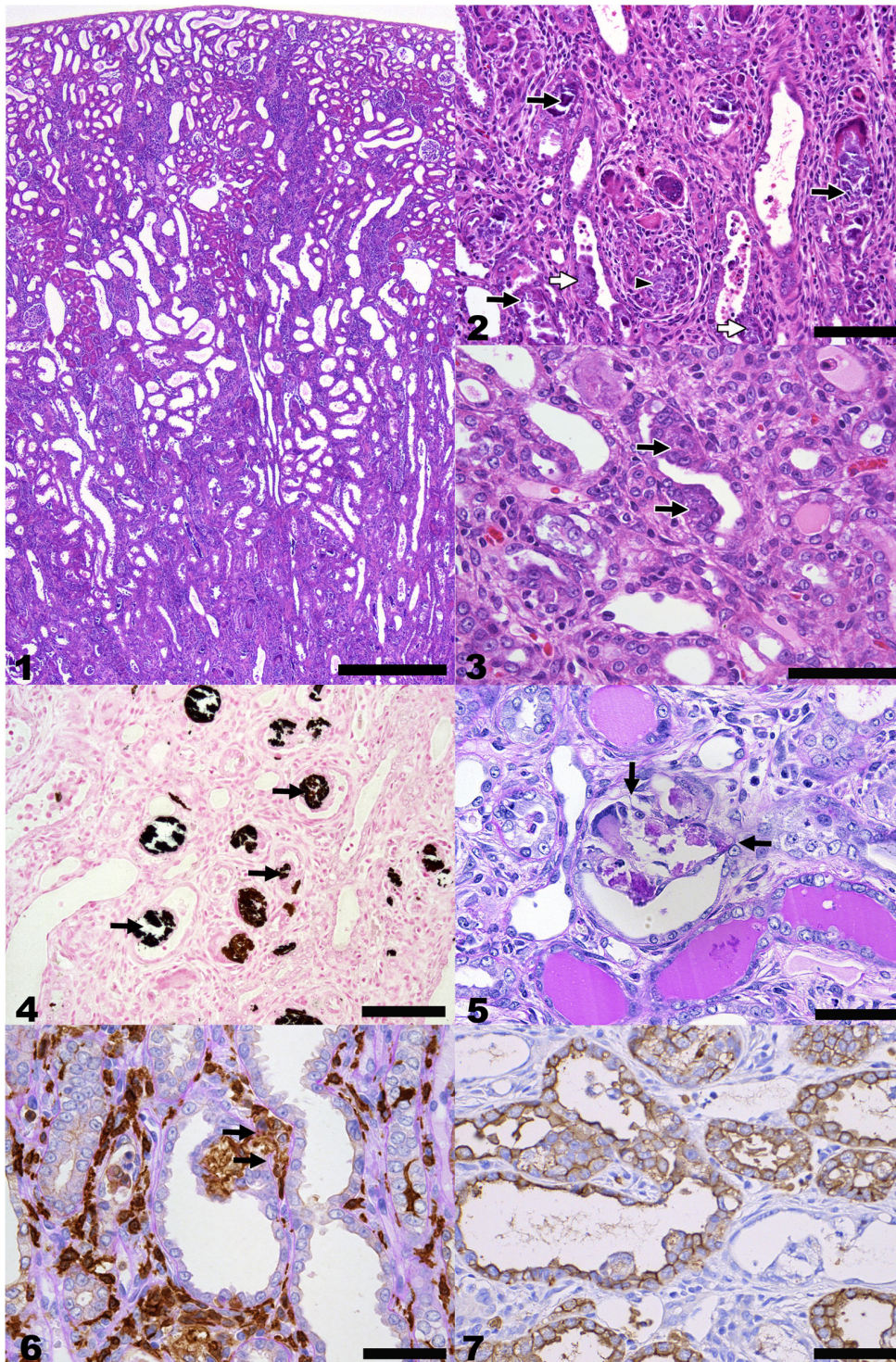
Fig. 1. Dilated and occluded tubules in the cortex and outer medulla. Bar = 500 µm. HE stain.

Fig. 2. Degeneration and necrosis of tubular epithelial cells are seen with tubular obstruction by cell debris and mineralization (arrows). Mineralization is observed mainly within the tubular lumen and to some extent in the subepithelium (open arrows) and interstitium (arrowhead). Infiltration of multinuclear foreign-body giant cells and fibrotic macrophages. Bar = 100 µm. HE stain.

Fig. 3. Protruded tubular epithelial cells envelope minerals (arrows). Bar = 100 µm. HE stain.

Fig. 4. Minerals are positive for Von Kossa's stain. Protruded tubular epithelial cells envelope minerals (arrows). Bar = 100 µm. Von Kossa's method.

Fig. 5. A tubular basement membrane (arrows) is disrupted by mineralization and foreign-body giant cells. Bar = 50 µm. PAS reaction.

Fig. 6. Iba-1-positive macrophages infiltrate from the interstitium into the subepithelial mineralization area, penetrating the basal lamina (arrows). Bar = 50 µm. PAS reaction and immunohistochemical staining for Iba1.

Fig. 7. Damaged and dilated tubules show various levels of immunopositivity for AQP-1. Bar = 50 µm. Immunohistochemical staining for AQP-1 and hematoxylin counterstain.

References

1. Evan AP, Mong SA, Connors BA, Aronoff GR, and Luft FC. The effect of alloxan, and alloxan-induced diabetes on the kidney. Anat Rec. **208**: 33–47. 1984. [Medline] [CrossRef]

2. Vargas L, Friederici HH, and Maibenco HC. Cortical sponge kidneys induced in rats by alloxan. Diabetes. **19**: 33–44. 1970. [Medline] [CrossRef]

3. Bruckmann G, and Wertheimer E. Alloxan studies; the action of alloxan homologues and related compounds. J Biol Chem. **168**: 241–256. 1947. [Medline]

4. de Water R, Noordermeer C, Houtsmuller AB, Nigg AL, Stijnen T, Schröder FH, and Kok DJ. Role of macrophages in nephrolithiasis in rats: an analysis of the renal interstitium. Am J Kidney Dis. **36**: 615–625. 2000. [Medline] [CrossRef]

5. Boevé ER, Ketelaars GA, Vermeij M, Cao LC, Schröder FH, and De Bruijn WC. An ultrastructural study of experimentally induced microliths in rat proximal and distal tubules. J Urol. **149**: 893–899. 1993. [Medline]

6. de Bruijn WC, Boevé ER, van Run PR, van Miert PP, Romijn JC, Verkoelen CF, Cao LC, and Schröder FH. Etiology of experimental calcium oxalate monohydrate nephrolithiasis in rats. Scanning Microsc. **8**: 541–549, discussion 549–550. 1994. [Medline]

7. Lieske JC, Spargo BH, and Toback FG. Endocytosis of calcium oxalate crystals and proliferation of renal tubular epithelial cells in a patient with type 1 primary hyperoxaluria. J Urol. **148**: 1517–1519. 1992. [Medline]

8. Khan SR. Calcium oxalate crystal interaction with renal tubular epithelium, mechanism of crystal adhesion and its impact on stone development. Urol Res. **23**: 71–79. 1995. [Medline] [CrossRef]

9. Mann PC, Vahle J, Keenan CM, Baker JF, Bradley AE, Goodman DG, Harada T, Herbert R, Kaufmann W, Kellner R, Nolte T, Rittinghausen S, and Tanaka T. International harmonization of toxicologic pathology nomenclature: an overview and review of basic principles. Toxicol Pathol. **40**(Suppl): 7S–13S. 2012. [Medline] [CrossRef]

10. Elsner M, Tiedge M, Guldbakke B, Munday R, and Lenzen S. Importance of the GLUT2 glucose transporter for pancreatic beta cell toxicity of alloxan. Diabetologia. **45**: 1542–1549. 2002. [Medline] [CrossRef]

11. Weaver DC, McDaniel ML, and Lacy PE. Alloxan uptake by isolated rat islets of Langerhans. Endocrinology. **102**: 1847–1855. 1978. [Medline] [CrossRef]

12. Lenzen S. The mechanisms of alloxan- and streptozotocin-induced diabetes. Diabetologia. **51**: 216–226. 2008. [Medline] [CrossRef]

Case Report

Accumulation of Mott cells in the spleen in a CB6F1-Tg rasH2 mouse

Tomoya Sano[1*], Yuichi Takai[1], Hisashi Anayama[1], Takeshi Watanabe[1], and Ryo Fukuda[1]

[1] Drug Safety Research Laboratories, Takeda Pharmaceutical Company Limited, 26-1 Muraoka-Higashi 2-chome, Fujisawa, Kanagawa 251-8555, Japan

Abstract: Mott cells are a variant form of plasma cells in humans and laboratory animals. This report describes the morphological characteristics of Mott cells observed in a 33-week-old female CB6F1-Tg rasH2 mouse. Microscopically, a large number of round cells with abundant eosinophilic globules, which were variable in size, were observed in the spleen and were densely distributed in the red pulp adjacent to the marginal zone. A few similar cells were present in the submandibular lymph node and bone marrow. Neither systemic nor local chronic inflammatory changes were seen in this animal. These cells were positive for mouse immunoglobulins. Ultrastructurally, the dilated rough endoplasmic reticulum had a homogenous substances with an intermediate electron density. On the basis of the above findings, these cells were identified as Mott cells. The present lesion is thought to be a spontaneous lesion, an unusual appearance of Mott cells without any associated pathological conditions. (DOI: 10.1293/tox.2016-0023; J Toxicol Pathol 2016; 29: 265–268)

Key words: Mott cell, plasma cell, Tg rasH2 mice

Mott cells (grape cells or morular cells) are a variant form of plasma cells that are characterized by a reddish cytoplasm located peripherally and are commonly observed in the spleen of an autoimmune disease mouse models such as New Zealand Black (NZB) mice and the IgM-Fc receptor (FcμR)-deficient autoimmune mice[1, 2]. This types of cells is known to produce immunoglobulin (Ig), which, rather than being secreted, accumulates in rough endoplasmic reticulum-derived vesicles known as Russell bodies.

The CB6F1-Tg rasH2 (Tg rasH2) mouse is a hemizygous transgenic mouse carrying multiple copies of the human c-Ha-ras gene with its own promoter and enhancer[3]. A short term carcinogenicity assay using this mouse model was endorsed and validated as an alternative to conventional 2-year carcinogenicity bioassays in mice. However, there have been few published reports about the spontaneous lesions in Tg rasH2 mice[4]. Recently, we encountered unusual accumulation of Mott cells in hematopoietic tissues, especially in the spleen, in a female Tg rasH2 mouse in the control group of a 26-week carcinogenicity study. Here, we report on the histological features of this splenic change.

The experimental procedures were approved by the Institutional Animal Care and Use Committees of Shonan Research Center, Takeda Pharmaceutical Company Limited. A 6-week-old female CB6F1 Tg rasH2 mouse was purchased from CLEA Japan (Shizuoka, Japan), housed in a metal cage in an animal room at Takeda Pharmaceutical Company Limited (Kanagawa, Japan) with a temperature of 20°C to 26°C, a relative humidity of 40% to 80% and a 12-hour light/dark cycle, and fed a commercial diet (CE-2, CLEA Japan., Tokyo, Japan) and tap water *ad libitum*. A methylcellulose solution (0.5 w/v%), which is generally used as a vehicle in toxicity studies, was administered once daily via oral gavage at 10 mL/kg to the mouse for 26 weeks begining at 7-weeks of age. At 33 weeks of age, the animal was euthanized by exsanguination from the abdominal aorta under inhalation anesthesia with isoflurane. There were no clinical signs or necropsy findings. In addition, no abnormalities were observed in its blood chemistry, including the serum albumin and albumin/globulin ratio (data not shown), and hematology compared with the other vehicle control animals in the same study (Table 1). All organs were fixed in 10 vol% neutral buffered formalin, embedded in paraffin, sectioned, and stained with hematoxylin and eosin (HE; all organs) and periodic acid-Schiff (PAS; spleen only). For identification of cell type, spleen sections were immunohistochemically stained with anti-mouse immunoglobulin G (IgG), anti-mouse immunoglobulins-complex (Igs; react with IgG, IgA, and IgM; fluorescein isothiocyanate (FITC) labelling), anti-mouse CD45R/B220 monoclonal antibody, and anti-mouse F4/80 polyclonal antibody. Details of the primary antibodies used are summarized in Table 2. Briefly, after the pretreatments and incubation with primary antibodies, the sections were immunohistochemically stained by the polymer immunocomplex method using Histofine Simple Stain Mouse MAX PO (Rat) (Nichirei, Tokyo, Japan) for CD45R/

Table 1. Hematological Parameters of the Present Case and the Control Data from the Same Study

	Neutrophils ($\times10^2$/µL)	Lymphocytes ($\times10^2$/µL)	Monocytes ($\times10^2$/µL)	Eosinophils ($\times10^2$/µL)	Basophils ($\times10^2$/µL)
Present case	5.9	14.9	0.2	0.8	0.1
Vehicle control (mean, n=25)	5.1	14.8	0.3	0.7	0.2
SD	2.1	6.3	0.2	0.3	0.1

Table 2. Primary Antibodies and Reaction Conditions for Immunohistochemistry

Primary antibody	Supplier	Host	Dilution	Antigen retrieval
IgG	Vector	Mouse	1:800	Trypsin for 30 min at 37°C
Igs-FITC	DAKO	Mouse	1:1	Proteinase K for 10 min at room temperature
CD45R/B220	BD Pharmingen	Rat	1:100	Autoclaved at 121°C for 10 min with citrate buffer (pH 6.0)
F4/80	AbD Serotec	Rat	1:100	
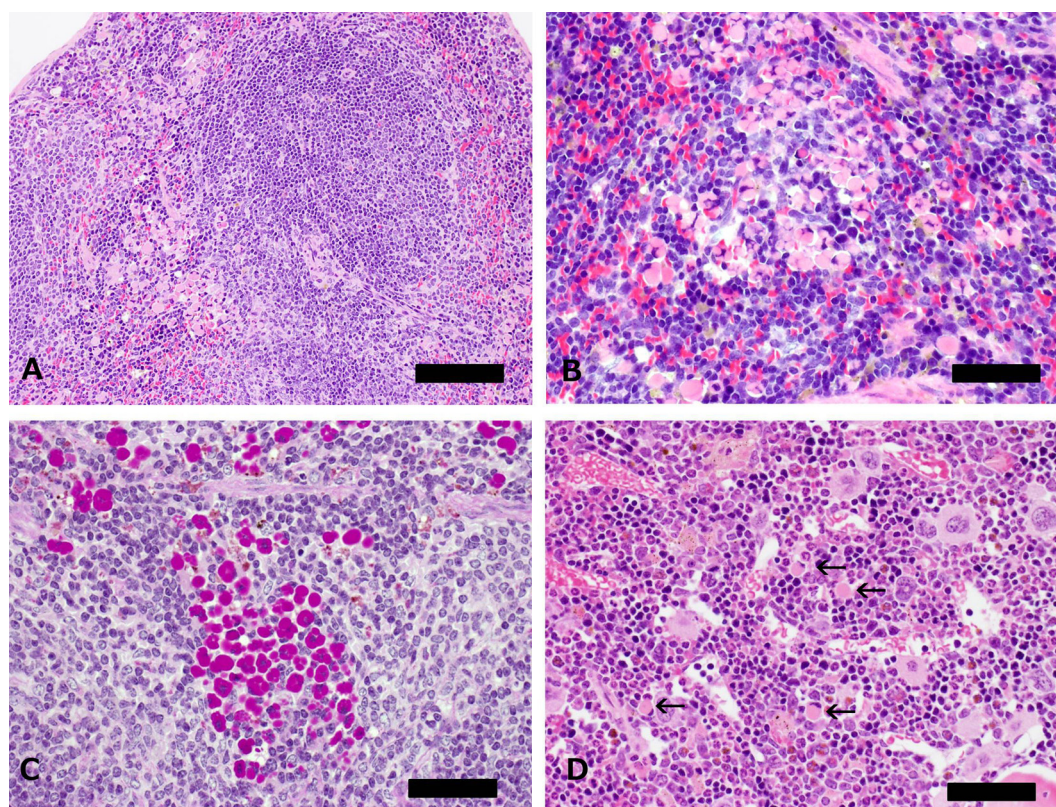
Fig. 1. Spleen and bone marrow from a 33-week-old Tg rasH2 mouse. A: The normal architecture of the spleen is well preserved, and a large number of round cells with abundant cytoplasm containing eosinophilic globules are distributed in the red pulp adjacent to the marginal zone (bar: 200 µm). B: A large number of round cells have a nucleus with peripherally clumped chromatin and variable sizes of eosinophilic globules in the cytoplasm (bar: 100 µm). C: Eosinophilic globules were positive for PAS stain (bar: 100 µm). D: Smaller numbers of round cells with abundant cytoplasm containing eosinophilic globules are evident in the bone marrow (arrows, bar: 100 µm).

B220 and F4/80 and a VECTASTAIN Elite ABC kit (Vector Laboratories, Burlingame, CA, USA) for IgG, and then the sections were counterstained with hematoxylin.

For electron microscopy, formalin-fixed spleen tissues were trimmed and fixed with 2.5% glutaraldehyde, postfixed in 1% osmium tetroxide solution (pH 7.4) for 2 hours, and processed into resin. Semithin sections were cut and stained with toluidine blue. Ultrathin sections were cut and stained with uranyl acetate and lead citrate and then examined under an electron microscope (H-7600, Hitachi, Tokyo, Japan).

Microscopically, a large number of round cells with abundant cytoplasm containing various sizes of eosinophilic globules were distributed in the red pulp adjacent to the marginal zone (Figs. 1A and 1B), and these eosinophilic
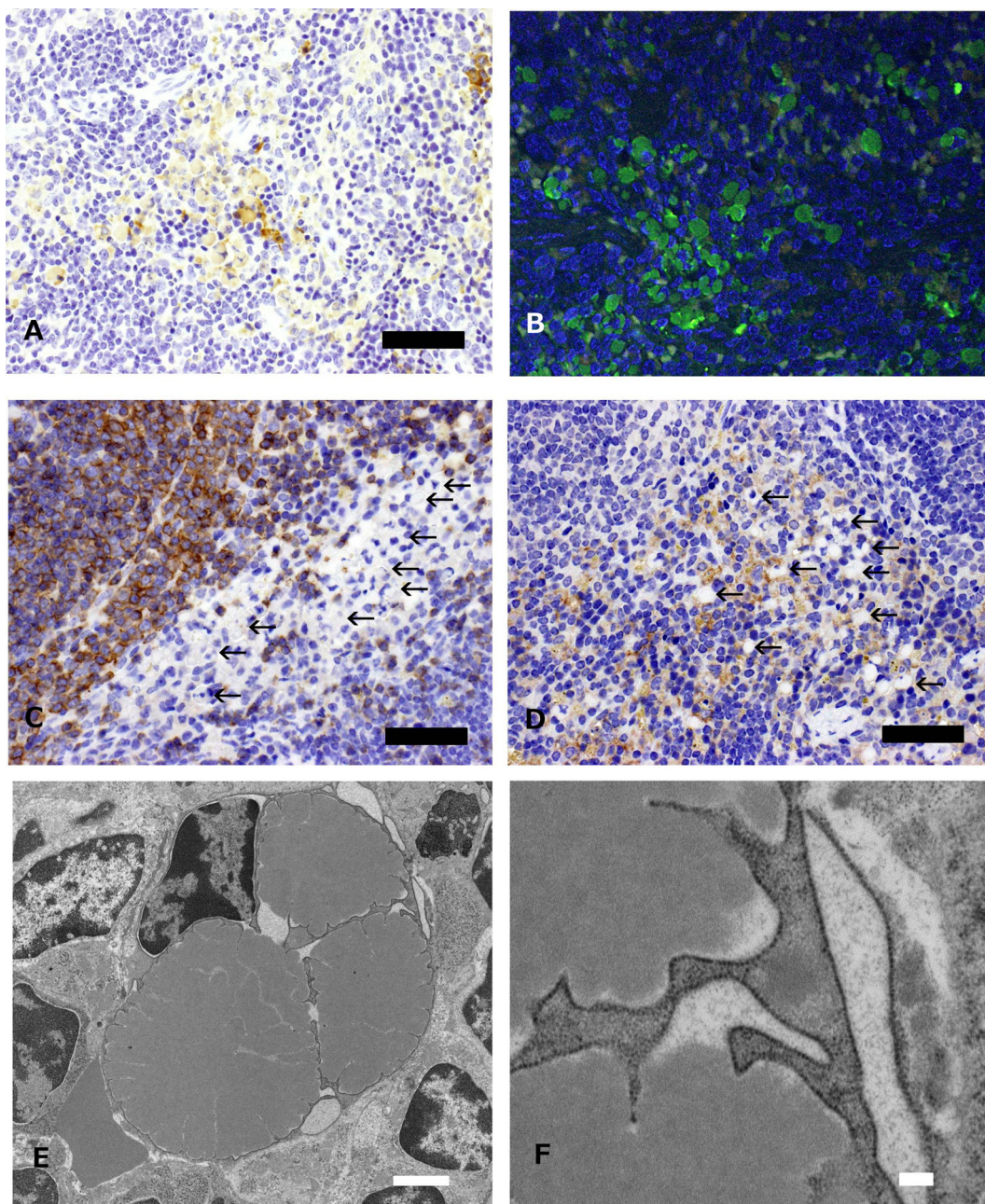
Fig. 2. Immunohistochemical staining and electron micrographs of Mott cells in a 33-week-old Tg rasH2 mouse. A: The cells with eosinophilic globules are positive for IgG (bar: 100 μm). B: The cells with eosinophilic globules are positive for fluorescent immunoglobulins (green: Igs-FITC; blue, nuclei, DAPI (4',6-diamidino-2-phenylindole); bar: 100 μm). C: The cells with eosinophilic globules are negative for CD45R/B220 (arrows, bar: 100 μm), whereas marginal zone lymphocytes are positive for CD45R/B220. D: The cells with eosinophilic globules are negative for F4/80 (arrows, bar: 100 μm), whereas macrophages in the red pulp are positive for F4/80. E: A homogeneous substance with an intermediate electron density is observed in the cisternae of the rER in Mott cells, and most of the nuclei show apparent distortion of the outline or are compressed because of the dilated rER (bar: 2 μm). F: Higher magnification of Fig. 2E (bar: 200 nm).

globules were positive for PAS stain (Fig. 1C). Smaller numbers of them were evident in the submandibular lymph node and bone marrow but not in the mesenteric lymph node and Peyer's patch (Fig. 1D). In addition, there were no inflammatory changes in any tissues, and no hematopoietic proliferative lesions were observed in this animal. In immunohistochemistry, the cytoplasmic eosinophilic globules were

reactive with mouse IgG and the fluorescent labeling mouse Igs (Figs. 2A and 2B), but negative for CD45R/B220 and F4/80, which are B cell and macrophage markers, respectively (Figs. 2C and 2D). Ultrastructurally, these cells have a nucleus with peripherally clumped chromatin, and the rough endoplasmic reticulum (rER) was markedly dilated and contained a large amount of a homogeneous substance

with an intermediate electron density. The dilated rER compressed the nucleus, and its contour often appeared distorted (Figs. 2E and 2F).

Based on the above findings, the cells that had a dilated rER containing immunoglobulins and characteristic nuclei were considered Mott cells distributed in the hematopoietic tissues, especially in the spleen.

Plasma cells in the spleen are thought to develop from marginal zone B cells and follicular B cells, from germinal center B cells, and from memory B cells[5]. When marginal zone B cells encountered an antigen in the spleen, they were able to rapidly differentiate into plasma cells, and marginal zone B cells are also known to migrate into red pulp and form foci of plasmablasts[5]. Follicular B cells are also known to develop into plasma cells or to move to the germinal center, and differentiate from memory B cells or plasmablasts to plasma cells, which can migrate into bone marrow[5]. Considering the distribution of Mott cells in the spleen and their presence in the bone marrow, both marginal zone and follicular B cells could be a possible source of the Mott cells in the present case[5].

Mott cell formation is a consequence of a disorder of abnormal synthesis, degradation, and/or secretion of Ig and is related to various pathological conditions including autoimmune diseases, reactive plasmacytosis, and several types of hematolymphoid malignancies[1, 2, 6]; however, neither inflammatory changes nor hematopoietic tumors were observed in this case. In Ig light chain-deficient mice, it was postulated that the mechanism of Mott cell formation was lack of Ig light chains, which prevents antibody aggregation, leading to Ig heavy chain aggregation, which is known as Russell body formation[7].

On the basis of the histopathologic and electron microscopic findings, the present lesion is thought to be an unusual appearance of Mott cells. To the best of our knowledge, this is the first case showing Mott cell accumulation without any pathological conditions in mice. The etiology of this change in Tg rasH2 mice remains unclear, but we believe this case will provide useful information regarding spontaneous background findings in Tg rasH2 mice.

Disclosure of Potential Conflict of Interest: The authors declare no conflict of interest associated with this paper.

References

1. Jiang Y, Hirose S, Hamano Y, Kodera S, Tsurui H, Abe M, Terashima K, Ishikawa S, and Shirai T. Mapping of a gene for the increased susceptibility of B1 cells to Mott cell formation in murine autoimmune disease. J Immunol. **158**: 992–997. 1997. [Medline]
2. Honjo K, Kubagawa Y, Suzuki Y, Takagi M, Ohno H, Bucy RP, Izui S, and Kubagawa H. Enhanced auto-antibody production and Mott cell formation in FcμR-deficient autoimmune mice. Int Immunol. **26**: 659–672. 2014. [Medline] [CrossRef]
3. Tamaoki N. The rasH2 transgenic mouse: nature of the model and mechanistic studies on tumorigenesis. Toxicol Pathol. **29**(Suppl): 81–89. 2001. [Medline] [CrossRef]
4. Paranjpe MG, Shah SA, Denton MD, and Elbekai RH. Incidence of spontaneous non-neoplastic lesions in transgenic CBYB6F1-Tg(HRAS)2Jic mice. Toxicol Pathol. **41**: 1137–1145. 2013. [Medline] [CrossRef]
5. Shapiro-Shelef M, and Calame K. Regulation of plasma-cell development. Nat Rev Immunol. **5**: 230–242. 2005. [Medline] [CrossRef]
6. Rampisela D, and Donner LR. An unusual self-limited clonal Mott cell proliferation with lymphoplasmacytic lymphoma-like features in a child with the Wiskott-Aldrich syndrome and Von Recklinghausen's neurofibromatosis. Pathol Res Pract. **206**: 467–471. 2010. [Medline] [CrossRef]
7. Corcos D, Osborn MJ, Matheson LS, Santos F, Zou X, Smith JA, Morgan G, Hutchings A, Hamon M, Oxley D, and Brüggemann M. Immunoglobulin aggregation leading to Russell body formation is prevented by the antibody light chain. Blood. **115**: 282–288. 2010. [Medline] [CrossRef]

Case Report

A case report of a metastatic yolk sac carcinoma in the pulmonary artery of a young female Sprague-Dawley rat

Yohei Sakamoto[1*], Takaharu Nagaoka[2], Kei Tamura[1], and Hideshi Kaneko[1]

[1] Toxicology Research Department, Pharmaceutical Development Research Laboratories, Teijin Pharma Limited, 4-3-2 Asahigaoka, Hino-shi, Tokyo 191-8512, Japan
[2] Safety Research Laboratory, Shin Nippon Biomedical Laboratories, 2438 Miyanoura, Kagoshima-shi, Kagoshima 891-1394, Japan

Abstract: Yolk sac carcinoma is an extremely rare tumor in rats and is usually found in the genital system of aged animals. We encountered a yolk sac carcinoma in the pulmonary artery of an 18-week-old female Sprague-Dawley rat. In a repeated dosing toxicity study (once weekly for 4 weeks, intraperitoneal), this rat was unexpectedly found dead on the 55th day after the final administration of the test article. At necropsy, grayish white nodules were found on the lung surface. Histopathologically, tumor emboli were observed in the trunk and branch of the pulmonary artery. Tumor cells with slightly basophilic vacuolated cytoplasm and large vesicular nuclei formed nests or clusters and were embedded in a homogenous eosinophilic and periodic acid-Schiff reaction positive matrix. The tumor cells and matrix were immunoreactive for laminin. The embolic tumor resembled yolk sac carcinoma showing a parietal pattern in rodents. Although the primary site was unknown, the tumor was considered to be a metastatic yolk sac carcinoma. (DOI: 10.1293/tox.2016-0025; J Toxicol Pathol 2016; 29: 269–273)

Key words: yolk sac carcinoma, pulmonary artery, lung, rat, young, female

Yolk sac carcinoma is a very rare malignant tumor in rodents which is considered to be a variant of germ cell tumors and microscopically resembles a yolk sac, an extraembryonic membrane. The incidence of yolk sac carcinoma in rats is extremely low, with only 1 case occurring in more than 40,000 female F344 rats used in previous carcinogenicity studies[1]. There have been some other reports of yolk sac carcinomas that developed in the ovary or uterus in aged female rats[2–4]. Nakazawa and colleagues reported an instance of testicular yolk sac carcinoma in an aged Sprague-Dawley (SD) rat[5]. Yolk sac carcinoma can also be experimentally induced in rats by surgical procedures, such as fetectomy with or without additional injection of mouse sarcoma virus[6, 7], puncture of the pregnant uterus wall in mid gestation[8], and implantation of an embryo under the kidney capsule of a syngeneic rat[9]. As described above, yolk sac carcinomas in rats are generally encountered in older animals and observed in genital systems. Here, we report a case of metastatic yolk sac carcinoma in the pulmonary artery of a young female rat.

The female SD rat was obtained from Charles River Laboratories Japan, Inc. (Kanagawa, Japan) at 5 weeks of age. The rat was housed alone in a stainless-steel cage in an air conditioned animal room controlled at a temperature of 24 ± 3°C with a humidity of 50 ± 20% and a 12 hour light/dark cycle, was fed a solid diet (CRF-1; Oriental Yeast Co., Ltd.), and was provided with drinking water *ad libitum*. The toxicity study was approved by the Institutional Animal Care and Use Committee and was performed in accordance with the animal welfare bylaws of Drug Safety Research Laboratories, Shin Nippon Biomedical Laboratories, Ltd. After a 2-week acclimation period, the rat was allocated to the high dose group in the study, and the test material (a biodegradative material) was intraperitoneally administered via a paramedian incision of 1 to 2 cm once a week for 4 weeks under anesthesia with intramuscular injection (0.2 mL/kg, each) of medetomidine hydrochloride and ketamine hydrochloride.

On the 55th day of the recovery period after the final administration of the test material (at 18 weeks of age), the rat, which had not exhibited any abnormalities in its general condition, body weight, or food consumption during the study, was unexpectedly found dead. At necropsy, small grayish white nodules were observed on the surface of the lung (Fig. 1). The heart weight was approximately twice than the other rats in the study, which were sacrificed at the end of recovery period (at 23 weeks of age). At necropsy, the right ventricular wall exhibited hypertrophy. Some of the remaining test material was observed in the abdominal

Fig. 1. Gross appearance of the lung. Some grayish white nodules (enclosed by a circle) were observed on the surface of the left lobe.

cavity at necropsy, however, this finding was normally observed following the intraperitoneal administration of this material.

The principal organs and tissues from the whole body, including the lung and heart with the pulmonary artery, were fixed in 10% phosphate-buffered formalin and embedded in paraffin. Paraffin sections were stained with hematoxylin and eosin. Sections from the lung and heart were processed with periodic acid-Schiff (PAS) reaction and phosphotungstic acid-hematoxylin (PTAH) stain. Immunohistochemical staining was performed in the sections from the lung and heart with anti-human cytokeratin mouse monoclonal antibody (AE1/AE3, ×1, Dako North America, Inc., Carpinteria, CA, USA), anti-laminin rabbit polyclonal antibody (×5,000, Dako Cytomation, Inc. Denmark), and alpha-fetoprotein (AFP) antibody (C-19, ×100, Santa Cruz Biotechnology, Inc., Dallas, TX, USA) and the sections were subjected to a subsequent chromogenic reaction with the streptavidin-biotin complex method.

In the histopathological examination of the lung, multiple intravascular emboli were observed in the branches of the pulmonary artery. Emboli were present in the left and right (posterior) lobes of the lung. Large and small emboli appeared to be occlusive, with close approximation or adherence to the vascular endothelium, and were considered to be the cause of death via obstruction of blood flow (Fig. 2A). A similar embolus was also seen in the trunk of the pulmonary artery (Fig. 2B). In the heart, fibrosis and mononuclear cell infiltration were observed in the right ventricular wall and interventricular septum, respectively. In the liver, congestion was observed. Together with the heart weight increase and right ventricular hypertrophy, these histopathological findings in the heart and liver suggested circulatory

disturbance.

The intravascular emboli were mainly characterized by the presence of small nests or clusters of undifferentiated cells embedded in a prominent homogenous eosinophilic matrix (Fig. 2C, 2D). In a few areas, it appeared as if similar cellular foci were growing within the lung parenchyma, which is indicative of invasion (Fig. 2E). The appearances of multiple emboli in the trunk and branches of the pulmonary artery and the evidence of invasion were indicative of metastasis of a neoplastic tumor.

The predominant cell type within the tumor emboli appeared as irregularly shaped slightly basophilic cells with vacuolated cytoplasm and large vesicular nuclei containing one or two nucleoli. Tumor cells within the nests or clusters appeared closely arranged and attached to each other. Infrequent hyaline droplets were present in tumor cells, suggesting that the eosinophilic matrix around the cell clusters was produced by the tumor cells (Fig. 2D). Individual cell necrosis of tumor cells was present throughout the neoplastic process. Mitoses were evident but few (Fig. 2E).

From the appearance of the H&E sections as described above, we suspected yolk sac carcinoma and conducted a PAS reaction and immunohistochemistry to cytokeratin, laminin, and AFP. The characteristic eosinophilic matrix was intensively positive for the PAS reaction and laminin (Fig. 3A, 3B). The cytoplasm of tumor cells was intensely positive for laminin and weakly and partially positive for AFP and cytokeratin (Fig. 3B, 3C, 3D), respectively. All of the morphological, histochemical, and immunohistochemical findings were highly comparable to the previously reported cases of yolk sac carcinoma in rodents[2, 4, 5, 10]. PTAH staining was performed to differentiate the possibility of thrombi and produced a negative result.

In the necropsy and histopathological examination, no other neoplastic lesions were identified in any other organ, including female reproductive organs, despite additional sectioning of the ovaries and uterus after the regular histopathological examination. Therefore, the organ in which the tumor originated was unknown.

Histologically, yolk sac carcinoma in rodents is described as having two components that resemble a parietal yolk sac and visceral yolk sac. The parietal component is characterized by a cluster of polygonal or cuboidal tumor cells with a surrounding PAS-positive eosinophilic matrix. The visceral component consists of cylindriform tumor cells arranged in a papillary pattern without an eosinophilic matrix, and sometimes a thin basement membrane between the endoderm and the mesenchyme can be observed[2]. In the present case, a visceral pattern was not obvious, and the majority of the components showed a parietal pattern; however, the results of PAS reaction and immunohistochemistry for laminin strongly supported the diagnosis of this tumor as a yolk sac carcinoma. Cytokeratin has also been reported to be positive in rat yolk sac carcinoma cells[4]. Increased levels of AFP were detected in the sera of rats or humans bearing yolk sac carcinomas. Using immunohistochemistry, it was found that AFP was secreted by the yolk sac carcinoma cells
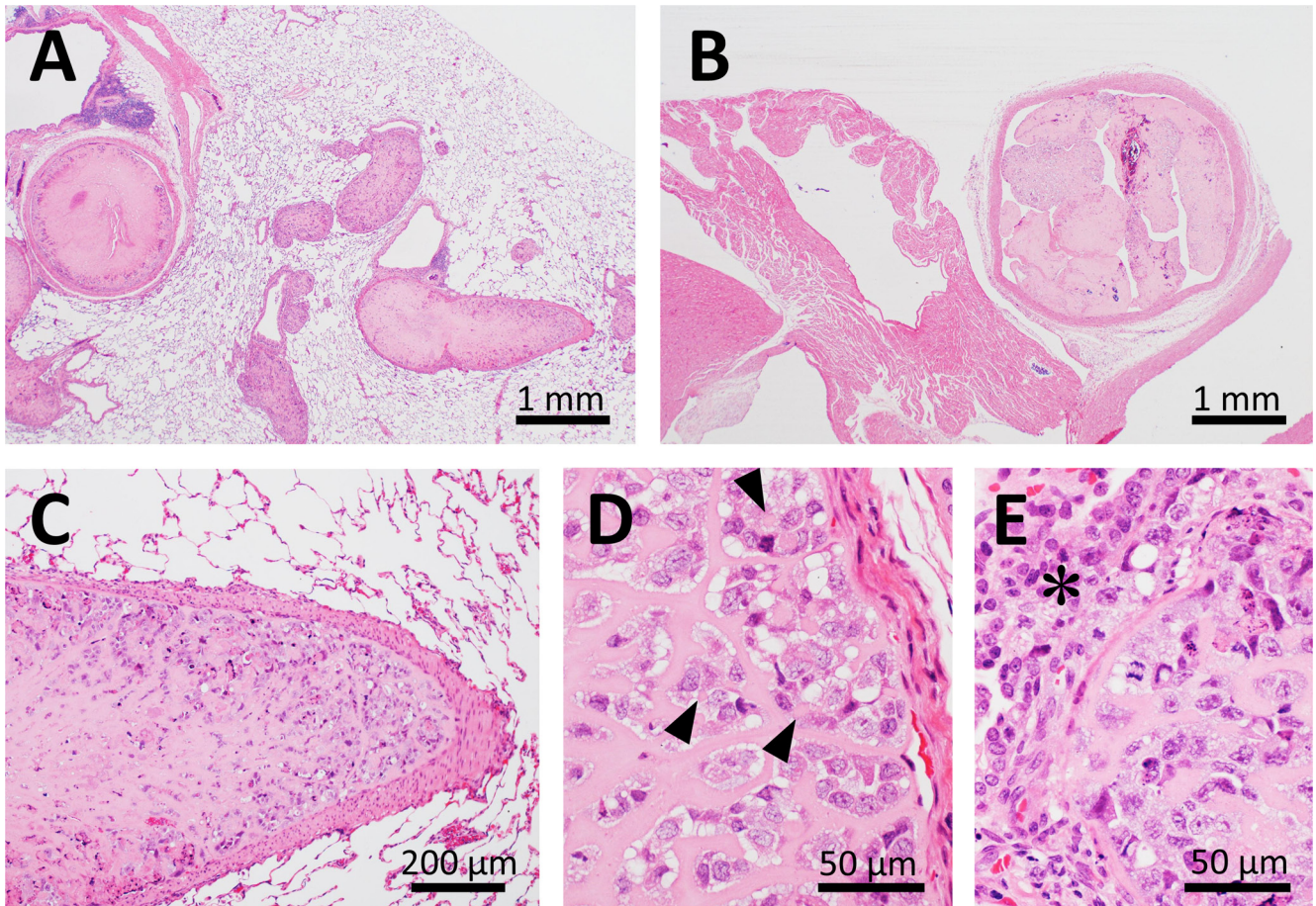
Fig. 2. Photomicrographs of the emboli. Hematoxylin and eosin stain. A) Multiple emboli were observed in the branches of the pulmonary artery. B) An embolus was also observed in the origin of the pulmonary artery. C) Nests or clusters of the neoplastic cells were surrounded by an eosinophilic matrix. D) The neoplastic cells exhibited basophilic vacuolar cytoplasm with large vesicular nuclei. Cytoplasmic hyaline droplets were evident (arrow heads). E) Necrosis and mitosis were present in the neoplastic cells. The presence of tumor cells in the extravascular space indicated invasion (asterisk).

displaying the visceral type[10, 11]. Thus it was reasonable that AFP was not intensely observed in the present case, which exhibited a parietal pattern.

This case is interesting and unique because of the animal's younger age and the lack of gross or microscopic evidence of a primary tumor. Pirak and colleagues[12] reported that choriocarcinoma, another germ cell tumor variant, developed in the cervical lymph nodes and lung (pleural surface) of a 15-week-old SD rat; however, its pathogenesis was considered to be different from our case, in which tumor cells were only observed in the pulmonary artery. Although it has not been published in the English literature, Kajikawa and colleagues[13] reported at the annual meeting of the Japanese Society of Toxicologic Pathology in 2006 that metastatic yolk sac carcinoma was found in the right ventricle and lung in a 10-week-old female SD rat. Kajikawa's case is similar to the present case in two aspects, namely, the presence of tumors in the right ventricle and/or pulmonary artery and the undetected origin of the tumors. Given the intravascular growth pattern of this tumor, it should be considered that a

primary tumor in the gonads or an extragonadal region become necrotic and resorbed following metastasis.

In contrast to rodents, there are some reports indicating that yolk sac carcinoma occurred in the lung in humans with no evidence of a gonadal lesion[14–18]. The origin of pulmonary germ cell tumors in humans is not well known, but it is possible that primordial germ cells remain in the region of the mediastinum or lungs at the time of migration along the gonadal ridge during embryogenesis and become the tumor "seed", eventually developing extragonadal germ cell tumor[17–19]. The origin of the pulmonary germ cell tumors in these human cases is more similar to that in Pirak's report[12] than that in the present case. When a germ cell tumor occurs in the rat lung, we have to consider the following two possibilities for its origin: metastasis from the gonadal or extragonadal primary tumor and a locally occurred tumor which was developed from a migrated primordial germ cell.

It was surprising that the animal did not show abnormal clinical signs or a decrease in body weight prior to death, despite a number of emboli in the pulmonary artery. It was
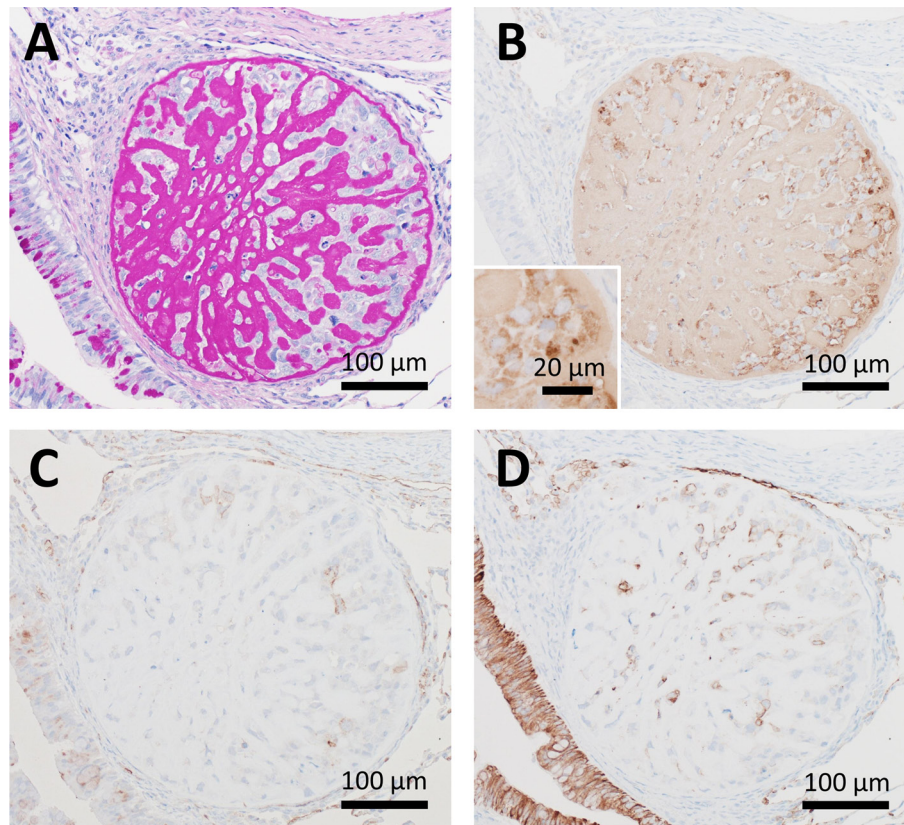
Fig. 3. Photomicrographs of PAS reaction and immunohistochemistry. A) The extracellular matrix showed a strongly positive PAS reaction. Some PAS-positive droplets were evident in the cytoplasm of the tumor cells. B) The extracellular matrix and tumor cells (see insert) were positive for laminin. C and D) A few tumor cells were slightly positive for alpha fetoprotein (C) and cytokeratin (D).

possible that a large embolus developed in the right ventricle and dropped into the trunk of the pulmonary artery, delivering the fatal blow.

The present case was considered to be a spontaneous tumor for the following reasons: there were no other reports of chemically induced yolk sac carcinoma, there was only one case in the study, and it was too early after administration of the test material, which has no genotoxic potential, for it to be the cause of induction and development of the tumor.

In conclusion, this was a very rare case of yolk sac carcinoma that developed in and embolized the pulmonary artery of 18-week-old female SD rat. The tumor cells showed characteristics of a parietal pattern of yolk sac carcinoma, such as cluster formation with a surrounding PAS- and laminin-positive, eosinophilic matrix. To the best of our knowledge, this is the first report of a metastatic pulmonary yolk sac carcinoma in the pulmonary artery without a clear primary site in a rat in the published English literature.

Disclosure of Potential Conflicts of Interest: The authors declare that they have no conflicts of interest with respect to the research, authorship, and/or publication of this article.

References

1. Alison RH, and Morgan KT. Ovarian neoplasms in F344 rats and B6C3F1 mice. Environ Health Perspect. **73**: 91–106. 1987. [Medline] [CrossRef]
2. Sobis H. Yolk sac carcinoma, rat. In: Monographs on the Pathology of Laboratory Animals – Genital System. TC Jones, U Mohr, and RD Hunt (eds). Springer-Verlag, Berlin. 127–133. 1987.
3. Cooper TK, Dumpala PR, and Whitcomb TL. Diagnostic exercise: ascites, abdominal masses, and diffuse peritoneal nodules in a rat. Vet Pathol. **51**: 659–662. 2014. [Medline] [CrossRef]
4. Sakamoto A, Yamaguchi Y, Yamakawa S, Nagatani M, and Tamura K. Highly metastatic ovarian yolk sac carcinoma in a rat. J Toxicol Pathol. **24**: 81–85. 2011. [Medline] [CrossRef]
5. Nakazawa M, Tawaratani T, Uchimoto H, Kawaminami A, Ueda M, Ueda A, Iwakura K, Sumi N, and Kura K. Testicular yolk sac carcinoma in an aged Sprague-Dawley rat. J Toxicol Pathol. **11**: 203–204. 1998. [CrossRef]
6. Sakashita S, Tsukada Y, Nakamura K, Tsuji I, and Hirai H. Experimental yolk-sac tumors produced by fetectomy without virus infection in rats. Int J Cancer. **20**: 83–86. 1977. [Medline] [CrossRef]
7. Van Hove L, Sobis H, and Vandeputte M. Viral-versus non-viral-induced yolk sac tumors in the rat. Oncodev Biol Med.

3: 97–109. 1982. [Medline]

8. Wewer U, Albrechtsen R, and Ruoslahti E. Laminin, a non-collagenous component of epithelial basement membranes synthesized by a rat yolk sac tumor. Cancer Res. **41**: 1518–1524. 1981. [Medline]

9. Damjanov I, and Sell S. Yolk sac carcinoma grown from rat egg cylinders. J Natl Cancer Inst. **58**: 1523–1525. 1977. [Medline]

10. Majeed SK, Alison RH, Boorman GA, and Gopinath C. Ovarian yolk sac carcinoma in mice. Vet Pathol. **23**: 776–778. 1986. [Medline]

11. Delacourt MC, Sobis H, and Vandeputte M. Immunofluorescent localization of alpha fetoprotein in yolk sac carcinomas of the rat. J Natl Cancer Inst. **57**: 1375–1377. 1976. [Medline]

12. Pirak M, Waner T, Abramovici A, Scolnik M, and Nyska A. Histologic and immunohistochemical study of a spontaneous choriocarcinoma in a male Sprague Dawley rat. Vet Pathol. **28**: 93–95. 1991. [Medline] [CrossRef]

13. Kajikawa S, Takeuchi A, Shirakai K, Nakano K, Izumisawa N, and Oishi Y. Spontaneous yolk sac carcinoma metastasizing to the heart and lung in a 10-week-old female Sprague-Dawley rat. 22nd JSTP Meeting abstract. 2006.

14. Arora S, Patel H, Mir P, Mishra S, Kalra A, Sawhney H, Duffoo F, Macera M, Abdu A, and Thelmo W. A bilateral primary yolk sac tumor of the lung associated with chromosome 3 polysomy: understanding the Oct 3/4 and Sox 2 interaction. Cancer Biol Ther. **14**: 1–4. 2013. [Medline] [CrossRef]

15. Inoue H, Iwasaki M, Ogawa J, Shohtsu A, Abe Y, Satoh S, and Osamura Y. Pure yolk-sac tumor of the lung. Thorac Cardiovasc Surg. **41**: 249–251. 1993. [Medline] [CrossRef]

16. Pelosi G, Petrella F, Sandri MT, Spaggiari L, Galetta D, and Viale G. A primary pure yolk sac tumor of the lung exhibiting CDX-2 immunoreactivity and increased serum levels of alkaline phosphatase intestinal isoenzyme. Int J Surg Pathol. **14**: 247–251. 2006. [Medline] [CrossRef]

17. Abdel Rahman AR, Ebied EN, Nouh MA, Gal AA, and Mansour KA. Primary yolk sac tumor of the lung. Ann Thorac Surg. **87**: 1925–1926. 2009. [Medline] [CrossRef]

18. Basoglu A, Sengul AT, Buyukkarabacak YB, Yetim TD, and Yildiz L. Pure yolk-sac tumor of the lung. Asian Cardiovasc Thorac Ann. **16**: 410–411. 2008. [Medline] [CrossRef]

19. Pont J, Pridun N, Vesely N, Kienzer HR, Pont E, and Spital FJ. Extragonadal malignant germ cell tumor of the lung. J Thorac Cardiovasc Surg. **107**: 311–312. 1994. [Medline]

Case Report

Spontaneous extraskeletal osteosarcoma in the duodenum of a Crlj:CD1 (ICR) mouse

Ryo Ando[1*], Shinichiro Ikezaki[1], Yuko Yamaguchi[1], Kazutoshi Tamura[1], and Toru Hoshiya[1]

[1] Gotemba Laboratory, BoZo Research Center Inc., 1284 Kamado, Gotemba-shi, Shizuoka 412-0039, Japan

Abstract: Extraskeletal osteosarcoma is a very rare tumor in humans and animals. This paper describes a case of extraskeletal osteosarcoma observed in the duodenum of a male ICR mouse. Grossly, a solid mass pushing up the tunica serosa was observed in the duodenal wall. Histologically, the tumor was located in the lamina propria mucosae and tela mucosa. Neoplastic cells densely proliferated in these areas, and replaced of the normal tissue components. A small amount of osteoid and a small clump of bone tissue were observed in the area of neoplastic cell proliferation, especially in the lamina propria mucosae. Neoplastic cells consisted of atypical polygonal cells and pleomorphic spindle-shaped cells, and the former were predominant. Mitotic figures were occasionally observed. Neither invasion of vessels in the duodenum nor metastasis to distant organs was observed. There were no skeletal tumors in the body. Immunohistochemically, the neoplastic cells were positive for anti-osteocalcin, osteonectin, vimentin, and S-100 protein. Judging from these results, the present tumor was diagnosed as extraskeletal osteosarcoma. This is the first report of spontaneous extraskeletal osteosarcoma arising from the duodenum of a mouse. (DOI: 10.1293/tox.2016-0043; J Toxicol Pathol 2016; 29: 275–278)

Key words: extraskeletal osteosarcoma, duodenum, spontaneous tumor, mouse

Extraskeletal osteosarcoma, which occurs in tissues having no relation to the bone or peritoneum, is a very rare tumor both in humans and animals, and there are only a few reports of its occurrence in rats and mice. Specifically, it has been reported in the skin (mouse)[1], subcutaneous tissue (rat)[2, 3], thoracic cavity (rat)[4], abdominal wall (mouse)[5], stomach (rat)[6], and cecum (rat)[7]. This paper describes the first case of spontaneous extraskeletal osteosarcoma detected in the duodenum of a mouse.

The animal was a male Crlj:CD-1 (ICR) mouse purchased from Charles River Laboratories Japan Inc. (Kanagawa, Japan) that served as a monitor in a 2-year carcinogenicity study and was found dead at 75 weeks of age. The animals used in the study were housed individually in suspended stainless-steel wire mesh cages in an animal room maintained at a temperature of $23 \pm 3°C$ and relative humidity of $50 \pm 20\%$ with air ventilation 12 to 17 times per hour and 12 hours of illumination (7:00 to 19:00). Pellet diet (irradiation sterilized CRF-1, Oriental Yeast Co., Ltd., Tokyo, Japan) and tap water were provided *ad libitum*. The experiment was conducted in compliance with the laws or guidelines relating to animal welfare including the Standards Relating to the Care and Management, etc. of Experimental Animals (Notification No. 6 of the Prime Minister's Office, Japan March 27, 1980) and Guidelines for Animal Experimentation (Japanese Association for Laboratory Animal Science, May 22, 1987).

Macroscopically, a solid mass ($6 \times 5 \times 5$ mm in size) pushing up the tunica serosa was palpable from the serous surface of the duodenum (Fig. 1). The mass, which showed a whitish cut surface, was located in the duodenal wall and did not protrude into the duodenal cavity. There were no macroscopic findings indicating skeletal or other tumors in the body. After complete necropsy, all tissues including the tumor mass were fixed in 10% neutral-buffered formalin, embedded in paraffin, sectioned, and stained with hematoxylin and eosin (HE). Additional sections from the tumor mass were also subjected to immunohistochemistry by the peroxidase-labeled polymer method using an EnVision+ kit (anti-rabbit or anti-mouse, Dako, Glostrup, Denmark). The primary antibodies used were osteocalcin (polyclonal, 1:100, Santa Cruz Biotechnology, Dallas, TX, USA), osteonectin (polyclonal, 1:500, LSL, Tokyo, Japan), vimentin (polyclonal, 1:100, Abcam, Cambridge, UK), S-100 (polyclonal, 1:500, Dako), Iba-1 (polyclonal, 1:100, Wako Pure Chemical Industries, Osaka, Japan), α-smooth muscle actin (α-SMA) (monoclonal, 1:100, Dako), and keratin/cytokeratin (polyclonal, ready-to-use, Nichirei, Tokyo, Japan).

Histologically, the tumor was located in the lamina propria mucosae and tela mucosa (Fig. 2). In the lamina propria mucosae, in addition to neoplastic cell proliferation, formation of small clumps of bone tissue was prominent
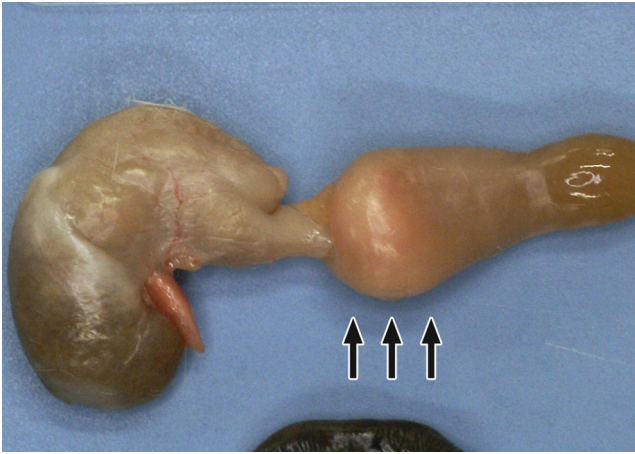
Fig. 1. Macroscopic appearance of the duodenum. A solid mass pushing up the tunica serosa (arrows) is palpable from the serous surface.
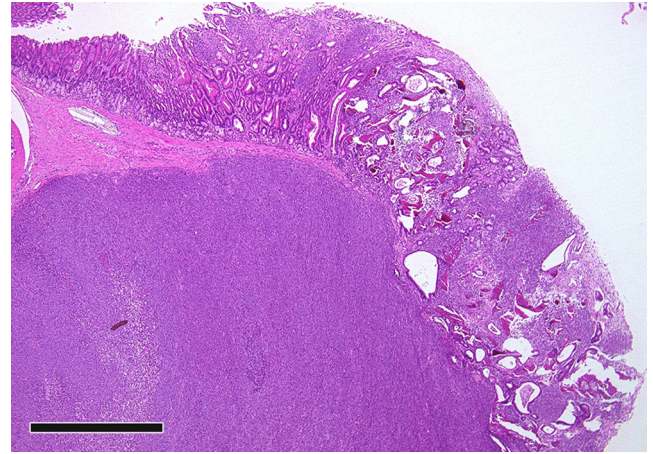

Fig. 2. Microscopic features of the tumor in the duodenal wall. The tumor is located in the lamina propria mucosae and tela mucosa. HE stain. Bar = 1,000 μm.
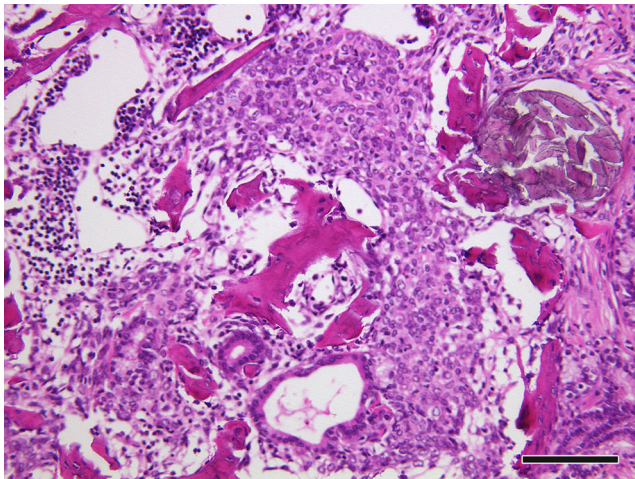

Fig. 3. A part of the lamina propria mucosae. Proliferation of polygonal cells and formation of small clumps of bone tissue in the lamina propria mucosae. HE stain. Bar = 100 μm.
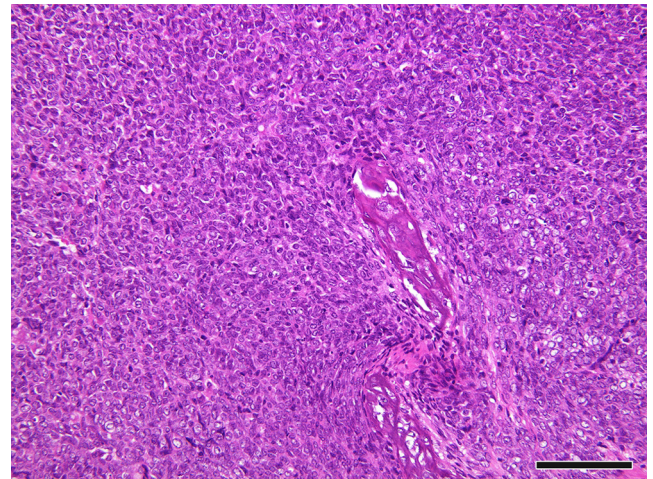

Fig. 4. A part of the tela mucosa. Marked proliferation of polygonal cells and spindle-shaped cells together with a small amount of osteoid and a small clump of bone tissue in the tela mucosa. HE stain. Bar = 100 μm.

(Figs. 2 and 3). The mucosal surface became flattened with disappearance of intestinal villi, and the remaining intestinal crypts generally showed luminal dilatation (Fig. 2). Neoplastic cells proliferated densely into the tela mucosa through the lamina muscularis mucosae, and replaced almost all of the normal tissue components including duodenal glands (Fig. 2). Neoplastic cells partially infiltrated into the tunica muscularis but not into the tunica serosa.

Neoplastic cells consisted of polygonal cells suggesting atypical osteoblasts and spindle-shaped cells, and polygonal cells were predominant (Figs. 3 and 4). Both types of neoplastic cells generally had a scanty basophilic or faintly eosinophilic cytoplasm and a pleomorphic plump nucleus (Figs. 3 and 4), and they occasionally showed mitosis. A few multinucleated cells resembling osteoclasts were also

found. In the tela mucosa, a small amount of osteoid and a small clump of mature bone tissue also sporadically formed in the area of dense neoplastic cell proliferation (Fig. 4). In addition, chondroid elements were not identified morphologically in either area of neoplastic cell proliferation. Neither invasion of vessels in the duodenum nor metastasis to distant organs was observed.

Immunohistochemically, both polygonal and spindle-shaped neoplastic cells were positive for anti-osteocalcin, osteonectin, vimentin, and S-100 protein (Fig. 5), and the latter were also occasionally positive for α-SMA (Fig. 5). In addition, a few Iba-1-positive osteoclast-like multinucleated cells were found intermingled with neoplastic cells (Fig. 5). Such immuno-positive neoplastic cells were mainly observed around small clumps of bone tissue, especially in
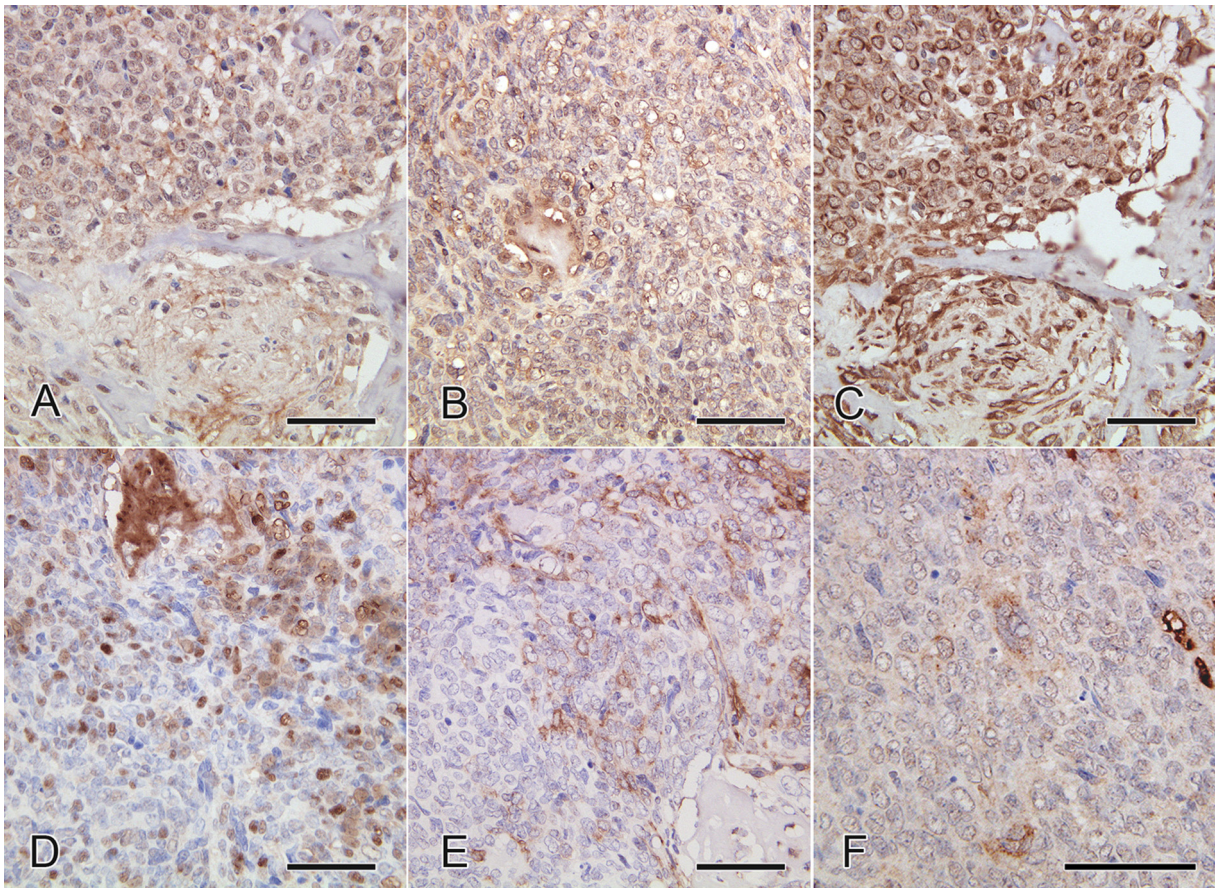
Fig. 5. Immunohistochemistry. Positive reactions for A) osteocalcin, B) osteonectin, C) vimentin, and D) S-100 protein in polygonal and spindle-shaped cells, E) α-SMA in spindle-shaped cells, and F) Iba-1 in multinucleated cells. Bar = 50 μm.

the lamina propria mucosae, except for those that were vimentin positive.

Osteocalcin and osteonectin are well-known reliable markers for osteogenic tumors, and some extraskeletal osteosarcomas are said to positively react with anti-vimentin, S-100 protein, and α-SMA antibodies[2, 3, 5, 6]. Judging from the abovementioned results, the present tumor was diagnosed as an extraskeletal osteosarcoma originating from the duodenum. In addition, the cause of demise of this animal was considered to be intestinal obstruction caused by the tumor.

Mouse osteosarcoma is classified into the following eight subtypes depending upon the morphologic characteristics of the tumor[8]: 1) the eburnating type, which is mainly composed of osteoma-like tumor osteoid/bone but with pleomorphic and infiltrating cells at the tumor periphery; 2) the osteoblastic type, which is composed of neoplastic osteoblasts and highly differentiated with varying amounts of osteoid and bone tissue; 3) the fibroblastic type, which is composed of spindle-shaped cells simulating a pattern of fibrosarcoma and a variable amount of osteoid; 4) the osteoclastic type, which is predominantly composed of osteoclast-like giant cells; 5) the chondroblastic type, which is composed of immature cartilage and bone; 6) the vascular type, which is composed of large blood-filled sinuses with variable amounts of osteoid and tumor cells; 7) the anaplastic type, which is composed of poorly differentiated pleomorphic tumor cells with scanty osteoid formation; and 8) the mixed type, which is composed of a combination of two or more histologic types. Judging from the abovementioned histological findings, the present osteosarcoma was considered to be the osteoblastic type.

In conclusion, this paper revealed the morphological and immunohistochemical characterization of the present tumor and described the first case of spontaneous duodenal extraskeletal osteosarcoma in a mouse.

Disclosure of Potential Conflicts of Interest: The authors declare that they have no conflicts of interest.

References

1. Historical Controls report NTP. ALL Routes and Vehicles, Mice. November 2014, from National Toxicology Program website: https://ntp.niehs.nih.gov/ntp/historical_controls/ntp2000_2014/histcont2014mice_all_routes_508.pdf.
2. Nagaike M, Sakai K, Tsuchiya S, Shimada F, Inui K, and Uratani M. Extraskeletal osteosarcoma with pulmonary metastasis in a female f344 rat. J Toxicol Pathol. **24**: 75–79. 2011. [Medline] [CrossRef]
3. Yoshizawa K, Matsumoto M, Oishi Y, and Nyska A. Extraskeletal osteosarcoma with cystic appearance in an aged Sprague-Dawley rat. Toxicol Pathol. **33**: 762–765. 2005. [Medline] [CrossRef]
4. Minato Y, Yamamura T, Takada H, Kojima A, Imaizumi K, Wada I, Takeshita M, and Okaniwa A. An extraskeletal osteosarcoma in an aged rat. Nippon Juigaku Zasshi. **50**: 259–261. 1988. [Medline] [CrossRef]
5. Ito T, Katoh Y, Shimada Y, Ohnuma-Koyama A, Takahashi N, Kuwahara M, and Harada T. Spontaneous extraskeletal osteosarcoma with various histological growth patterns in the abdominal wall of an ICR mouse. J Toxicol Pathol. **29**: 39–43. 2016. [Medline] [CrossRef]
6. Okazaki S, Ando R, Matsushima K, Hoshiya T, and Tamura K. Spontaneous extraskeletal osteosarcoma in the stomach of an aged f344 rat. J Toxicol Pathol. **23**: 157–159. 2010. [Medline] [CrossRef]
7. Elwell MR, and McConnell EE. Small and large intestine. In: Pathology of the Fischer Rat. Boorman GA, Eustis SL, Elwell MR, Montgomery Jr. CA, and MacKenzie WF (eds). Academic Press, San Diego. 43–61. 1990.
8. Ernst H, Long PH, Wadsworth PF, Leininger JR, Reiland S, and Konishi Y. Skeletal system and Teeth. In: International Classification of Rodent Tumors: The Mouse. Mohr U (ed). Springer-Verlag Berlin Heidelberg, New York. 389–415. 2001.

Short Communication

Histopathological localization of cadmium in rat placenta by LA-ICP-MS analysis

Yoshikazu Yamagishi[1], Satoshi Furukawa[1*], Ayano Tanaka[1], Yoshiyuki Kobayashi[2], and Akihiko Sugiyama[3]

[1] Biological Research Laboratories, Nissan Chemical Industries, Ltd., 1470 Shiraoka-cho Shiraoka, Saitama 349-0294, Japan
[2] Chemical Research Laboratories, Nissan Chemical Industries, Ltd., 2-10-1 Tsuboi-nishi Funabashi, Chiba 274-8507, Japan
[3] Courses of Veterinary Laboratory Medicine, School of Veterinary Medicine, Faculty of Agriculture, Tottori University, 4-101 Koyama-cho Minami, Tottori 680-8553, Japan

Abstract: In order to clarify the histological localization of cadmium (Cd) in the placenta, we analyzed paraffin sections of placentas from rats with a single Cd exposure on gestation day 18 by the LA-ICP-MS imaging method compared with the histopathological changes. The placentas were sampled at 1 hour, 2 hours, 3 hours, 6 hours, and 24 hours after treatment. Histopathologically, the trophoblasts in the labyrinth zone of the Cd group showed swelling at 1 hour. At 2 and 3 hours, the trophoblasts showed swelling and vacuolar degeneration. At 6 and 24 hours, the syncytiotrophoblasts selectively underwent necrosis/apoptosis, resulting in a decrease in number. Remarkable metallothionein expression was observed in the trophoblastic septa, particularly cytotrophoblasts at 24 hours. The LA-ICP-MS analysis detected the localization of Cd in the fetal part of the placenta from 1 hour onwards. In particular, the intensity of Cd was prominent in the labyrinth zone and tended to increase with the progression of trophoblastic septa damages. The LA-ICP-MS analysis using the paraffin sections detected the localization of Cd in the fetal part of the placenta, and this methodology will be one of the valuable tools to detect heavy metals in toxicological pathology. (DOI: 10.1293/tox.2016-0022; J Toxicol Pathol 2016; 29: 279–283)

Key words: cadmium, LA-ICP-MS, placenta, rat

Cadmium (Cd) is known to be one of the most toxic heavy metals that induce damage to various organs, which is caused by a diversity of toxic effects[1]. Cd induces nephrotoxicity, osteotoxicity, lung toxicity, hepatotoxicity, reproductive toxicity, carcinogenicity, and teratogenicity. Regarding reproductive toxicity, Cd exposure during pregnancy in mice, rats, and hamsters results in teratological effects, such as skeletal malformations and exencephaly in the early gestation stage and fetal death and placental necrosis in the late gestation stage. Although Cd can cross the placenta and accumulates in fetal tissues, fetal toxicity in rats is considered to be caused by Cd-induced placental or maternal dysfunction, not by a direct effect of Cd on fetuses[2]. The placenta is known to be a primary target for Cd toxicity during pregnancy[3] and is one of the major Cd accumulation tissues in rats[4]. Histologically, the rat placenta is composed of the fetal part (labyrinth zone and basal zone) and the maternal part (decidua and metrial gland)[5, 6]. However, the his-

tological localization of Cd in each part of the placenta has not been reported.

In recent years, elemental detection of thin tissue sections by means of laser ablation-inductively coupled plasma-mass spectrometry (LA-ICP-MS) has been developed for imaging trace elements (metals, metalloids, and nonmetals) and isotopes in biological materials, providing accurate and reliable data for quite different applications[7]. LA-ICP-MS analysis has become the method of investigation of elemental distributions in biological tissue sections due to its high sample throughput, high sensitivity, and spatial resolution down to 4 µm. Cryosections[7, 8] or fixed sections[9, 10] are possible sources for elemental bioimaging with LA-ICP-MS. Therefore, LA-ICP-MS analysis is becoming one of the important tools for pathology[11]. In the present study, in order to clarify the histological localization of Cd in the placenta, we used the LA-ICP-MS imaging method to analyze paraffin sections of placentas from rats exposed to Cd.

Non-pregnant specific pathogen-free Wistar Hannover rats (Japan Laboratory Animals, Inc., Tokyo, Japan) were purchased at approximately 10–14 weeks of age. Each female rat was housed together with a male rat. The occurrence of copulation was established by daily inspection for a vaginal plug. Mated female rats were utilized in this study. Gestation day (GD) 0 was designated as the day on when the presence of a vaginal plug was identified. The animals were single-housed in plastic cages on softwood chip bed-

ding in an air-conditioned room (22 ± 2°C; humidity, 55 ± 10%; light cycle, 12 hr/day). Feed (CRF-1, Oriental Yeast Co., Ltd., Tokyo, Japan) and water were available *ad libitum*. Fifteen pregnant rats were randomly allocated to the control group of 5 rats and the Cd group of 10 rats. Cadmium chloride (CdCl$_2$) (Wako Pure Chemical Industries, Ltd., Osaka, Japan) was dissolved in sterile 0.75% saline solution. CdCl$_2$ was subcutaneously administered to rats at doses of 0 mmol/kg with sterile 0.75% saline solution (the control group) or 0.04 mmol/kg CdCl$_2$ (the Cd group) with a volume of 1 ml/100 g body weight on GD 18. Previously, treatment with this dose level on GD 18 was reported to induce fetal death and placental necrosis[12]. All treatments were performed between 7 and 9 a.m. One dam in the control group and two dams in the Cd group each were sampled at 1 hour, 2 hours, 3 hours, 6 hours, and 24 hours after treatment. The dams were euthanized by exsanguination under anesthesia and necropsied. All fetuses were removed from the placentas. Five placentas/litter were randomly obtained from embryos/fetuses of all dams in both groups at the sampling time points. All placentas were fixed in 10% neutral buffered formalin, embedded in paraffin, sectioned at 4 μm thickness, and stained routinely with hematoxylin and eosin (HE) for histopathological examination. In order to figure the localization of Cd, immunohistochemical staining of metallothionein (MT) antibody against rat MT-1/MT-2 (MTE9, DakoCytomation, Carpinteria, USA) was performed according to the avidin-biotin complex (ABC) method (VECTSTAIN ABC Kit, Vector Laboratories, Inc., Burlingame, California, USA). These experiments were conducted according to the Guidelines for Animal Experimentation, Japanese Association for Laboratory Animal Science.

An LSX 213 laser ablation system (Teledyne CETAC Technologies, Omaha, USA) working at a wavelength of 213 nm with a scanning camera was coupled to a quadruple-based iCAP Qc ICP-MS (Thermo Fisher Scientific, Waltham, USA) in such a way that the aerosol from the laser ablation unit was directly introduced into the injector pipe of the ICP-MS by a carrier gas through a tygon tube (Fig. 1). The laser parameters, such as laser energy, scan rate and frequency, were optimized to receive accurate lateral elemental information. A spot size of 150 um was selected. The scan rate was 50 um/s. The used laser energy was adjusted to 15.13 mJ, while the laser was operated at a shot repetition rate of 20 Hz. For the present study, a HelEx™ 2-volume cell was utilized. For tuning of the instrument, a fully automated adjustment approach was programmed using the provided functionality of the Qtegra software. For this purpose, parameters like the position of the torch, extraction voltage, and additional carrier gas flow of argon, as well as the most relevant ion lenses in front of the mass analyzer, were optimized for maximum intensity and low levels of oxides and doubly charged ions. As a carrier gas (0.65 L/min), helium was used to obtain an improved washout behavior. Additional ICP-MS conditions were as follows: a nickel sampler and skimmer without insert and a quartz injector pipe with an inner diameter of 3.5 mm; RF power, 1,550 W; auxiliary
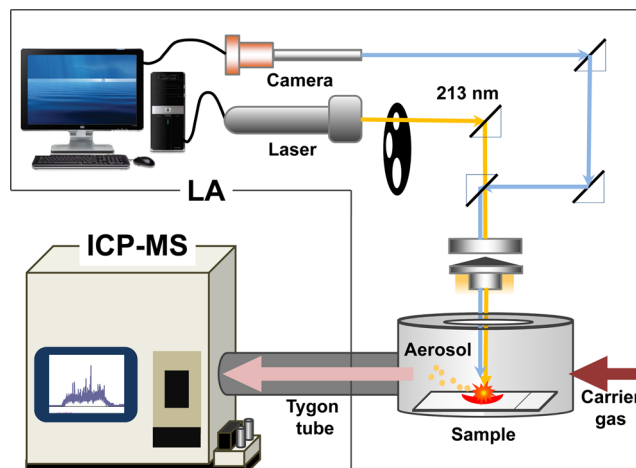

Fig. 1. LA-ICP-MS. Laser ablation system (LA): sample extraction from an unstained paraffin section slide by laser ablation with a 213 nm laser beam with camera scanning. Inductively coupled plasma-mass spectrometry (ICP-MS): analysis of a sample-derived aerosol from LA.

gas flow rate, 0.8 L/min; dwell time, 0.22 s; and isotopes monitored, [111]Cd and [114]Cd. Because of the absence of isobaric interference for the investigated mass to charge ratios (blank signal, 400 cps), the analysis was performed in the standard mode of the ICP-MS instrument. One placenta on the unstained paraffin section slide from one dam at each sampling time in the both groups was measured with the LA-ICP-MS under the above condition. Placentas showing typical lesions at each sampling time were selected for the LA-ICP-MS analysis. After the LA-ICP-MS analysis, the used slides were stained routinely with HE staining for histopathological examination.

There were no deaths of dams in the either group. Fetal death was observed from 6 hours onwards after treatment in the Cd group (Fig. 2). Histopathologically, the trophoblasts in the labyrinth zone of the Cd group showed swelling at 1 hour (Fig. 2). At 2 and 3 hours, the trophoblasts showed swelling and vacuolar degeneration (Fig. 2). At 6 and 24 hours, the syncytiotrophoblasts selectively underwent necrosis/apoptosis resulting in a decrease in number. Some placentas showed congestion and hemorrhage, resulting from thinning of the trophoblastic septa (Fig. 2). During the experimental period, there were no lesions in the basal zone, decidua, or metrial gland in the Cd group or in any zones in the control group.

The MT expression at each sampling time point in each zone is shown in Table 1. In the labyrinth zone, remarkable MT expression was observed in the trophoblastic septa, particularly in cytotrophoblasts at 24 hours in the Cd group, compared with in the control group (Fig. 2). There was no remarkable difference in MT expression in the basal zone, decidua, or metrial gland at any sampling time between the control and Cd groups.

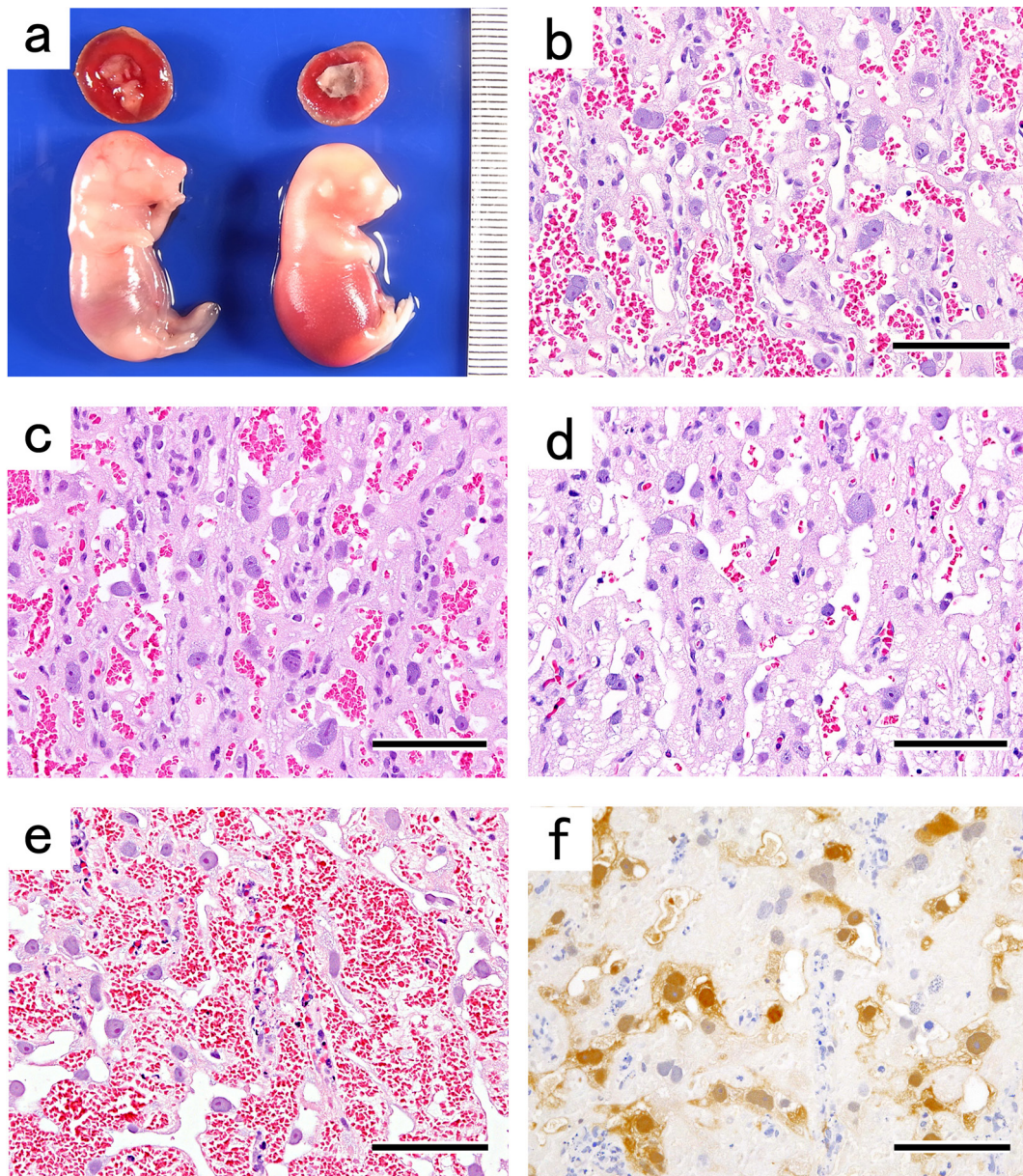The LA-ICP-MS intensity of Cd at each sampling time

Fig. 2. Gross appearance and histopathological changes in labyrinth zone. a) Gross appearance of fetus and placenta at 24 hours after treatment. Control group (left) and Cd group (right). In Cd group, macerated fetus immediately after death and geographic discoloration of fetal surface of placenta. b) At 1 hour in control group. (HE staining) c) At 1 hour in Cd group. Swelling of trophoblasts. (HE staining) d) At 3 hours in Cd group. Swelling and vacuolar degeneration of trophoblasts. (HE staining) e) At 24 hours in Cd group. Selective necrosis/apoptosis of syncytiotrophoblasts. Congestion and hemorrhage with thinning of trophoblastic septa. (HE staining) f) At 24 hours in Cd group. MT expression in trophoblastic septa, particularly cytotrophoblasts. (MT immunohistochemical staining) Bar = 100 μm.

point in each zone is shown in Table 1 and Figure 3. In the labyrinth zone, the intensity of Cd was detected from 1 hour onwards and showed a marked increase at 24 hours in the Cd group. In the basal zone, the intensity of Cd was detected at 1 hour, 2 hours, and 24 hours in the Cd group, but the levels were less than those in the labyrinth zone. The intensity of Cd could not be detected in the decidua or metrial gland in the Cd group, or in any zones in the control group.

These results revealed that the LA-ICP-MS analysis us-ing the paraffin sections detected the localization of Cd in the fetal part of the placenta, but not in the maternal part of the placenta. In particular, the intensity of Cd was promi-nent in the labyrinth zone and tended to increase with the progression of trophoblastic septa damage. Immunohisto-chemically, MT expression was increased in the labyrinth zone, although it was only detected at only 24 hours. It has been known that MT expression is observed in the yolk sac and decidua, but not in the labyrinth zone, in the normal

Table 1. LA-ICP-MS Intensity and MT Immunohistochemical Expression in Placenta

Part of placenta	LA-ICP-MS intensity (average of cps in part)						MT immunohistochemical expression					
	Control	Cadmium					Control	Cadmium				
		1 hr	2 hr	3 hr	6 hr	24 hr		1 hr	2 hr	3 hr	6 hr	24 hr
Labyrinth zone	N.D.	3,690	4,305	5,419	3,714	7,099	−	−	−	−	−	+++
Basal zone	N.D.	616	439	N.D.	N.D.	821	±	±	±	±	±	±
Decidua basalis	N.D.	N.D.	N.D.	N.D.	N.D.	N.D.	±	±	±	±	±	+
Metrial gland	N.D.	N.D.	N.D.	N.D.	N.D.	N.D.	±	±	±	±	±	±

N.D.: not detected. −, negative; ± , minimal, +, mild; ++, moderate; +++, severe.

developing rat placenta[13]. Therefore, the MT immunohistochemical data seems to support the results of the localization of Cd by the LA-ICP-MS analysis broadly. In addition, it is considered that the positive reaction of MT immunohistochemistry was observed 6 hours or more than after Cd deposition at earliest. LA-ICP-MS analysis was sensitive tool to detect Cd deposition in the paraffin sections compared with MT immunohistochemistry.

 The fetal part of the placenta on GD 19 is primarily composed of four kinds of trophoblasts; cytotrophoblasts and syncytiotrophoblasts in the labyrinth zone and spongiotrophoblasts and trophoblastic giant cells in the basal zone[14]. It has been known that Cd mainly injuries the syncytiotrophoblasts as a result of the cellular and mitochondrial damage and that the cytotrophoblasts remain relatively unaffected early stage in the labyrinth zone[12, 15]. In the present study, although Cd deposition was observed in these trophoblasts, the highest affinity cells for Cd were cytotrophoblasts, and the most severely damaged cells were spongiotrophoblasts. Thus, it is considered that the sensitivity to Cd toxicity is different among these trophoblasts. Further detailed investigations of the treatment on an earlier gestation day are necessary to clarify the differential sensitivity of the Cd toxicity among these trophoblasts.

 It is known that LA-ICP-MS can be applied as microscopic detector of exogeneous heavy metals (Cu, Fe, Zn, Pt, etc.) at the tissue level[9, 16]. In addition, paraffin section slides that have been analyzed with LA-ICP-MS can be subjected to HE staining or special staining. Furthermore, the HE-stained slides can also be subjected to LA-ICP-MS analysis[16]. Therefore, it is possible to identify the location of metal deposition by LA-ICP-MS analysis in comparison with histopathological changes. The LA-ICP-MS methodology will be exploited in future toxicological pathology for a mode of action approach.

 In conclusion, LA-ICP-MS analysis using paraffin sections detected the localization of Cd in the fetal part of the placenta, particularly in the labyrinth zone, and this methodology will be one of the valuable tools to detect heavy metals in toxicological pathology.
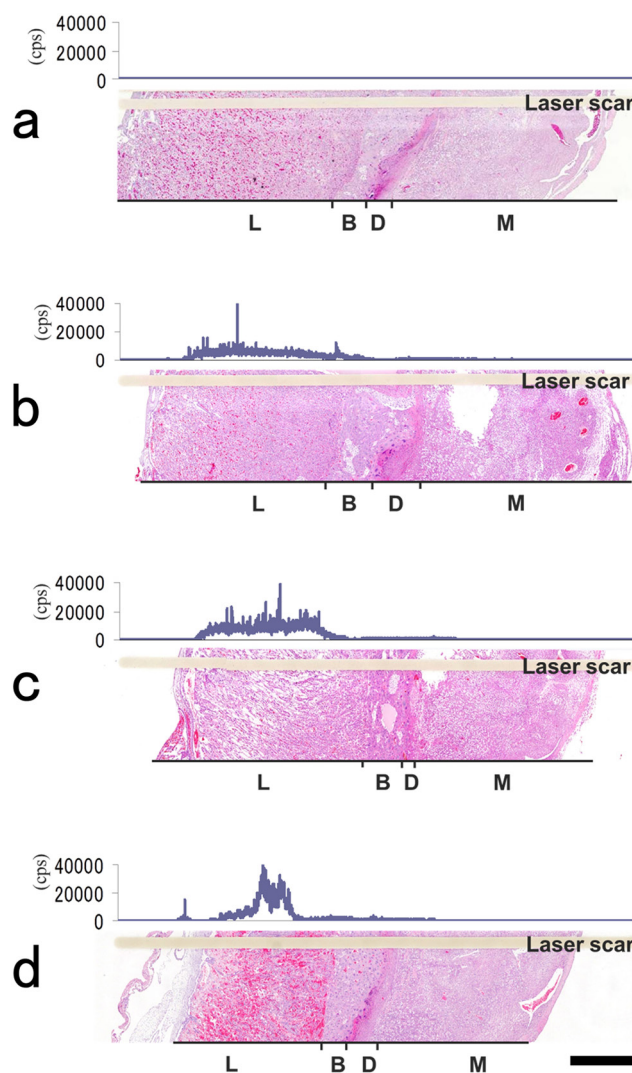
Fig. 3. LA-ICP-MS chromatography and histopathology. a) At 1 hour in control group. b) At 1 hour in Cd group. c) At 3 hour in Cd group. d) At 24 hour in control group. L, labyrinth zone; B, basal zone; D, decidua basalis; M, metrial gland. (HE staining) Bar = 1 mm.

Disclosure of Potential Conflicts of Interest: The authors declare that they have no conflicts of interest.

Reference

1. Rani A, Kumar A, Lal A, and Pant M. Cellular mechanisms of cadmium-induced toxicity: a review. Int J Environ Health Res. **24**: 378–399. 2014. [Medline] [CrossRef]
2. Levin AA, and Miller RK. Fetal toxicity of cadmium in the rat: maternal vs fetal injections. Teratology. **22**: 1–5.1980.
3. Daston GP. Relationships between maternal and developmental toxicity. In: Developmental Toxicology, 2nd ed. CA Kimmel, and J Buelke-Sam (eds). Raven Press, New York. 189–212. 1994.
4. Goyer RA, and Cherian MG. Role of metallothionein in human placenta and rats exposed to cadmium. IARC Sci Publ. **118**: 239–247. 1992. [Medline]
5. Furukawa S, Hayashi S, Abe M, Hagio S, Irie K, Kuroda Y, Ogawa I, and Sugiyama A. Background data on developmental parameters during the gestation period in rats. J Toxicol Pathol. **26**: 83–88. 2013. [Medline] [CrossRef]
6. Furukawa S, Kuroda Y, and Sugiyama A. A comparison of the histological structure of the placenta in experimental animals. J Toxicol Pathol. **27**: 11–18. 2014. [Medline] [CrossRef]
7. Becker JS, Kumtabtim U, Wu B, Steinacker P, Otto M, and Matusch A. Mass spectrometry imaging (MSI) of metals in mouse spinal cord by laser ablation ICP-MS. Metallomics. **4**: 284–288. 2012. [Medline] [CrossRef]
8. Pugh JA, Cox AG, McLeod CW, Bunch J, Writer MJ, Hart SL, Bienemann A, White E, and Bell J. Elemental imaging of MRI contrast agents: benchmarking of LA-ICP-MS to MRI. Anal Bioanal Chem. **403**: 1641–1649. 2012. [Medline] [CrossRef]
9. Sussulini A, and Becker JS. Application of laser microdissection ICP-MS for high resolution elemental mapping in mouse brain tissue: a comparative study with laser ablation ICP-MS. Talanta. **132**: 579–582. 2015. [Medline] [Cross-Ref]
10. Moraleja I, Esteban-Fernández D, Lázaro A, Humanes B, Neumann B, Tejedor A, Mena ML, Jakubowski N, and Gómez-Gómez MM. Printing metal-spiked inks for LA-ICP-MS bioimaging internal standardization: comparison of the different nephrotoxic behavior of cisplatin, carboplatin, and oxaliplatin. Anal Bioanal Chem. **408**: 2309–2318. 2016. [Medline] [CrossRef]
11. Egger AE, Kornauth C, Haslik W, Hann S, Theiner S, Bayer G, Hartinger CG, Keppler BK, Pluschnig U, and Mader RM. Extravasation of Pt-based chemotherapeutics - bioimaging of their distribution in resectates using laser ablation-inductively coupled plasma-mass spectrometry (LA-ICP-MS). Metallomics. **7**: 508–515. 2015. [Medline] [CrossRef]
12. Levin AA, Kilpper RW, and Miller RK. Fetal toxicity of cadmium chloride: the pharmacokinetics in the pregnant Wistar rat. Teratology. **36**: 163–170. 1987. [Medline] [CrossRef]
13. Furukawa S, Usuda K, Abe M, Hayashi S, and Ogawa I. Histological expression of metallothionein in the developing rat placenta. J Toxicol Pathol. **21**: 223–227. 2008. [CrossRef]
14. Furukawa S, Hayashi S, Usuda K, Abe M, Hagio S, and Ogawa I. Toxicological pathology in the rat placenta. J Toxicol Pathol. **24**: 95–111. 2011. [Medline] [CrossRef]
15. Di Sant'Agnese PA, Jensen KD, Levin A, and Miller RK. Placental toxicity of cadmium in the rat: an ultrastructural study. Placenta. **4**: 149–163. 1983. [Medline] [CrossRef]
16. Reifschneider O, Wehe CA, Raj I, Ehmcke J, Ciarimboli G, Sperling M, and Karst U. Quantitative bioimaging of platinum in polymer embedded mouse organs using laser ablation ICP-MS. Metallomics. **5**: 1440–1447. 2013. [Medline] [CrossRef]